



Modeling an industrial LDPE plant with Aspen Plus® and Aspen Polymers®

Artur Miguel Moutinho de Jesus

Thesis to obtain the Master of Science Degree in:

Chemical Engineering

Supervisors:

Eng. André Vilelas

Prof. Pedro Miguel Gil de Castro

Examination Committee:

Chairman: Henrique Anibal Santos de Matos

Supervisor: Prof. Pedro Miguel Gil de Castro

Member of the committee: Carlos Manuel Faria de Barros Henriques

October 2023

Declaration

I, Artur Miguel Moutinho de Jesus, student number 90787 of Instituto Superior Técnico, declare that this master thesis is the original work of my authorship, and it follows the requirements of the conduct code and good practices of the Universidade de Lisboa and of Instituto Superior Técnico.

Acknowledgments

I want to start for thank my father, sister, and paternal grandparents. To my father for everything. Without him, I would not be here today. All the support he provided to my sister and I, he was always there in both good and challenging moments to take care of us. To my sister who is with me since we born. I am grateful to have shared my entire journey with her, and for all the support and inspiration she has given me. To my grandma who sadly passed way before witness the graduation of me and my sister. I know this was one of her dreams, and she was one of the most important people who helped to accomplish it. To my grandfather to always lighten the mood, with his hilarious histories. To all four I am truly grateful, I love you all.

I want to express my gratitude to Eng^o André Vilelas for proposing this work and welcoming me into Repsol. I am very thankful to Eng^o João Amaro, Eng^a Rita Vidigal, Eng^a Raquel Nunes, and everybody in the LDPE team that received me warmly, allowed me to watch close their work, and generously answered my questions while providing invaluable suggestions for this project. It was the best part of this last 6 months, and I will all remember my time there hopefully one day we meet again someday.

I extend my appreciation to Prof^o Pedro Castro for his continuous communication and guidance throughout this work; his assistance was fundamental.

I would like to acknowledge Dr. Alberto Buchelli and Dr. Bryan Satola. Despite not knowing me personally, they offered their expertise, helping me overcome certain challenges I faced. Without their support, the results of this thesis would have been significantly different.

Finally, I want to thank to friends and family that helped me along my path and I might forgot to mention.

Resumo

O polietileno de baixa densidade (PEBD) representa 18% do mercado global de polietileno, com uma produção de 20Mt em 2020, sendo utilizado principalmente em filmes injeção e laminagem [1,2]. Devido à meta de zero emissões até 2050 da *Plastic Europe* [2] e às exigências dos consumidores em novos produtos adaptados às suas necessidades, esta indústria tem mostrado um interesse renovado na modelação dos seus processos.

Neste trabalho, modelou-se o processo de produção de PEBD na unidade de Sines da Repsol Polímeros, utilizando *Aspen Plus*[®] V11 e *Aspen Polymers*[®]. O reator, um autoclave com 5 zonas, opera a alta pressão (1200-2000 bar) e temperaturas elevadas (170-300 °C). Em contraste com autoclaves previamente modelados este possui 5 entradas etileno, ao qual são adicionados agentes de terminação (butano ou propileno) conforme o grau a produzir, para controlar o crescimento das cadeias poliméricas [3].

No *Aspen Plus*[®] V11 modelou-se o reator como 5 cinco *CSTRs*, representando as zonas do autoclave. Parâmetros cinéticos da literatura levaram a desvios elevados em relação às medidas da fábrica, motivando a obtenção de novos parâmetros cinéticos com a ferramenta *Data Fit*, usando dados reais do processo de 8 diferentes graus. As variáveis de output usadas foram a conversão, as massas molares médias (M_n e M_w) e as ramificações curtas (SCB).

Contudo, para se obter uma descrição satisfatória do comportamento do sistema com o modelo cinético de polimerização radical, foi necessário utilizar dois conjuntos de parâmetros cinéticos, num total de 78 parâmetros. Um conjunto para prever os outputs relacionados com a qualidade do polímero (M_n , M_w , Índice de Polidispersividade e SCB), e um segundo para descrever a conversão. Os resultados obtidos correspondem a desvios de $\pm 30\%$ para a maioria dos graus de PEBD.

O modelo de PC-SAFT foi utilizado para descrever as propriedades termodinâmicas do sistema. Os parâmetros binários do PC-SAFT (k_{ij}) foram manipulados de forma a replicar as fases de separação. Os compressores, responsáveis por grande parte da energia consumida no processo, também foram simulados.

Palavras-Chave: PEBD, Polietileno, Polimerização radical, Aspen Plus, Aspen Polymers

Abstract

The low-density polyethylene (LDPE) represents 18% of the polyethylene market worldwide with a production of 20 Mt in 2020, being mainly used in films, injection and moulding applications [1,2]. This industry has been evolving to develop polymers that can be tailored to the consumer's needs, and to minimize emissions to meet the 2050 net zero target of Plastic Europe [2]. Thus, there has been renewed interest in modeling the processes.

This work aims to model the LDPE production process at Repsol Polímeros' Sines unit using Aspen Plus® V11 and Aspen Polymers®. The reactor, an autoclave with 5 zones, operates at high pressure (1200-2000 bar) and elevated temperatures (170-300 °C). In contrast to the previously modeled autoclaves, this reactor has 5 ethylene inlets. Termination agents (n-butane or propylene) are also added to control the polymer chain growth and achieve the desired grade.

In Aspen Plus ® V11, the reactor was modeled as 5 CSTRs, representing the zones of the autoclave. Kinetic parameters from the literature led to significant deviations from the plant data. This motivated the determination of new kinetic parameters from real process data, gathered from 8 different grades, using the Data Fit tool. The output variables considered were conversion, both average molar masses (M_n and M_w), and short-chain branching (SCB).

Nevertheless, for a good description of the system behavior with the free-radical kinetic model, 2 sets of kinetic parameters were required (a total of 78 parameters). One set to describe the outputs related to polymer quality (M_n , M_w , Polydispersity Index, and SCB), and the other to describes the conversion. Overall, the model predictions were within $\pm 30\%$ for most LDPE grades.

The PC-SAFT model was employed to describe the system thermodynamic properties. The PC-SAFT binary parameters (k_{ij}) were also adjusted to replicate phase separation behavior. Since the compressors account for a large share of the energy consumption in the process, they were also simulated.

Keywords: LDPE, Polyethylene, Free-radical polymerization, Aspen Plus, Aspen Polymers

Table of contents

Declaration	i
Acknowledgments	ii
Resumo	iii
Abstract	iv
List of Figures	viii
List of Tables	xiv
List of Abbreviations	xv
1. Introduction.....	1
1.1. Polymers Overview.....	1
1.1.1. Polymers Properties	3
1.1.2. LDPE Reactor Technologies	4
1.2. Polymers Market Analysis	6
1.3. Polymers Simulation.....	9
1.3.1. Aspen Polymers®.....	10
2. Motivation	15
3. Repsol Polímeros	17
3.1. Process Description.....	17
3.2. Protocol Recipes for Polymer Grade Production	20
4. Free Radical Polymerization Reaction.....	21
4.1. Chain Initiation.....	21
4.2. Propagation	22
4.3. Termination.....	23

4.4.	Chain Transfer	23
4.4.1	Chain transfer to Agents (or solvent).....	23
4.4.2.	Chain transfer to monomer.....	24
4.4.3.	Chain transfer to polymer	24
4.5.	β -scission.....	25
4.6.	Backbiting.....	25
4.7.	Kinetic parameters from the literature	26
4.8.	Preliminary tests	29
5.	Polymer properties correlations	33
5.1.	Melt index	33
5.2.	Density.....	35
6.	Methodology.....	37
6.1.	Components definition.....	37
6.2.	Thermodynamic model.....	38
6.2.1.	PC-SAFT (Perturbed Chain Statistical Associating Fluid Theory)	38
6.3.	Process simulation	40
6.3.1.	Data Fit tool	43
6.3.2.	Parameters estimation.....	45
7.	Results and Discussion.....	58
7.1.	Reactor	58
7.1.1.	Initial Case.....	58
7.1.2.	Case 1	61
7.1.3.	Case 2	63
7.1.4.	Case 3	66

7.2.	Separation Stages.....	71
7.3.	Compressors.....	73
7.4.	Full plant.....	76
8.	Conclusions and Future Work.....	79
9.	References.....	81
	Appendix.....	88
A.	MWD.....	88
B.	PC-SAFT.....	89
C.	Reactor conditions.....	92

List of Figures

Figure 1. Representation of linear copolymers, statistical or random, alternate and block-copolymers [14].	2
Figure 2. Classification of polyethylene types according to branching structure and density [3].	3
Figure 3. Representation of how the short-chain branches (SCB) impact the lamellae formation [1].	4
Figure 4. Difference in the MWD obtained in an autoclave and a tubular reactor LDPE [1,23].	5
Figure 5. Annual production of plastics worldwide from 1950 to 2021 and forecast until 2050 [26,27].	7
Figure 6. Distribution of global plastic materials production in 2021, by region [2].	7
Figure 7. Distribution of plastics consumption by application [2].	8
Figure 8. Distribution of the global plastics production by type in 2021 [2].	9
Figure 9. Sustainable Development Goals approached on the Repsol Polímeros Sustainability Plan [49].	17
Figure 10. Simplified flowsheet of the process. Some of the main measurements in the plant are shown in blue: T – Temperature (°C); P – Pressure (barg); F – Mass Flow (kg/h); W – Power (kW).	19
Figure 11. Reactor zones temperature in each grade protocol.	20
Figure 12. M_n sensitive analysis to each reaction.	30
Figure 13. M_w sensitive analysis to each reaction.	30
Figure 14. PDI sensitive analysis to each reaction.	30
Figure 15. Ethylene conversion sensitive analysis to each reaction.	31
Figure 16. AT conversion sensitive analysis to each reaction.	31
Figure 17. SCB sensitive analysis to each reaction.	32
Figure 18. LCB sensitive analysis to each reaction.	32
Figure 19. Number-average molecular weight against Melt Index.	34

Figure 20. Weight-average molecular weight against Melt Index.	35
Figure 21. Relation between SCB and the final polymer density. Curve (a), (b) and (c) are generated with equations (22), (23) and (24), respectively.	36
Figure 22. The main difference between SAFT and PC-SAFT.	39
Figure 23. Conversion of the real reactor to the Aspen Plus [®] reactor model.	41
Figure 24. Trust Region Optimization [79].	43
Figure 25. Flowchart of the methodology used to treat the full plant.	46
Figure 26. Deviations between the model predictions and experimental conversions when using the kinetic parameters taken from the literature.	47
Figure 27. Deviations between the model predictions and experimental M_n when using the kinetic parameters taken from the literature.	47
Figure 28. Deviations between the model predictions and experimental M_w when using the kinetic parameters taken from the literature.	47
Figure 29. Deviations between the model predictions and experimental SCB when using the kinetic parameters taken from the literature.	48
Figure 30. Conversion RMSE for the different kinetic sets.	48
Figure 31. M_n RMSE for the different kinetic sets.	48
Figure 32. M_w RMSE for the different kinetic sets.	49
Figure 33. SCB RMSE for the different kinetic sets.	49
Figure 34. Flowchart of the iterative strategy to regress the kinetic parameters.	51
Figure 35. Flowchart of the strategy to regress the kinetic parameters related with the quality output variables.	52
Figure 36. Flowchart of the strategy to regress the kinetic parameters related with the conversion output variables.	53
Figure 37. Flowsheet with the two reactor systems (one for each set of kinetic parameters). ...	54
Figure 38. Flowsheet with the separation stages.	55
Figure 39. Final Flowsheet.	57

Figure 40. Experimental vs estimated ethylene conversion (initial case).	58
Figure 41. Deviation of the estimated ethylene conversion (initial case).	58
Figure 42. Experimental vs estimated M_n (initial case).	59
Figure 43. Deviation of the estimated M_n (initial case).	59
Figure 44. Experimental vs estimated M_w (initial case).	59
Figure 45. Deviation of the estimated M_w (initial case).	59
Figure 46. Experimental vs estimated SCB (initial case).	59
Figure 47. Deviation of the estimated SCB (initial case).	59
Figure 48. Experimental vs estimated butane conversion (initial case).	60
Figure 49. Deviation of the estimated butane conversion (initial case).	60
Figure 50. Experimental vs estimated propylene conversion (initial case).	60
Figure 51. Deviation of the estimated propylene conversion (initial case).	60
Figure 52. Experimental vs estimated ethylene conversion (case 1).	61
Figure 53. Deviation of the estimated ethylene conversion (case 1).	61
Figure 54. Experimental vs estimated M_n (case 1).	61
Figure 55. Deviation of the estimated M_n (case 1).	61
Figure 56. Experimental vs estimated M_w (case 1).	61
Figure 57. Deviation of the estimated M_w (case 1).	61
Figure 58. Experimental vs estimated SCB (case 1).	62
Figure 59. Deviation of the estimated SCB (case 1).	62
Figure 60. Experimental vs estimated butane conversion (case 1).	62
Figure 61. Deviation of the estimated butane conversion (case 1).	62
Figure 62. Experimental vs estimated propylene conversion (case 1).	62
Figure 63. Deviation of the estimated propylene conversion (case 1).	62

Figure 64. Experimental vs estimated ethylene conversion (case 2).....	63
Figure 65. Deviation of the estimated ethylene conversion (case 2).	63
Figure 66. Experimental vs estimated M_n (case 2).	63
Figure 67. Deviation of the estimated M_n (case 2).	63
Figure 68. Experimental vs estimated M_w (case 2).	63
Figure 69. Deviation of the estimated M_w (case 2).....	63
Figure 70. Experimental vs estimated SCB (case 2).	64
Figure 71. Deviation of the estimated SCB (case 2).	64
Figure 72. Experimental vs estimated butane conversion (case 2).	64
Figure 73. Deviation of the estimated butane conversion (case 2).....	64
Figure 74. Experimental vs estimated propylene conversion (case 2).	64
Figure 75. Deviation of the estimated propylene conversion (case 2).....	64
Figure 76. System instability sensitivity analysis.....	66
Figure 77. Experimental vs estimated M_n (case 3).	67
Figure 78. Deviation of the estimated M_n (case 3).	67
Figure 79. Experimental vs estimated PDI (case 3).....	67
Figure 80. Deviation of the estimated PDI (case 3).	67
Figure 81. Experimental vs estimated SCB (case 3).	67
Figure 82. Deviation of the estimated SCB (case 3).	67
Figure 83. Experimental vs estimated ethylene conversion (case 3).....	68
Figure 84. Deviation of the estimated ethylene conversion (case 3).	68
Figure 85. Experimental vs estimated butane conversion (case 3).	69
Figure 86. Deviation of the estimated butane conversion (case 3).....	69
Figure 87. RMSE of the ethylene conversion for the different scenarios.	70

Figure 88. RMSE of the butane conversion for the different scenarios.	70
Figure 89. RMSE of the M_n for the different scenarios.....	70
Figure 90. RMSE of the PDI for the different scenarios.....	70
Figure 91. RMSE of the SCB for the different scenarios.	70
Figure 92. Experimental vs estimated high-pressure flash top output stream (before the fit). ...	72
Figure 93. Deviation of the estimated high-pressure flash top output stream (before the fit).	72
Figure 94. Experimental vs estimated low-pressure flash top output stream (before the fit).....	72
Figure 95. Deviation of the estimated low-pressure flash top output stream (before the fit).	72
Figure 96. Experimental vs estimated high-pressure flash top output stream (after the fit).	73
Figure 97. Deviation of the estimated high-pressure flash top output stream (after the fit).....	73
Figure 98. Experimental vs estimated low-pressure flash top output stream (after the fit).....	73
Figure 99. Deviation of the estimated low-pressure flash top output stream (after the fit).	73
Figure 100. Experimental vs estimated CP power (after the fit).	74
Figure 101. Deviation of the estimated CP power (after the fit).	74
Figure 102. Experimental vs estimated output temperatures in each CP stage (after the fit). ...	74
Figure 103. Deviation of the estimated output temperatures in each CP stage (after the fit).	74
Figure 104. Experimental vs estimated CS power (after the fit).	75
Figure 105. Deviation of the estimated CS power (after the fit).	75
Figure 106. Experimental vs estimated output temperatures in each CS stage (after the fit). ...	76
Figure 107. Deviation of the estimated output temperatures in each CS stage (after the fit).	76
Figure 108. Deviation of the estimated conversion (full plant scenario).	77
Figure 109. Deviation of the estimated M_n (full plant scenario).....	77
Figure 110. Deviation of the estimated PDI (full plant scenario).	77
Figure 111. Deviation of the estimated SCB (full plant scenario).	77

Figure 112. Deviation of the estimated CP power (full plant scenario).	77
Figure 113. Deviation of the estimated CS power (full plant scenario).	77
Figure 114. Estimated and experimental MWD for different grades. (a) and (b) are the A but with different batches with different protocols, (c) is E, (d) F, and (e) B.	78
Figure 115. Invalid distribution due to the presence of some side reactions.	88
Figure 116. Ethylene vapor pressure with the PC-SAFT [75]	89
Figure 117. Supercritical ethylene calorific capacity with the PC-SAFT [72]	89
Figure 118. Supercritical ethylene density with PC-SAFT [72]	90
Figure 119. LDPE density with PC-SAFT[74]	90
Figure 120. Liquid-Vapor equilibrium between LDPE and ethylene with PC-SAFT [76]	91
Figure 121. Relation between the flowrate and the strokes/min of the initiator pumps. $Q(L/h) = 0.0038(\text{Strokes/min})^2 + 0.6004(\text{Strokes/min}) - 0.0521, R^2=0.9996$	96

List of Tables

Table 1. Pressure, termination agent and type of initiator used in each zone for each grade protocol (the number in front of the initiator type in the initiators columns represents its concentration in the mixture injected).	20
Table 2. Summary of the ethylene free-radical polymerization reactions	26
Table 3. Kinetic constants of the initiators' decomposition [57]	27
Table 4. Kinetic parameters in the literature	28
Table 5. List of the compounds used in the simulation with their ID, type, and database.	37
Table 6. PC-SAFT parameters used in the simulation.....	40
Table 7. List of inputs and outputs for Data Fit	49
Table 8. Coupling between validation variables and adjusted parameters.....	50
Table 9. Kinetic parameters used to predict quality attributes- set number 1.....	68
Table 10. Kinetic parameters used to predict conversion- set number 2.....	69
Table 11. PC-SAFT binary parameters before and after the fit	73
Table 12. Primary compressor efficiencies after the fit	75
Table 13. Secondary compressor efficiencies after the fit	76
Table 14. Data for the reactor inputs for the grades with butane as termination agent	92
Table 15. Data for the reactor inputs for the grades with propylene as termination agent	94
Table 16. Data for the reactor inputs for the grades without termination agent	95

List of Abbreviations

BHP	Brake horsepower
CP	Primary Compressor
CS	Secondary Compressor
CTA	Chain Transfer to Agent
E_A	Activation Energy
EOS	Equation of State
EVA	Ethylene Vinyl Acetate
EBA	Ethylene Butyl Acrylate
HDPE	High-density Polyethylene
IHP	Indicated horsepower
k	Boltzmann constant
k_0	Pre-exponential Factor
LCB	Long Chain Branch
LDPE	Low-density Polyethylene
LLDPE	Linear Low-density Polyethylene
m	Segment number
MI	Melt Index
M_n	Number-Average Molecular Weight
M_w	Weight-Average Molecular Weight
P	Pressure
PC-SAFT	Perturbed-Chain Statistical Associating Fluid Theory
PDI	Polydispersity Index
R	Gas constant
RMP	Medium pressure return
RMSE	Root Mean Squared Error
SCB	Short Chain Branch
T	Temperature
V_A	Activation Volume
Greek letters	
ϵ	Segment energy
η	Efficiency
ρ	Density
σ	Segment diameter

1. Introduction

In this first chapter, we will start with a brief overview of the history, properties, and production process of polymers, with a specific focus on low-density polyethylene (LDPE). Next, we will conduct a market analysis to highlight the significance of the polymer industry and its economic value. Finally, we will introduce the modelling of polymerization processes and explain how Aspen Polymers®, an extension of the Aspen Plus® software, works.

1.1. Polymers Overview

The term “polymer” was coined by J. Berzelius in 1833 to distinguish between two types of isomers. The polymer was used to describe two substances with identical relative compositional formulas but different absolute compositional formulas. A long time after, in 1922, H. Staudinger introduced the term “macromolecule” for the description of large covalently bonded organic chain molecules, comprising more than 10^3 atoms [4–7]. So, today, the polymers are defined as all synthetic and natural substances constituted by macromolecules made by multiple smaller molecules (monomers) [8]. Although the definition and discovery of polymers were only documented in the 19th and 20th centuries, they have always been around with natural polymers such as nucleic acid, polysaccharides, proteins, etc. However, the synthetic polymers in fact only start appearing at the last half of the nineteenth century and the first of the twentieth, which were marked by the accidental discoveries of many synthetic polymers by organic chemists during their investigations.

For example, in 1933, during an experiment performed at Imperial Chemical Industries (ICI), involving the reaction of benzaldehyde and ethylene at high pressure and temperature, a white waxy solid was obtained, which was not a product of the benzaldehyde-ethylene reaction, but an ethylene polymer, nowadays known as low-density polyethylene. This was the first polyolefin to be discovered and then commercialized, in 1939. The biggest breakthrough of LDPE and other polymers happened during World War II. The application of LDPE in insulating radio cables, Nylon for parachutes, ropes, body armor, etc., explain why in the United States plastics production increased over 300% during this time [9–12].

As it was said before, polymers are made of monomers. The monomer molecules can be of the same type, classifying the polymer as a homopolymer (like in polyethylene where there is only the ethylene as monomer), but polymers can also be constituted by two or more different monomers, being called a copolymer. An example is the ethylene butyl acrylate (EBA), which is constituted by ethylene and butyl acrylate monomers. In the copolymers category there are multiple arrangements of the repeating units over the chain, as it is represented in Figure 1. The alternating copolymer has two types of units which are arranged alternately along the chain. Statistical copolymers are the ones where the distribution of the segments along the chain obeys

statistical laws. The random copolymers are a special case of the statistical group with the distribution being truly random. The block copolymers are when the repeating units only exist in long sequences of the type [13].

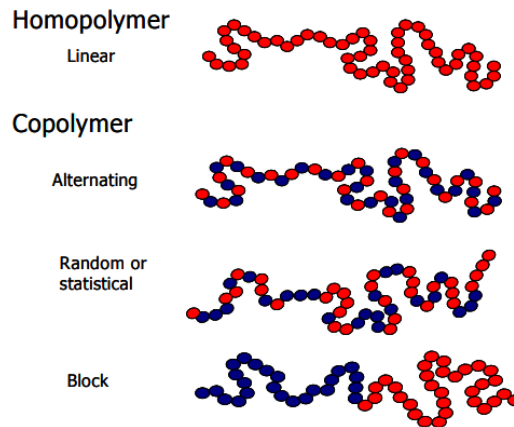


Figure 1. Representation of linear copolymers, statistical or random, alternate and block-copolymers [14].

One very significant group of polymers is the polyolefins. The polyolefins are polymers made from olefins (hydrocarbons with one double bond). They are mostly derived from natural gas or from lower weight constituents of petroleum, and their most prominent members are ethylene and propylene that originate the polyethylene and polypropylene, respectively. [15]

The polyethylene has three main types of resins that are classified according to the respective density range: Low-Density Polyethylene (LDPE), Linear Low-Density Polyethylene (LLDPE), and High-Density Polyethylene (HDPE). The HDPE, LLDPE are produced with coordination catalysts while the LDPE is made with free radical initiators. The LDPE has both long and short chain branches, while the polyethylene made by the coordination catalysts only have the short chain branches. The microstructure of the three main types and the density ranges are in Figure 2. [3]

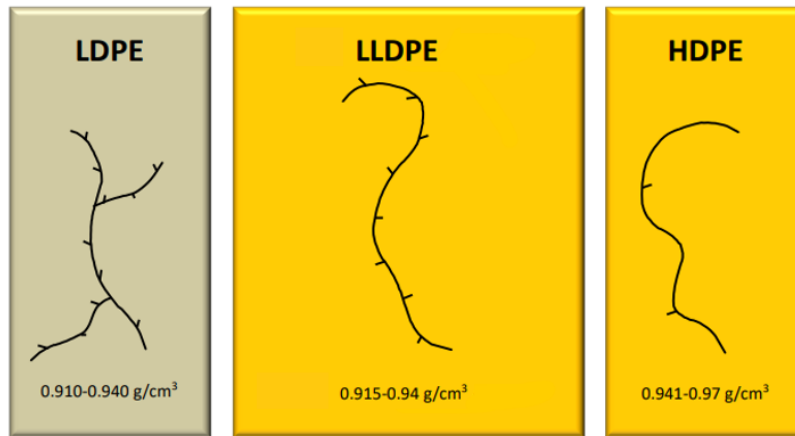


Figure 2. Classification of polyethylene types according to branching structure and density [3].

1.1.1. Polymers Properties

The polymers are characterized by not having a fixed molecular structure, instead they are constituted by many molecular species of different sizes. So, the molecular weight distribution is the most fundamental micro-structural distribution of any polymer due to its influence on polymer properties such as stiffness, hardness, strength, and viscoelasticity, which contribute for defining the polymer applications [16]. Nevertheless, in most cases, it is not necessary to know the full molecular weight distribution, just the first few averages. Two average molecular weights and corresponding average chain lengths are typically defined [17] where M_i is the molecular weight of chain length i , and N_i is the number of polymer molecules of chain size i .

$$Total\ weight = \sum_{i=1}^{\infty} N_i M_i \quad (1)$$

$$Total\ number\ of\ molecules = \sum_{i=1}^{\infty} N_i \quad (2)$$

$$M_n = \frac{\sum_{i=1}^{\infty} N_i M_i}{\sum_{i=1}^{\infty} N_i} \quad (3)$$

$$M_w = \frac{\sum_{i=1}^{\infty} N_i (M_i)^2}{\sum_{i=1}^{\infty} N_i M_i} \quad (4)$$

Another important property of the polymers is the branching, related to the final product density. The density is determined by crystallinity of the polymer. So, the polymer when it is conceived it is melted and does not show any organization, being an agglomerate of long polymeric chains

randomly distributed. When the polymers transition to the solid phase, a crystallization process occurs, where the chains start packing in high density lamellas. The crystallization is a slow process due to the necessary time to fold the polymeric chain into the lamellae, and that is why the polymers are semi-crystalline, comprising crystalline domains separated by amorphous regions. Therefore, polymers with a higher crystallinity have a higher density. One of the key factors that determine the crystallinity is the number of short-chain branches (SCBs). These SCBs act like defects, that do not allow the chains to pack properly, ejecting the chain in the amorphous region [18].

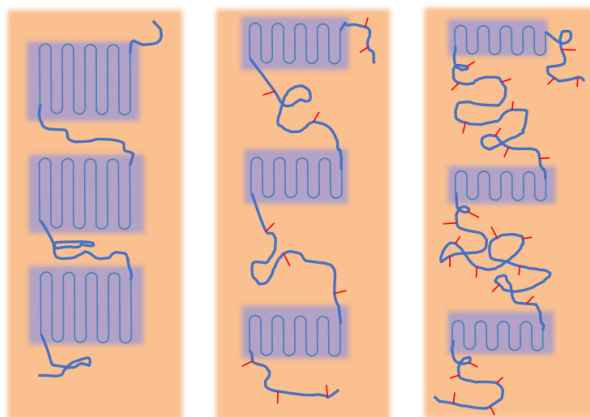


Figure 3. Representation of how the short-chain branches (SCB) impact the lamellae formation [1].

1.1.2. LDPE Reactor Technologies

Since the 1930s, LDPE is commercially produced by essentially two continuous high-pressure technologies. One uses an autoclave reactor and the other, a tubular reactor. Both reactors operate at high pressures (around 1000 to 3000 bar) and high temperatures (about 150°C to 330 °C).

The first commercial process to produce LDPE (and in fact every polyethylene in general) was the autoclave reactor process developed by ICI, which started production in 1939 [9]. These reactors are usually long vertical vessels with a length-to-diameter ratio as high as 20, and volumes chosen to give residence times between 30 and 60 s [19]. They may be divided in two or more reaction zones in series, that are separated by baffles incorporated in the body of the agitator. The reaction condition in each zone (temperature, concentration of initiator, etc.) can be adjusted independently to produce a broad range of molecular weights. The initiators used are exclusively organic peroxides. The injection of the initiators in each zone, controls the zone temperature. These reactors tend to be smaller than the tubular, and thus have a lower production rate. The operation is essentially adiabatic, with the heat being only removed by the fresh ethylene entering the reactor and the discharge of molten polymer and unreacted gas. Therefore,

conversion per pass in the autoclave, which is around 15-20%, is limited to the allowed temperature rise (one practical rule is $\%conversion=0.075 \times \Delta T$, where $\Delta T(^{\circ}C)$ is the difference between the inlet and the outlet temperature of the reactional mixture) [10,19,20]. Despite their lower capacity, autoclave reactors have been maintained due to their ability to produce other copolymers such as Ethylene Vinyl Acrylate (EVA) or Ethylene Butyl Acrylate (EBA), for example [1].

The second technology is the tubular reactor, which consists of a spiral wound jacketed metal tube. The length-to-diameter ratio of these reactors is very large, with lengths in the range of 500-1500 m and internal diameters that typically do not surpass 60 mm. The thickness of the tube is obviously very large due to the pressure that it needs to sustain. The fluid flowing through the reactor shell partially removes the heat of the reaction. In the tubular reactor, various types of zones can be distinguished, based on the initiator status and heat demands, such as preheating, and multiple reaction and cooling zones [1,21].

The major advantages of the tubular reactor, when compared to the autoclave, include higher conversion of ethylene (about 20-35%) and less frequent reaction decomposition events. This is due to the better temperature control, making it possible to identify sudden jumps in temperature early, giving the operators time to actuate and reduce the reaction rate [22].

Even with similar operating conditions, the flow pattern is different. Therefore, the residence time distributions are quite different, and so, the polymer produced by each technology is not the same. Figure 4 shows the difference between the product produced by the two reactors. Essentially, the residence time distribution of the tubular reactor will be narrower due to its lower degree of back-mixing, resulting in an also narrower MWD. From a microstructure standpoint, the polymer will have fewer long branches [1,10,23].

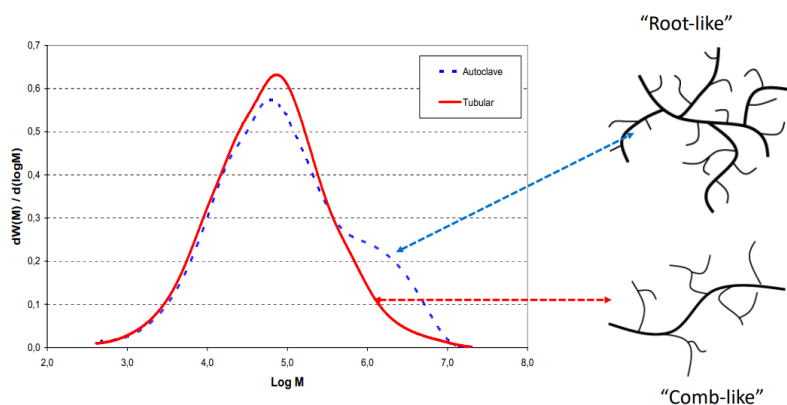


Figure 4. Difference in the MWD obtained in an autoclave and a tubular reactor LDPE [1,23].

1.2. Polymers Market Analysis

Most consider synthetic polymers the material of the 20th century. Over the last 80 years, they have been playing a huge role in the quotidian of many people, due to their different applications. Their versatility allowed them to compete in new markets, replacing a variety of materials. Nowadays, plastics are everywhere: in bike helmets, toothbrushes, bottles, bags, cars, clothes, etc. [24]. Quoting author Susan Freinkel, “In product after product, market after market, plastics challenged traditional materials and won, taking the place of steel in cars, paper and glass in packaging, and wood in furniture.” [25].

However, over the years, the way plastics are looked upon by society have been shifted from an unambiguous positive product, towards a product associated with environmental problems. This shift occurred mainly during the 1970s and 1980s, where plastics reputation declined, mainly due to the growing concerns about waste from many disposable plastic products. This problem is reinforced by the fact that once discarded, plastic remains in the environment indefinitely. The first response to this problem came from the plastics industry, which proposed recycling as a solution. Throughout the 1980s, the sector led a forceful campaign to encourage local authorities to incorporate the collection and processing of recyclable materials into their waste management systems. However, despite their efforts, recycling did not prove itself as flawless solution, as most plastic wastes still end up in landfills or polluting the environment [11].

Despite the lately growing suspicion, plastics are crucial to modern life. Plastics lightweight and good insulation saved, over the years, a lot of fossil fuels in transportation and heating. And now with the electrification of many sectors, they are projected to have even a bigger role [2,11].

Figure 5 demonstrates the evolution of polymers production between 1950 and 2021. The production, besides the pandemic year, when it stagnated, has been increasing steadily. The latest report of PLASTICS EUROPE [2], indicated a production of 390.7 Mt in 2021, which represented a recovery from the stagnation caused due to the COVID-19 pandemic. It also presented forecasts until 2050, with an expected 50% rise in the production, to 589 Mt [2,26].

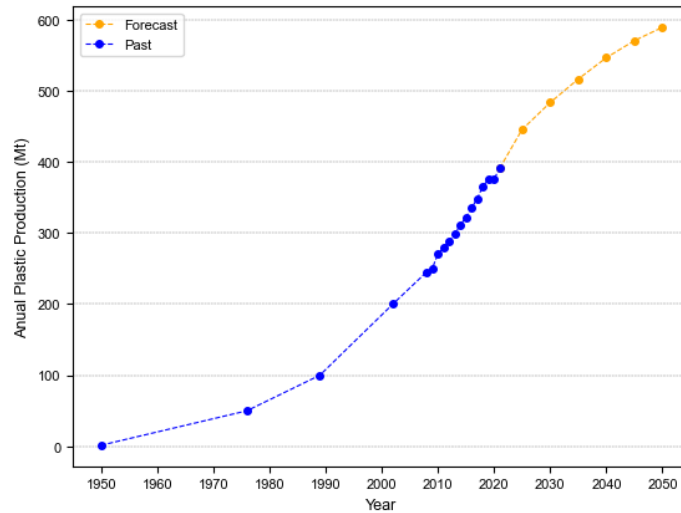


Figure 5. Annual production of plastics worldwide from 1950 to 2021 and forecast until 2050 [26,27].

This production has its major share located in Asia (nearly 52%) with a big contribution from China, that produces 32% of the plastics in the world. Europe’s share has been declining over the last years (it decreased from 19% in 2020 to 15% in 2021). A trend that is expected to be intensified by energy and logistics crises resulting from the war in Ukraine [2].

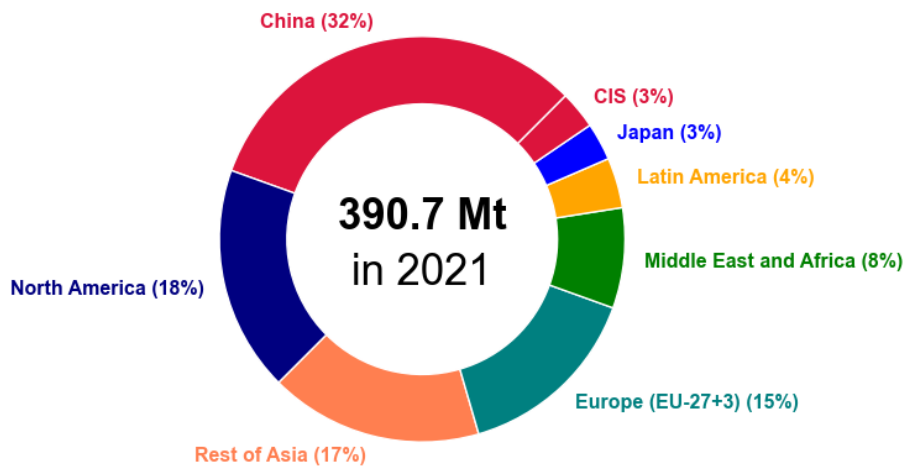


Figure 6. Distribution of global plastic materials production in 2021, by region [2].

In Figure 7, the most common plastics application continues to be packaging, although there are other significant areas like building and construction, agriculture, electrical and electronics, automotive, etc. All these applications justify the predicted growth of the plastics industry. In fact, the automotive industry is expected to increase its plastics consumption since, authorities have implemented strict regulations with the target of reducing automotive emissions. This motivates manufacturers to adopt lightweight plastic materials in several applications. As the

automotive industry grows by more than 4% annually, the plastics demand is expected to increase [2,28].

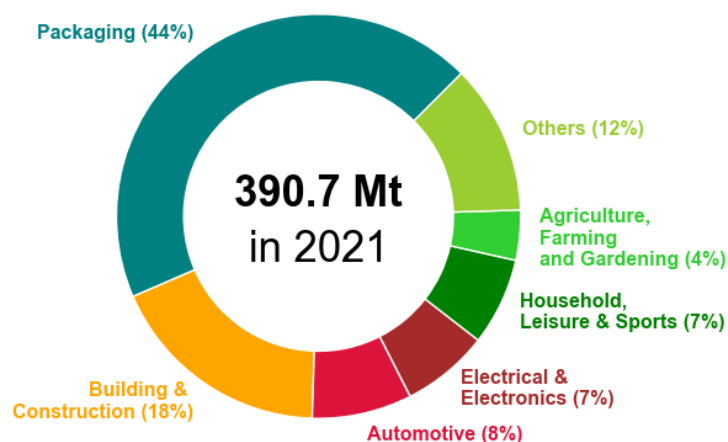


Figure 7. Distribution of plastics consumption by application [2].

The urge to transform the plastic industry into a more sustainable one, has been growing over the last few years. In Europe, companies have been making huge efforts to meet the PLASTICS EUROPE 2050 net zero and circularity targets. Consequently, the production of recycled plastics and bio-based/ bio-attributed plastics increased over the last years. In Europe, these represented 5.5 Mt of the total production in 2021, an increase of 20% face to 2020 [2,29].

Figure 8 shows that despite the efforts for using more recycled and sustainable plastics, the current market continues to be dominated by the fossil-fuel based polymers, which account for 90.2% of the 2021 polymers production. In the fossil-fuel based polymers, a lot of credit should be given to the polyolefins that represent 51% of the fossil-fuel based polymers. Although it has a lower share, LDPE still represents about 18% of the polyethylene market, which is about 20 Mt. The utilization of LDPE in various sectors, including agriculture, edible and frozen foods, packaging, electrical cables, and others for sheets, films, and coatings is anticipated to drive the market growth in the near future [1,28,30,31]. Like other types of polymers, LDPE is commonly employed in diverse areas of the automotive industry, which range from electrical components to upholstery and liquid reservoirs. So, the LDPE, as it was said before, will also benefit from the demand for lightweight plastic materials in several applications of the automotive sector [26,28,32,33].

Another indicator of the high demand for LDPE is the plant's ability to sell every product generated in the process. Even off-spec production, while yielding lower profit margins compared to Prime First Pass and Prime Final Pass products, is still sold. Remarkably, even the side-product wax (oligomers), finds buyers in the market [1,28,30,31].

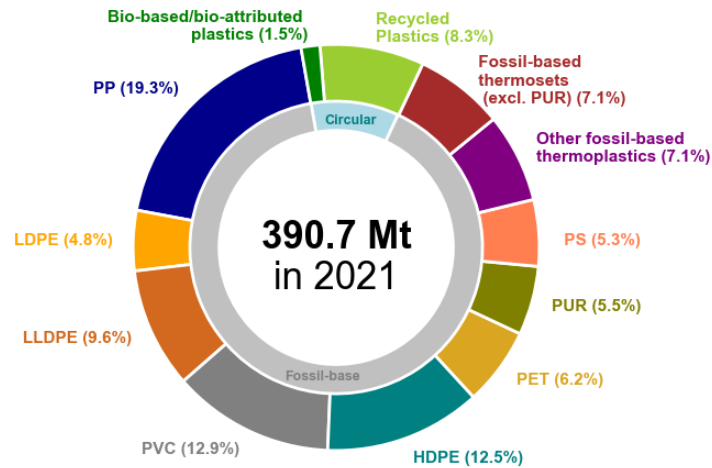


Figure 8. Distribution of the global plastics production by type in 2021 [2].

1.3. Polymers Simulation

Over the years, there has always been an interest in modeling polymerization processes. The LDPE processes were not an exception, with several mathematical models being developed, and published. These models had four focuses:

1. Physical state of the reaction mixture (one-phase versus two-phase system);
2. Kinetic mechanism and estimation of associated parameters;
3. Reactor flow conditions and mixing effects;
4. Variation of the physical properties of the reaction mixture.

The steady-state computer model comprises nonlinear differential equations, for the tubular reactor, or algebraic equations, for the autoclave reactor, which describe the conservation of the various molecular species, mass, energy, and momentum balances within the reactor. Additionally, a set of algebraic equations accompanies the model equations, accounting for variation of kinetics, physical and transport parameters, according to the reactor conditions. A detailed model should be able to relate monomer and initiator consumption, reaction temperatures, radical moments, polymer size distributions, the degree of long and short chain branching and the number of unsaturated double bonds in the polymer chains, to operating conditions such as initiator concentration, temperature, pressure, chain transfer agent concentration, heat transfer coefficient and other process design and operating variables [34].

Models built so far, have been mainly developed in MATLAB and SIMULINK or FORTRAN. As most of the models were developed during the last half of the 20th century and the

early years of the 21st, the computational power was not the same as is today, and so simulations that took days to run, today take only a few minutes or seconds. Polymerization simulations are known for the being computationally intensive, which explains why the models available on the literature are mainly built just for the reactor, not considering further stages. Also in these models, the thermodynamics were very simplified to reduce the complexity of the calculations.

Another negative aspect of these types of models is the limitation regarding its durability at the actual plant sites. This is due to the complexity involved on these types of models, with very extensive code and with the parameters for tuning of the model typically deep embedded in the code. Hence, these models tend to be used only while the person who developed them stays in the company/project/plant [35].

This work is done in collaboration with the industry, and the long-term life of the model needs to be considered. Thus, a user-friendlier package software was preferred. The software employed was the Aspen Plus[®] with the Aspen Polymers[®] extension, developed by Aspen Technology Inc. This was preferred over other simulation packages such as gPROMS[®] or Predici[®] since there was already a familiarity with the Aspen[®] Plus in the company (including software licenses).

1.3.1. Aspen Polymers[®]

The Aspen Polymers[®] is an extension of the Aspen Plus[®] software, dedicated to the simulation of polymers. As all the models developed with Aspen Plus, we begin with the components' definition. Contrarily to what happens in the Aspen Plus[®] V11 simulation where there are only present conventional compounds, when there are polymers involved, Aspen Polymers[®] expands Aspen Plus[®] by encompassing further types of elements. More specifically, there are three new types:

Segment: A segment does not represent a true compound, and so does not appear in the stream results sheet. The segments are used to define the polymers and oligomers structures. They can be the repeating unit, a termination group, or a branch point. The segments are also used to compute the polymers/oligomers properties.

Oligomer: An oligomer is a specific molecule made of two or more segments. They are used to represent low molecular weight polymers, that appear in the process, usually as a by-product since they are chains that did not grow enough. The oligomers have a different treatment compared to the polymers because they got a well-defined structure that doesn't change throughout the simulation, i.e., the type and number of segments that constitute the oligomer are specified when the compound is defined. Besides that, the oligomers can be volatile, in fact, they usually have high volatilities, in contrast to the polymers which are non-volatile.

Polymer: A polymer is not a specific molecule but a distribution long polymeric chain, constituted by many segments. Their characterization is the most particular of the three types since the polymer is not a well-defined molecule, but a distribution of molecules with different chain sizes. In Aspen Plus® V11, polymers are characterized by two different independent systems. The first system is the polymer component attributes, which is based on the method of moments, and is always necessary. Attributes are used in many property models. This system is used to track average properties such as moments, chain size, molecular weight, chain composition, branching frequency, etc. The attributes needed depend on the type of polymerization reaction, and in Aspen Plus® V11, there are many built-in attribute groups like Ziegler-Natta, Free-radical, Cationic, Anionic, etc. Additional attributes may be required to predict specific properties and may be added as necessary. The other system is the polymer molecular weight distribution. This system is optional, and it is based on the method of instantaneous properties where it is assumed the Flory's most probable distribution is formed at each instant. This allows to obtain the molecular weight distribution curve that can be compared to the experimental distribution that is obtained by Gel Permeation Chromatography (GPC). To use this system, we need to tick the box to perform the GPC distribution calculation, define the number of points and the upper limit of the distribution [36,37].

After the definition of the compounds, we need to select a thermodynamic model, before entering the simulation environment. Aspen Plus® has some dedicated thermodynamic models for addressing the polymers properties. These methods include the Equation of State (EOS) of Sanchez-Lacombe, PC-SAFT, SAFT, etc.

In the simulation environment, the definition of the polymerization reaction is done in the reactions folder, where we select the type of reaction (free-radical in the present case, but it could be Ziegler-Natta, Ionic, Emulsion, etc.) The intervenient species are then defined (polymer, monomers, monomer-segments, initiators, transfer agents, solvent, etc.). Aspen Plus uses this information to generate the reactions, although the user can add or remove reactions.

1.3.1.1. Polymer Component Attributes

It is convenient to examine the molecular properties of polymers in terms of averages rather than considering the full distribution. The average properties from actual distributions can be determined through distribution moments or instantaneous properties.

The polymer average properties that constitute the components attributes include the segment fraction, segment flow, number and weight average degree of polymerization/molecular weight, the Z-average degree of polymerization/molecular weight, the zeroth through third moment of chain distributions, number and frequency of long and short chain branches, and others. Component attributes are available to track most of these properties for dead polymer and

live polymer. Existing two sets of polymers attributes: the Composite Polymer Set and the Composite Live Polymer Set. The first contains the basic attributes required for any type of polymerization. The second has the necessary attributes to track the characteristics of live polymer chains in chain growth polymerization. (Note: There are 4 extra sets but are not relevant for the free-radical polymerization, for more information consult [38]). These properties are calculated resorting to the method of moments within kinetic models [36–38].

The distribution of a given property s , may be described by a frequency function f_s , if the property is a discrete variable, or by a density function $f(s)$, if it is a continuous variable. Hence, the f_s and $f(s)$ represent the fraction of the population whose property is exactly s or stands between s and $s+\Delta s$.

The frequency and the density functions are respectively:

$$F_s = \sum_{s_0}^s f_s \quad (5)$$

$$F(s) = \int_{s_0}^s f(s) ds \quad (6)$$

In Aspen Plus®, the distribution moments are defined from the origin of the average property, i.e., the point where the property is equal to zero. Thus, the general form of the relationship between the distribution moment and the distribution function is the next one.

$$\mu_k = \begin{cases} \sum_{all\ s} s^k f_s, & \text{for frequency function} \\ \int_{all\ s} s^k f(s) ds, & \text{for density function} \end{cases} \quad (7)$$

Where μ is the moment, k the moment order, s the property value (chain length, molecular weight, particle size, etc.).

For the chain length distribution, the moments frequency distribution is given by.

$$\lambda_m = \sum n^m Q_n \quad (8)$$

Where λ is the moment, m the moment order, n is the chain length or the degree of polymerization, and Q_n is the number of moles of polymer of length n .

Then the average properties are then computed as:

$$DP_n = \frac{\lambda_1}{\lambda_0} \quad (9)$$

$$DP_w = \frac{\lambda_2}{\lambda_1} \quad (10)$$

$$DP_z = \frac{\lambda_3}{\lambda_2} \quad (11)$$

The respective molecular weights are calculated multiplying the average degrees of polymerization by the average segment molecular weight ($\overline{M_{seg}}$).

$$M_i = DP_i \times \overline{M_{seg}} \quad , \quad i = n, w, z \quad (12)$$

The polydispersity index (PDI) can also be computed as a function of the moments.

$$PDI = \frac{M_w}{M_n} = \frac{\lambda_2 \lambda_0}{\lambda_1^2} \quad (13)$$

1.3.1.2. Polymer Molecular Weight Distributions

Previously, it was mentioned that the Polymer Molecular Weight Distributions system is not mandatory. Nevertheless, there is a great demand to know the full molecular weight distribution (MWD), which is crucial to optimize the rheological and mechanical properties of the final product. Aspen Plus[®] employs the instantaneous properties method to calculate the distributions. This method is preferred over the moments method for computing the distribution, since the moments method would require a larger number of moments to be computed. Also, knowing the leading moments of a distribution does not provide sufficient information to unambiguously construct a complex distribution. A better approach proposed by Hamielec et al. for constructing the MWD is to store reaction rate data throughout kinetic calculations and then utilize them to build the full distribution of polymer accumulated in the reaction system [38,39].

The instantaneous method, although not valid for all the cases, assumes that polymer molecules grow and deactivate quickly as the growing center deactivates, terminates, or moves to another monomer, solvent, or chain transfer agent molecule. The method also considers that once the polymer chain is dead, it does not suffer further modifications. These assumptions make this method only suitable for addition polymerization. Furthermore, the assumption that the polymer molecules are conserved after their formation can be invalid in the presence of certain side reactions like thermal scission, which destroys polymer molecules, and the chain transfer to polymer that reactivates the dead chains. This would lead to very different values of the PDI computed by the moments and the distribution method. (See the example in Figure 115 at the Appendix)

The previous curve is the cumulative MWD, which is calculated by adding up the MWD formed at each instant. The cumulative weight fraction of polymer of chain length with a length equal to n is calculated with the following expression.

$$W(n) = \frac{\sum_z m_p(z)W(z, n)}{\sum_z m_p(z)} \quad (14)$$

Where $m_p(z)$ is the mass of polymer produced at instant z , which in the context of a flowsheet refers to the contribution by each reactor in series. $W(z, n)$ is the instantaneous weight fraction of polymer with a size equal to n produced at instant z . This instantaneous weight fraction is computed with the following expression.

$$W(z, n) = (\tau + \beta) \left(\tau + \frac{\beta}{2} (\tau + \beta) (n - 1) \right) n e^{-(\tau + \beta) n} \quad (15)$$

Where τ is defined as the ratio between the termination reaction rates plus the transfers reaction rates and the propagation reaction rate. β is defined as the ratio of the termination by combination reaction rate and the propagation.

$$\tau = \frac{R_{tm} + R_{ts} + \dots + R_{td}}{R_p} = \frac{\text{transfer} + \text{termination}}{\text{propagation}} \quad (16)$$

$$\beta = \frac{R_{tc}}{R_p} = \frac{\text{termination by combination}}{\text{propagation}} \quad (17)$$

2. Motivation

The current trend in the chemical engineering process industry is towards models that can describe accurately the plants. After the validation of the models, these can be used to optimize the design and/or operation and provide a better understanding of the process.

The polymer plants produce different products, a mix between commodity products that are produced in large amounts and lower quantities of more specific products. There are frequent grades transition, which require these plants to be extremely versatile. The appropriate model of the process will provide an important design and predictive tool, providing insights into the free radical polymerization of ethylene process, which may lead to a better quality and quantity control of the product. It is also expected that the model could help to design operational changes to produce new grades tailored to meet specific requirements of the clients and/or optimize the current conditions used to manufacture different grades, with minimum plant disturbance, contrarily to what happens with a trial-and-error approach.

Therefore, the main goal of this work is to establish a simulation model in Aspen Plus® V11 that describes the operation at Sines' plant. The plant can be divided into three main sections: compression, reaction, and separation. The first is the reaction, where the target is to optimize the kinetic parameters involved in the free radical polymerization of ethylene, to accurately predict the quality and quantity for the different LDPE grades produced. At the separation phase, there are three gas-liquid separators that operate at different pressures, so we will pursue a thermodynamic model and its respective parameters that could replicate the separations processes. Finally, in the compression stage, the goal is predicting the energy consumption and close the recycling streams to have the full plant simulated.

In the literature, a few studies exist describing the hydrodynamics of the reactors and the kinetics of the polymerization [21,34,35,40–46]. Yet, there is a lack of consistency between the reported values, due to the different assumptions and methodologies followed by each author. Some of these studies were performed in a real plant [21,34,35,40,44], although, the type of reactor is different to the one implemented at Repsol. Specifically, previous studies focused on tubular reactors, or autoclaves with only one or two gas feed streams, whereas at Sines, the autoclave reactor has five inlet gas streams.

Only two models were found for the free radical polymerization of ethylene built in Aspen Plus® and Aspen Polymers®. The first was built by Bokis et al. [21] and focused on a tubular reactor, different from the one considered in this thesis. The model developed by Alleyne [35], considered a full plant model with a single inlet stream autoclave reactor producing EVA, whereas the reactor in this study has five inlet streams and produces LDPE. Alleyne [35] optimized grade transitions, thus neglecting the MWD, and placed the focus on the melt index that was computed

with an end-user correlation. Both works regressed the model parameters using real-life industrial plant data, the first from Equistar Chemicals and the second from AT Plastics.

3. Repsol Polímeros

Repsol Polímeros is one of the biggest chemical companies in Portugal and one of the top 10 exporters. Located in Sines (Portugal), Repsol Polímeros petrochemical complex englobes 5 main different units:

- 1) Steam-Cracker unit, with a production capacity of 410 kt/year of ethylene and 220 kt/year of propylene;
- 2) Butadiene unit with a production capacity of 52 kt/year;
- 3) MTBE/ETBE (Methyl tert-Butyl Ether / Ethyl tert-Butyl Ether) unit with a total capacity of 53 kt/year of MTBE/ETBE;
- 4) LDPE/EBA unit with 140 kt/year of production capacity;
- 5) HDPE unit capable to produce 150 kt/year;

In 2025, they will accommodate two more units, which will produce LLDPE and Polypropylene (PP) each with a capacity of 300 kt/year [47,48].

In 2019, Repsol Polímeros became the first company in its sector to announce the goal of achieving zero net CO₂ emissions by 2050, demonstrating the company's commitment to global sustainability and the energy transition [48]. In 2023, Repsol Polímeros updated their sustainability plan, describing various actions taken within the petrochemical complex to support 10 of the 17 Sustainable Development Goals of the 2030 United Nations Agenda [49].



Figure 9. Sustainable Development Goals approached on the Repsol Polímeros Sustainability Plan [49].

3.1. Process Description

This work was performed in *Repsol Polimeros*, at Sines, where the production process is high-pressure low-density polyethylene autoclave process licensed by CdF Chemie. The plant possesses two identical independent production lines for LDPE, each with a capacity of 70 kt/year. One is a dedicated line, while the other is also used to produce grades of ethylene butyl-acrylate (EBA). The simplified flowsheet is observed in Figure 10.

The plant receives ethylene from the Steam-Cracker unit or the terminal port. The gas is fed to the feed drum. The ethylene goes through a filter from the drum before being fed to the primary compressor. The primary compressor (CP) is a piston-operated reciprocating compressor constituted by three compression stages with inter-stage cooling. The discharge pressure of this compressor is about 280 barg. The outlet gas of the primary compressor is then mixed with a recycling stream. A n-butane or propylene termination agent is added for certain grades, with the EBA grades also requiring the injection of the butyl acrylate comonomer.

The mixture (stream 3) proceeds to the secondary compressor. As it happens in the primary compressor, before being sucked in, the gas passes through a filter. The secondary compressor (CS) is a plunger-operated hyper compressor with two stages and inter-stage cooling. The discharge pressure of this second compressor is around 2100 barg. After the secondary compressor, the outlet gas is split into five different streams. The temperature of each stream is adjusted according to the reactor zone where it is going to enter.

The reactor features an agitator with four plates integrated into its body, dividing it into five different zones. The five streams are fed to the reactor in the following way: One stream enters the reactor through the agitator's motor, to cool it. The other four streams (stream 5, 6, 7, and 8) are fed to zones 1,2,3 and 4. In zone 5, only initiator or solvent is injected. The reactor operates at pressures between 1200 and 2000 barg. The temperatures of each zone are independent, with the top zone operating between 170 and 230 °C, and the bottom between 280 to 305 °C. Each zone's temperature is controlled by the corresponding initiator's injection rate. Due to exothermicity of the polymerization reaction and to the fact that ethylene explosively decomposes itself above 350 °C, the reaction must be carefully maintained under control. In the body of the reactor there is a jacket, where a thermal fluid flows. During start-up, it heats the reactor to a temperature that allows the reaction to occur. When the operation is stabilized, the flow of the thermal fluid is reduced to just compensate the heat losses to the environment. The ethylene conversion in the reactor is only around 15-20%. On the outlet of the reactor, an extrusion valve reduces the pressure to around 300 barg. The polymer and non-converted ethylene exit the reactor at high temperature, which is additionally increased due to the isenthalpic expansion at the control valve, which in this range of pressures leads to an increment of about 5-10 °C due to the negative sign of the Joule-Thompson coefficient. Even so, to maintain the polymer as a fluid, the line connecting the reactor to the separator is covered by a jacket with thermal fluid.

The liquid-vapor separator operates at about 300 barg and removes most of the non-converted ethylene. The gas stream is then sent to a series of coolers and cyclones, to remove the low molecular weight polymer that was dragged with the ethylene. This purification circuit of the gas is called medium pressure return (RMP). After this circuit, the ethylene is mixed with the outlet gas from the primary compressor into the secondary compressor. This circuit allows to recover around 30-40 t/h of ethylene. While the ethylene follows for the RMP circuit, the molten polymer is sent to a high-pressure flash.

The high-pressure flash operates at around 15 barg. This step allows to remove part of the ethylene still present after the separator. The gas removed in this stage (stream 15) is mostly sent to the feed drum, while a small fraction is purged to avoid the accumulation of inert compounds. After the high-pressure flash, the polymer (stream 16) goes to the low-pressure flash, which operates at about 0.5 barg. In this third step of purification, the ethylene that was not recovered in the previous units is removed. The gas (stream 17) is forwarded to the residual storage drum and then sent back to the Steam-Cracker unit through the residual compressor.

The polymer leaving the low-pressure flash to the extruder, has only a residual quantity of ethylene. The main function of the extruder is to homogenize the product and allow its granulation. In the outlet of the extruder, a granulator is placed, which has a cut chamber with flowing water that cools and solidifies the polymer, allowing it to be cut. The pellets are then transported out of the chamber, and dried. After removing the dust, the pellets are sent to the silage zone, for quality control, homogenization, storage, and packing of the product.

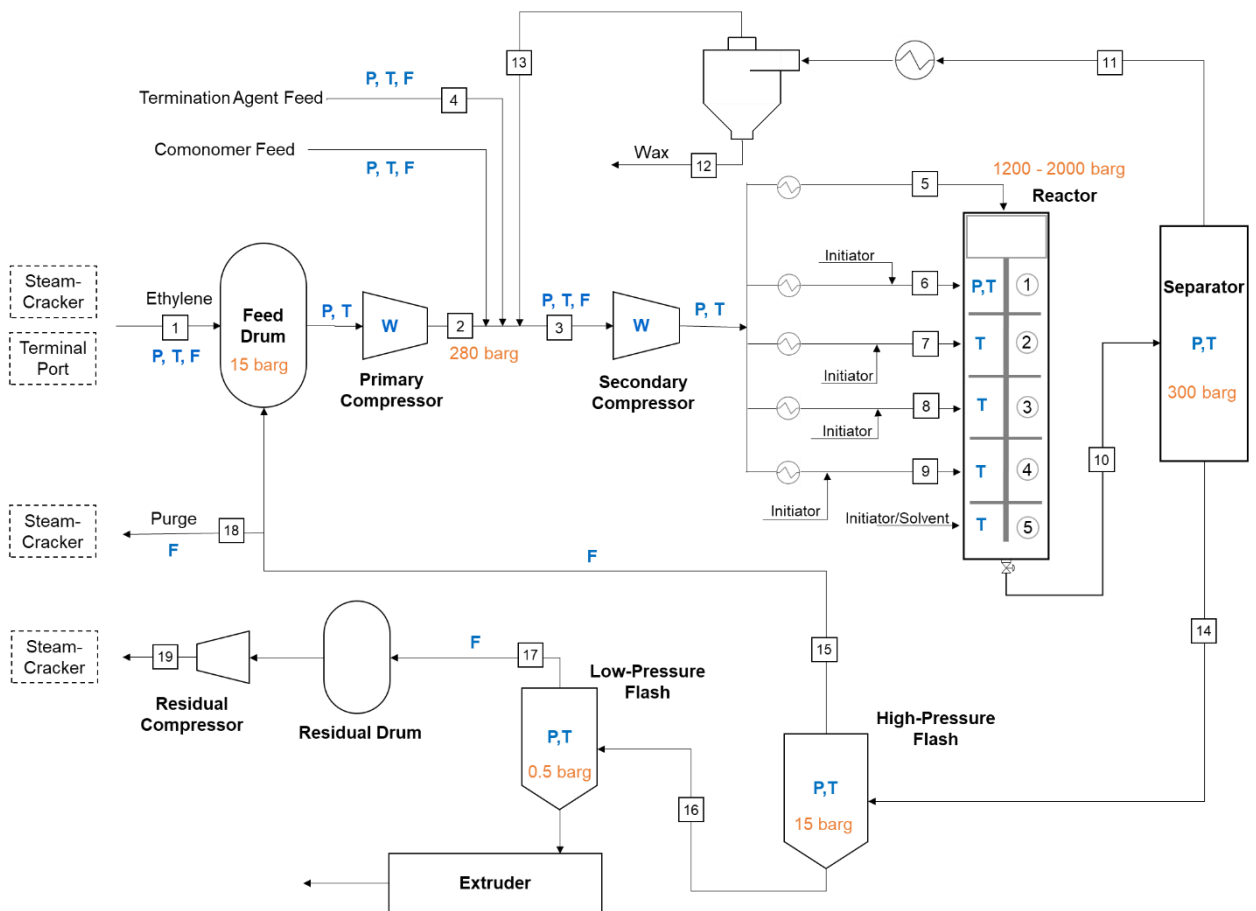


Figure 10. Simplified flowsheet of the process. Some of the main measurements in the plant are shown in blue: T – Temperature (°C); P – Pressure (barg); F – Mass Flow (kg/h); W – Power (kW).

3.2. Protocol Recipes for Polymer Grade Production

The plant produces 40 different grades of LDPE/EBA. Each specific grade has its own protocol recipe that indicates to the operators, the start-up and steady state conditions required to produce that grade. These conditions are essentially the type of initiators, termination agent and its flow rate (when a termination agent is needed), pressure, reactor zones temperatures, etc.

In this work, we considered 31 batches covering 8 different grades. The main information required from the process to introduce as inputs in the Aspen Plus® V11 reactor model was the temperature of each zone, pressure, termination agent flow rate, and the type of initiator. The reactor zones temperatures are presented in Figure 11, while the rest of the information can be found in Table 1. In the model, the values used were the actual values measured at plant (see appendix C), which are slightly different to those found in the protocols.

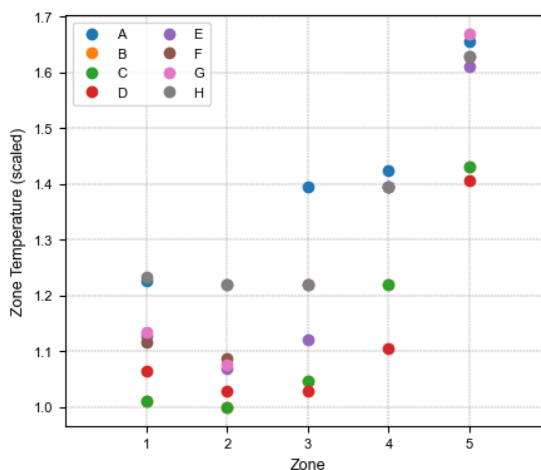


Figure 11. Reactor zones temperature in each grade protocol.

Table 1. Pressure, termination agent and type of initiator used in each zone for each grade protocol (the number in front of the initiator type in the initiators columns represents its concentration in the mixture injected).

Grade	Pressure (barg)	Butane (kg/h)	Propylene (kg/h)	Initiator 1	Initiator 2	Initiator 3	Initiator 4	Initiator 5
A	1440	67	0	25Y	25Y	4W+7.8Y	4W+7.8Y	3X+5Y
B	1950	70	0	15V	15V	15Z	15Y	4W+7.8Y
C	1950	80	0	15V	15V	15Z	15Y	4W+7.8Y
D	1950	120	0	15V	15V	15V	15Z	4W+7.8Y
E	1250	0	0	25Z	25Z	25Z	4W+7.8Y	3X+5Y
F	1320	0	0	25Z	25Z	25Y	4W+7.8Y	4X+6.7Y
G	1290	0	0	25Z	25Z	25Y	4W+7.8Y	3X+5Y
H	1950	0	185	25Y	25Y	4W+7.8Y	4W+7.8Y	3X+5Y

4. Free Radical Polymerization Reaction

The free-radical polymerization of ethylene occurs in the presence of very high pressures. The initiator, usually an organic peroxide, supplies free radicals to the reaction. These radicals react with the monomer originating a polymeric chain with only one monomer. From there on, the other monomer molecules are quickly added forming a long chain. Typically, due to the high pressures and temperatures, these processes have very short reaction times. The reactor residence time is in the order of 20 to 90 seconds [10].

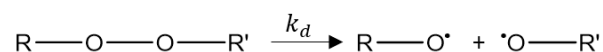
In free radical polymerization many reaction mechanisms exist that give the polymer its structure and, consequentially, its properties. The basic mechanisms that are common to almost every polymerization process are the chain initiation, propagation, and termination. Then there are other secondary reaction mechanisms that may or may not occur depending on the process conditions.

4.1. Chain Initiation

As with other chain growth mechanisms, free radical polymerization involves the sequential addition of a monomer to an active site. The difference between the free radical and the site-based mechanism is the type of active site, which in this case are radicals. [24]

In the first commercial processes, oxygen was used to produce free radicals because of the facility to be fed into the reactor. The development of high-pressure pumps and of new initiators made it possible to switch to liquid initiators, which allow for a better control of the reactor's temperature. The half-life of these initiators to meet the range of desired temperatures oscillates between 0.02 and 1 second. The initiators are compounds thermodynamically unstable, such as organic peroxides and azo compounds which can be decomposed by thermal or photocatalytic cleavage of the covalent bonds.

The most common way to generate radicals is through thermal decomposition of some compounds, such as peroxides, azo or disulfide compounds. The most used compounds in the production of LDPE are organic peroxides. These compounds generate free radicals due to the thermal cleavage of the oxygen-oxygen bonds, as it represented next [50]. The rate of the peroxide decomposition depends on its structure, that is, on the R and R' groups [10,24].

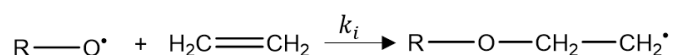


In the ICI process, the radicals generated in a LDPE production plant are obtained by thermal degradation of organic peroxides. The decomposition of the initiators has typically a high activation energy (around 30-40 kcal/mol), making the initiation process very dependent of the

temperature [50,51]. So, a peroxide has a narrow temperature range in which it can generate radicals at velocity that can be useful for the polymerization process. Outside this range, the decomposition could be very slow, and the peroxide might leave the reactor without decomposing, not generating radicals. Or in the other hand, the decomposition could be too fast, with the reaction taking all the available space. In this last case, the radicals are lost due to premature interaction between them or with the polymer chains. Both situations lead to a loss of efficiency in the initiation process. For this reason, to cover all the temperature ranges in which the process operates, a variety of initiators are used, depending on their temperature sensitivity. These initiators are independently injected into the different reactor zones, and its flow rates are manipulated to control the temperatures in each zone [51].

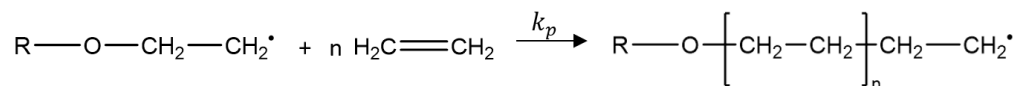
Nevertheless, even if the initiators are employed at the right temperature range, not all undergo radical formation capable of attacking the monomer. Moreover, a portion of the radicals are lost due to the “cage effect”. The radical pair is confined for a certain time in a “solvent cage”. Here the term “solvent” goes beyond its traditional definition, referring to the general environment, which includes polymer, inert substances, monomer, and so on [50]. Therefore, an initiator efficiency factor, f , is defined. This parameter can be expressed as the ratio between the initiating radicals and the total number of radicals that are formed and has values between 0.2 and 0.8.

After the formation of the radicals, the monomer molecule reacts with it to form a polymer radical with a chain length equal to one.



4.2. Propagation

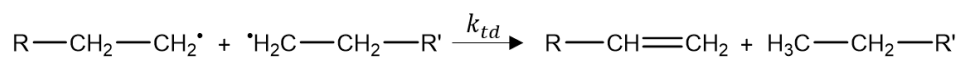
With the chain initiated, other monomer molecules are added, growing the chain. The radical position will keep moving away from the initial point to the last added monomer.



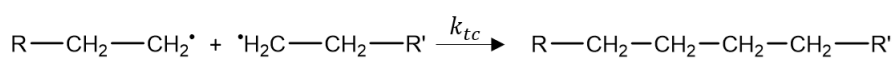
The growth of the chain continues until it is terminated by one of the possible mechanisms. The high pressures used in the production process favor the propagation reaction in detriment of the termination. Consequently, by operating at higher pressures, polymers with higher molecular weight are obtained. The average chain length is in the order of thousands ethylene segments.

4.3. Termination

In equilibrium conditions of the reaction, the rate of generation of free radicals is balanced by the rate of the reaction eliminating them from the system. The termination of the chain can be done via two different mechanisms: Termination by disproportion and termination by combination. The first one is when two living polymers react with each other to create two dead polymer chains.



In termination by combination, the two living polymers react with each other to originate one dead polymer chain.



4.4. Chain Transfer

The overall process of polymerization is much more complex than what is indicated in the previous reactions of initiation, propagation, and termination. In the case where only these reactions exist, each radical formed by the initiators, would produce a polymer molecule and this molecule would be linear. It is known that this is not the case, each initial radical produces more than one polymer molecule and those contain branches. This is because there are reactions that transfer the radical from a chain to another, without losing the activity of the free radical.

The chain transfer reactions involve the transfer of an active free radical on living polymeric chain to a solvent, monomer, or transfer agents. The radical can also break away from the live polymer or be transferred to another site in the same polymeric chain. These chain transfer reactions affect the size, structure, and the end groups of the polymer [21], but do not change the concentration of the active radical and so do not affect the monomer's conversion. Due to their nature and frequency, they are very important regarding the polymer molecular structure.

4.1.1 Chain transfer to Agents (or solvent)

The chain transfer can happen to the solvent or to a transfer agent. In some systems, a small amount of transfer agents is added to the feed. These agents are small molecules, such as small hydrocarbons like butane, propane, etc., and are often introduced in the reactional medium to control and reduce the molecular weight of the polymer produced.

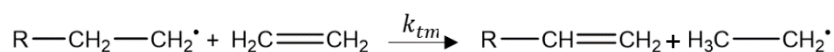
The rate of these reactions is dependent on the amount of weakly bonded atoms (normally hydrogen) present on the transfer agent, and their likelihood to be removed. For very

active compounds, the amount of agent added must be carefully controlled, to prevent a deviation of the polymer's molecular weights. In case of a large increase of the agent concentration, telomerization instead of polymerization may occur, and so the product will be composed majorly by low-molecular weight species [24]. The mechanism involves the removal of a hydrogen atom from the live polymer chain to the transfer agent, forming a dead polymer chain and a new radical [21,24].



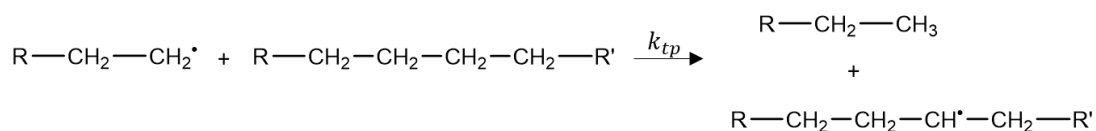
4.4.2. Chain transfer to monomer

Transfer of the active radical can occur between a live polymer chain and a monomer molecule. In this reaction, a dead polymer chain and a new polymer radical are formed. The reaction occurs through a hydrogen abstraction mechanism and leaves an unsaturated end at the dead polymer produced.

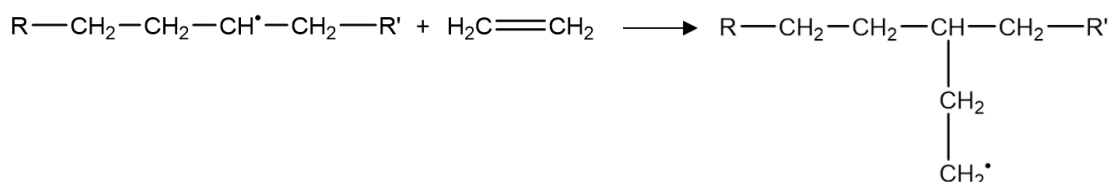


4.4.3. Chain transfer to polymer

The chain transfer to polymer involves the transfer of a radical from a live polymeric chain to a dead polymer chain.



Then the polymer continues to growth from that active site until is terminated, generating a long chain branch (LCB) [10].

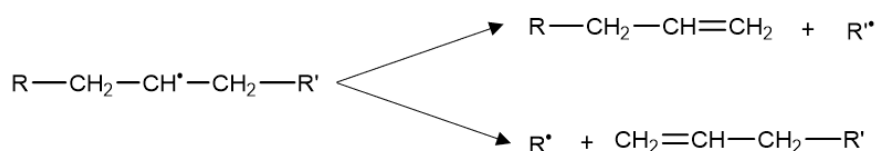


As the dead polymer chains are reactivated, this mechanism leads to an increase of the weight-average molecular weight (M_w) and consequentially to the broadening of the molecular weight distribution (MWD). This is why branched polymers, even with a low degree of branching

have a polydispersity index (PDI) between 5 and 15, while linear polymers present a PDI between 2 and 3 [24].

4.5. β -scission

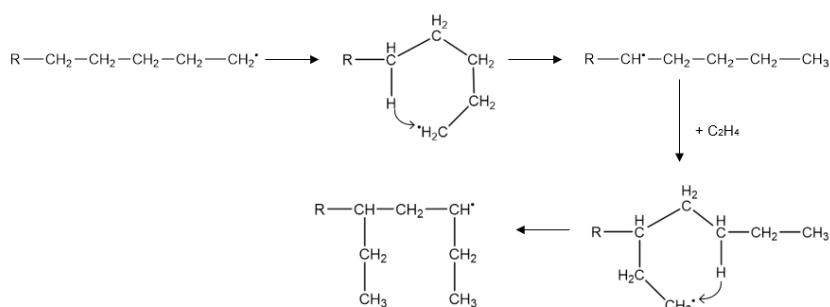
Oakes and Richards [52] have shown that at higher temperature conditions, the radical chain may undergo thermal degradation. The scission could happen either way, generating a short chain radical and a long chain with a double bond at the end, or otherwise, a short chain with a terminal double bond and a radical long chain. This reaction mechanism is illustrated next, for a scission on a secondary radical, although it can also occur on tertiary radicals, where the difference would just be having one more location where the scission could happen.



4.6. Backbiting

The LDPE presents short chain branches, of butyl and ethyl, that impact the crystallinity of the polymer. These branches are produced with a frequency between 8 and 50 branches per 1000 carbon atoms [31]. Roedel et al. [53] proposed an intramolecular mechanism for justifying the formation of the short branches, since until then, only the transfer to polymer was considered, which explained the long branches but not the short ones. The mechanism proposed lies on an intramolecular hydrogen transfer occurring via a transient 6 ring formation.

In summary, in this reaction, the active free radical site at the end of the live polymer chain is transferred to the fifth carbon from the end, by abstraction of one hydrogen atom. As the propagation continues from there, a butyl branch is formed. If, otherwise, a second back-biting reaction could occur, transforming the butyl branch into two ethyl branches [54,55].



The following table summarizes the reactions described.

Table 2. Summary of the ethylene free-radical polymerization reactions

Initiator decomposition	$I \rightarrow nR\bullet$
Chain Initiation	$R\bullet + C_2H_4 \xrightarrow{k_i} P_1$
Propagation	$P_n + C_2H_4 \xrightarrow{k_p} P_{n+1}$
Chain Transfer to monomer	$P_n + C_2H_4 \xrightarrow{k_{trm}} D_n + P_1$
Chain Transfer to polymer	$P_n + D_m \xrightarrow{k_{trp}} D_n + P_m$
Chain Transfer to transfer agent (or solvent)	$P_i + CTA \xrightarrow{k_{CTA}} D_i + R\bullet$
β-Scission	$P_n \xrightarrow{k_\beta} D_n + R\bullet$
Termination by disproportionation	$P_n + P_m \xrightarrow{k_{td}} D_n + D_m$
Termination by combination	$P_n + P_m \xrightarrow{k_{tc}} D_{n+m}$
Backbiting	$P_n \xrightarrow{k_{bb}} P_n$

In Aspen Polymers, the reaction rate constants are calculated from the modified Arrhenius law presented in Equation (18).

$$k = k_0 \exp \left[- \left(\frac{E_A + V_A P}{R} \right) \left(\frac{1}{T} - \frac{1}{T_{ref}} \right) \right] \quad (18)$$

Where k_0 is the pre-exponential factor (in s^{-1} for first order reactions and $m^3 mol^{-1} s^{-1}$ for second order), E_A the activation energy ($J mol^{-1}$), V_A the activation volume ($m^3 mol^{-1}$), R the gas constant ($J mol^{-1} K^{-1}$), P the pressure (Pa), T the temperature (K), and T_{ref} the reference temperature (K).

4.7. Kinetic parameters from the literature

There are many studies related with the simulation of the LDPE production process. However, most of them are for the tubular reactor process, while in this work there is an autoclave reactor process. The advantage of the tubular reactor simulation is that the kinetic parameters used on those studies should be suitable also for the present process. In the literature there are many values available for the kinetic parameters. However, there exists a huge disparity between the values reported by different authors, and not all of them use the same reaction mechanisms.

The first task of this work was to make a review of the kinetic parameters available in the literature and evaluate which ones could provide a good description of the process, compared to the real data collected from the plant.

The decomposition of the initiators was obtained directly from the suppliers' product data sheet, where besides information related to product characteristics, specifications, storage and other relevant data for the handling and storage of the product, it is also provided the activation energy and the pre-exponential factor for the peroxide decomposition (explained in chapter 4.1). The kinetic parameters used can be found in Table 3.

Table 3. Kinetic constants of the initiators' decomposition [57].

Initiator	k_0 (s ⁻¹)	E_A (J/kmol)	V_A (cm ³ /mol)	# of radicals
X	4.20×10^{15}	1.535×10^8	0	2
Y	1.54×10^{14}	1.249×10^8	0	2
W	9.30×10^{16}	1.541×10^8	0	4
Z	7.09×10^{14}	1.240×10^8	0	2
V	1.52×10^{14}	1.150×10^8	0	2

The kinetic parameters of other mechanisms were obtained from numerous papers, and other documents with such information. In the next table the parameters found in the literature are presented.

Table 4. Kinetic parameters in the literature.

	N. Agrawal et al. [58]			S. Goto et al. [59]			J. Y. Ham et al. [60]			P. Lorenzini et al. [61]			P.D. Iedema, et al. [62]			E. Saldívar-Guerra, et al. [63]		
	k_0	E_A	V_A	k_0	E_A	V_A	k_0	E_A	V_A	k_0	E_A	V_A	k_0	E_A	V_A	k_0	E_A	V_A
Chain initiation	4.00×10^5	17.4	-16.8	1.56×10^8	44.1	-18.5	1.0×10^6	27.1	-23.10	4.80×10^7	27.0	-17.30	1.25×10^8	33.7	-19.70	3.45×10^6	26.3	-52.70
Propagation	4.00×10^5	17.4	-16.8	1.56×10^8	44.1	-18.5	1.00×10^6	27.1	-23.10	4.80×10^7	27.0	-16.30	1.25×10^8	33.7	-19.70	3.45×10^6	26.3	-52.70
Chain Transfer to monomer	4.00×10^4	33.8	0.0	1.56×10^9	54.6	-23.5	1.00×10^6	49.31	19.80	----	----	----	1.25×10^5	33.7	-19.70	2.92×10^5	46.0	-20.00
Chain Transfer to polymer	5.20×10^4	36.8	-19.0	4.86×10^8	59.0	4.4	3.00×10^4	39.3	19.80	1.03×10^6	21.3	37.10	4.38×10^8	54.8	4.40	2.00×10^5	37.6	-19.80
Chain Transfer to butane	7.00×10^4	18.4	0.0	9.75×10^7	58.6	-16.7	7.00×10^4	18.4	19.80	1.47×10^8	53.3	-9.02	2.62×10^7	49.7	-19.50	2.40×10^9	52.7	63.20
Chain Transfer to propylene	7.00×10^4	18.4	0.0	6.11×10^7	55.3	-16.7	7.00×10^4	18.4	19.80	9.10×10^8	47.8	55.20	2.62×10^7	49.7	-18.50	2.40×10^9	52.7	64.20
B-Scission	7.70×10^9	87.4	-10.0	2.36×10^7	60.8	-18.5	2.43×10^7	40.7	0.00	1.11×10^7	33.9	-61.80	1.29×10^7	47.1	-16.80	2.36×10^7	60.7	-18.40
Termination by disproportion	8.70×10^8	15.3	9.2	8.33×10^7	12.6	13.0	3.00×10^8	16.5	0.00	2.06×10^9	64.4	12.60	1.25×10^9	4.2	13.00	----	----	----
Termination by combination	8.70×10^8	15.3	9.2	8.33×10^7	12.6	13.0	3.00×10^8	16.5	0.00	----	----	----	1.25×10^9	4.2	13.00	1.25×10^9	1.0	13.00
Backbiting	1.20×10^{10}	60.5	0.0	7.22×10^8	50.8	-14.0	2.43×10^7	40.6	0.00	6.80×10^8	40.1	17.20	7.80×10^8	37.9	-16.00	2.95×10^7	37.9	-23.50

The pre-exponential factor units are s^{-1} or $m^3/(kmol.s)$, depending on the reaction order. The activation energy units are kJ/mol, and the activation volume units are $m^3/kmol$.

4.8. Preliminary tests

This subsection pretends to provide insights into how each reaction of the ethylene free-radical polymerization influences output parameters of the model. To conduct this analysis, we used the condition of grade A, which uses butane as termination agent. It is important to note that the chain transfer to propylene does not occur due to its absence in the system. However, the conclusions for the transfer to butane can be extended to the transfer to propylene. Therefore, throughout this subsection, we refer to these reactions as chain transfer to agents although the reaction is the chain transfer to butane.

The kinetic set used to perform the analysis was the one that better described the real system which will be discussed more ahead on chapter 6.3.2.1. In each reaction, it was varied the pre-exponential factor, the activation energy, and the activation volume. It is important to note that these variables have an impact on the reaction rate constant. So, the variation on the three variables could be redundant. For instance, in the case of the propagation reaction, if the pre-exponential factor and the conversion increase, it is obvious that if the activation energy decreases, the conversion also increases. So, the conversion increases with the increase of the propagation reaction rate. That being said, in this stage, it does not matter to evaluate each parameter of the reaction rate but the reaction rate itself. So, we opted to vary only the pre-exponential factor, since it is proportional to the overall reaction rate, if this parameter increases by a factor of 2, it means that the reaction rate will also increase by a factor of 2.

The sensitivity study showed that the reactions which affect the number-average molecular weight (M_n) were the propagation, the chain transfer to monomer and to transfer agent, and the β -scission. However, the latter has a much lower impact compared to the other three reactions. The weight average molecular weight (M_w) is shown to be more dependent on the propagation, chain transfer to monomer, and chain transfer to polymer reactions. Although the polydispersity index (PDI) is the ratio between M_w and M_n , this parameter was also evaluated. The more important reactions for the PDI are the chain transfer to monomer, the chain transfer to polymer and the propagation (basically the reaction that affect M_w and M_n the most).

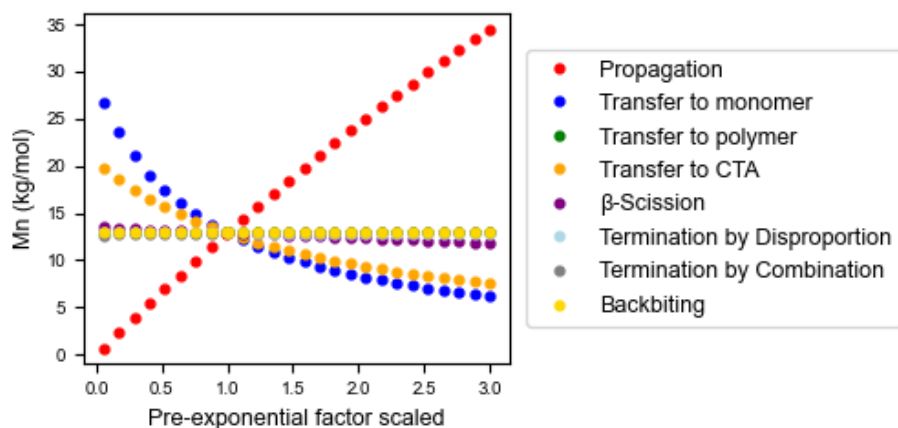


Figure 12. M_n sensitive analysis to each reaction.

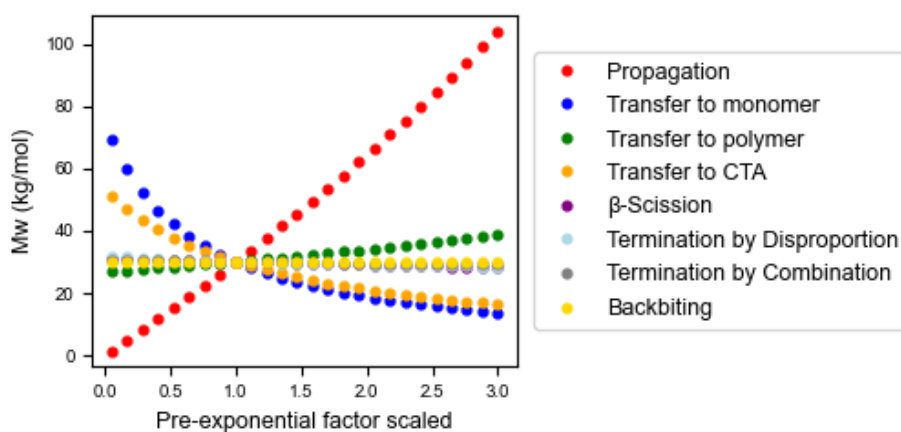


Figure 13. M_w sensitive analysis to each reaction.

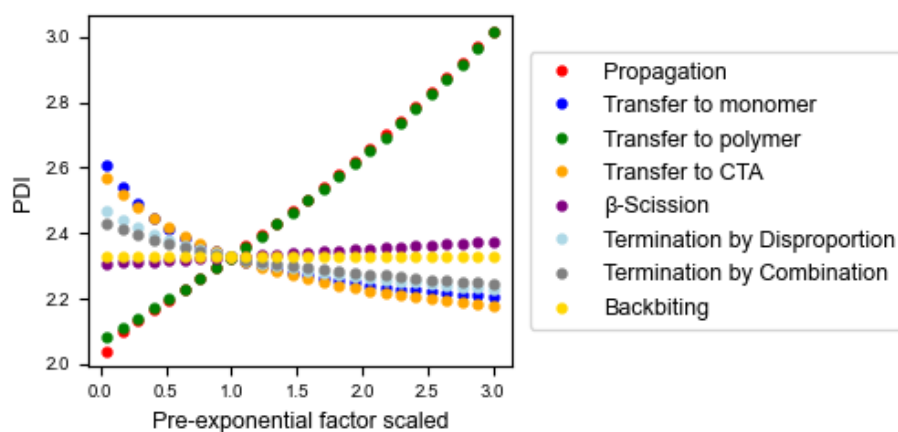


Figure 14. PDI sensitive analysis to each reaction.

All these reactions mentioned are related to the growth and the deactivation of the polymeric chains. The not significant impact of the termination reaction means that the

predominant termination mechanisms are the chain transfer reactions. Regarding the conversion, the reaction that showed a larger influence was the propagation, together with both termination reactions. Beyond this, the conversion is shown to be also sensitive to the initiators efficiency, where a larger efficiency means more radicals, which results in a larger conversion.

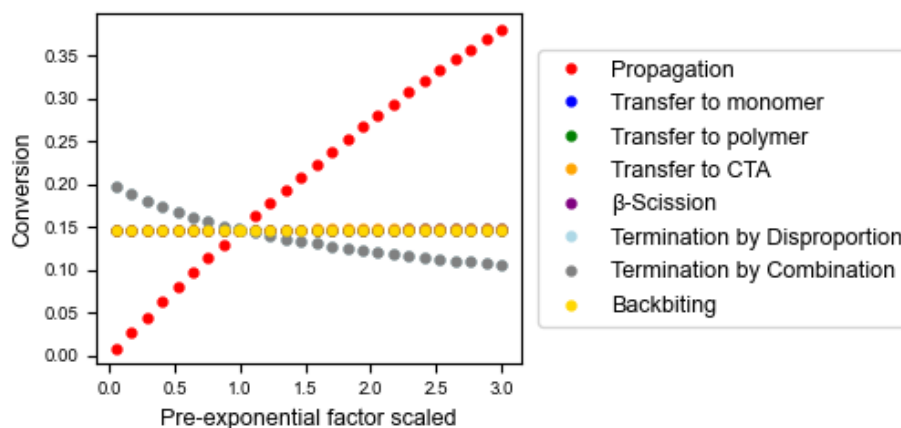


Figure 15. Ethylene conversion sensitive analysis to each reaction.

The conversions of the chain transfer agents are essentially only affected by the chain transfer to agents' reaction, since they are the only reaction that these agents take part. When they are not present, the reactions do not occur, as previously mentioned.

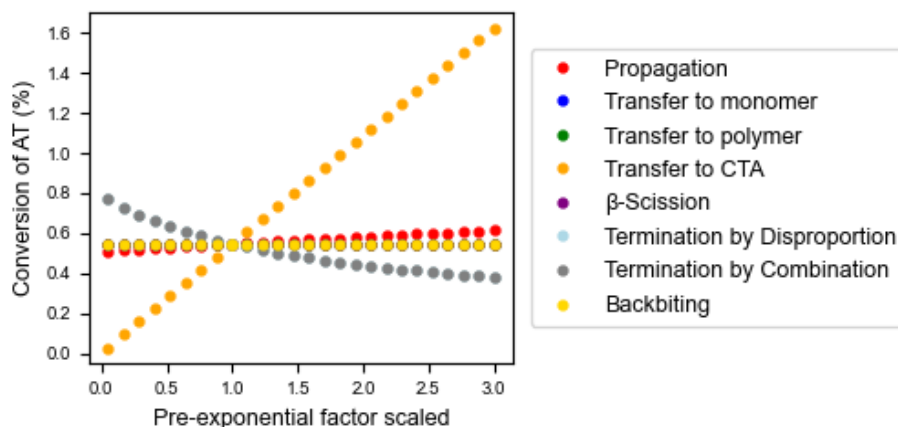


Figure 16. AT conversion sensitive analysis to each reaction.

The ramifications of the polymer were also evaluated (both SCB and LCB). Starting with the SCB, the reactions with more impact on the frequency of SCB were the propagation and the backbiting reactions. The backbiting reaction is in fact responsible for the formation of SCB, while the propagation does not directly affect the number of SCB but impacts its frequency, because

this is given in SCB/1000 segments, so with the increase of the propagation the chain will incorporate more segments, resulting in a lower frequency of SCB. The frequency of LCB is more sensitive to the chain transfer to polymer, which is responsible for the formation of the LCB. Both termination reactions are less important than the transfer to polymer, but still have impact on the frequency of LCB.

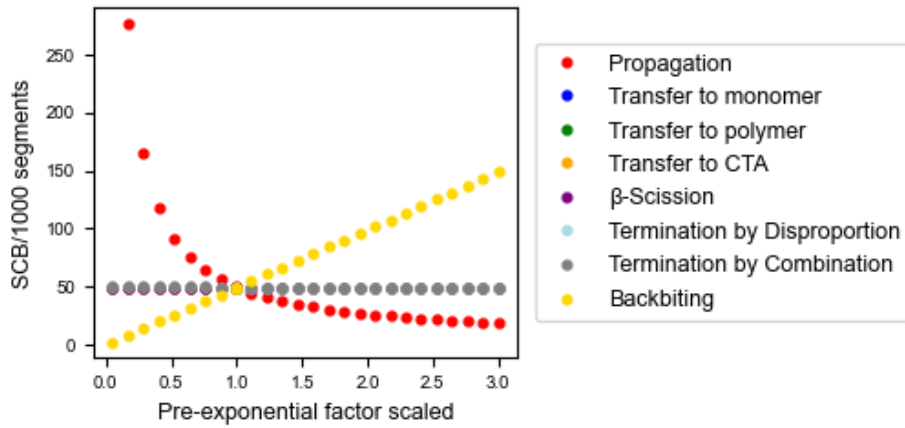


Figure 17. SCB sensitive analysis to each reaction.

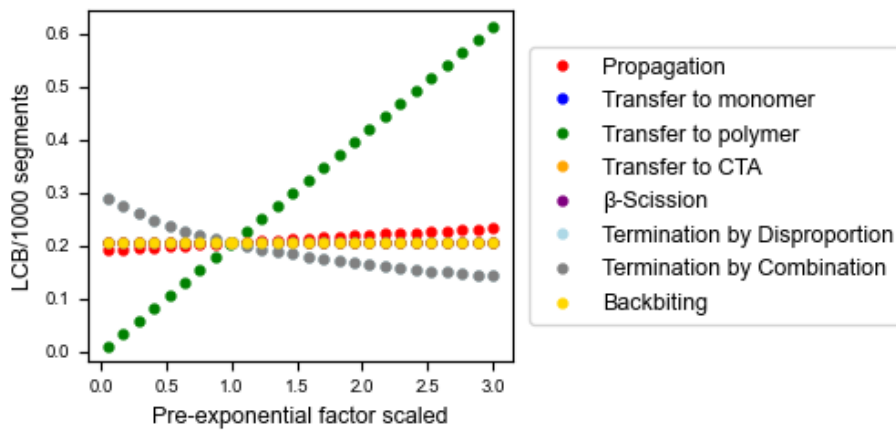


Figure 18. LCB sensitive analysis to each reaction.

5. Polymer properties correlations

In the industry, the polymer quality is quantified by empirical quality measures that are related to the processing and mechanical characteristics of the polymer. These measurements include the melt index, density, haze, gels, and so on.

5.1. Melt index

Amongst the properties used for quality control, the melt index and the density are the most important. The melt index is obtained from a standard test (ASTM D1238), which measures the amount of molten polymer extruded through a standard orifice opening during a certain time, usually 10 min. The test is performed under specific conditions of temperature, load and piston position in the barrel. The melt index is expressed in mass of polymer extruder per unit of time (g/10 min). The higher the value of MI, the softer the product. Its applications are totally different from the ones with lower MI that are stiffer [64].

In Aspen Plus[®], product quality measures such as melt index, density, haze, etc., are not directly computed. Only the information about the polymer molecular structure, such as molecular weights M_w and M_n , short and long chain branches (SCB and LCB), copolymer incorporation, are provided. However, these are not used to evaluate the quality of the product. Since expensive and time-consuming tests are required to obtain these last properties, such tests are only performed occasionally to access abnormal events in the plant or to perform studies aimed at optimizing the unit.

For the simulation model to be useful, a correlation between the molecular structure properties that are available in the output of Aspen Plus and the melt index is needed. It is known that the melt index is strongly correlated with the polymer's molecular weights and with the polymer viscosity. A smaller melt index implies a larger molecular weight and viscosity. Here the main interest is between the relationship between the melt index and the number/weight-average molecular weight, since it is the one that can relate the Aspen Plus[®] V11 outputs to the properties measured in the plant.

In the literature, many correlations are proposed to relate the number-average molecular weight of LDPE with the melt index. Sperati et al. proposed the following correlation, which was claimed to be valid for a range of M_n between 15000 and 50000 g/mol [65].

$$\log(MI) = 5.09 - 1.53 \times 10^{-4} M_n \quad (19)$$

Two other correlations were found. The first was developed by ICI (Equation (20)), while the second was developed by *Repsol YPF* and represents an improvement because it is valid for a larger range of melt indexes [66], Equation (21).

$$\log(MI) = 6.2649 - 0.1761 \sqrt{\frac{M_n}{28}} \quad (20)$$

$$\log(MI) = -3.153276 + \frac{2918.563}{\frac{M_n}{28}} \quad (21)$$

However, as it can be observed in Figure 19 and Figure 20, the data provided by the GPCs analysis of the different grades produced in *Repsol Polimeros* (for different batches), did not show evidence of a correlation between the molar weight and the melt index. Although, no clear correlation could be observed for all the data points, some relation could be observed for melt indices lower than 4. More data points over a broader range of melt index could be helpful to evaluate if a correlation for different ranges of melt index exists.

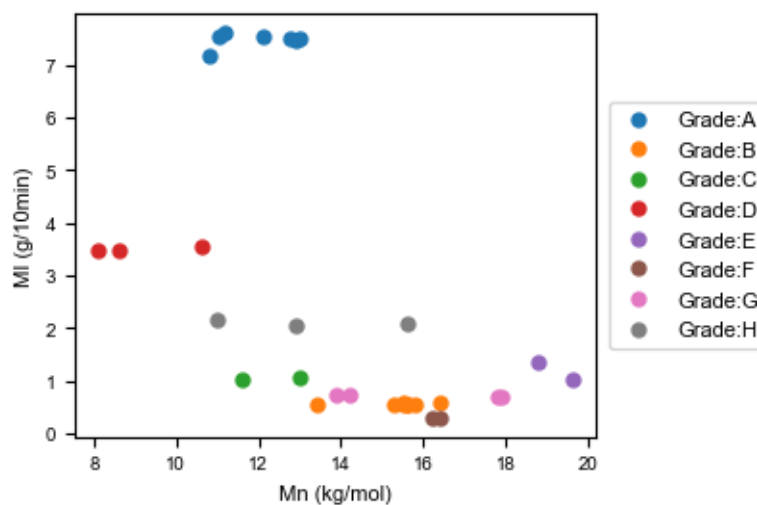


Figure 19. Number-average molecular weight against Melt Index.

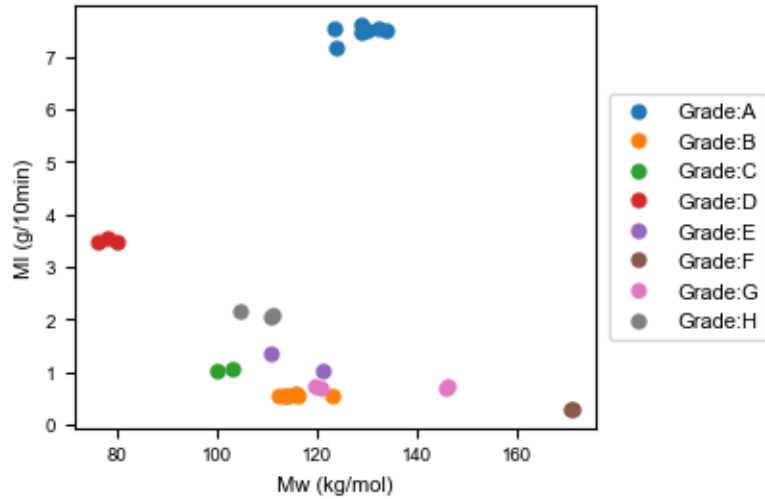


Figure 20. Weight-average molecular weight against Melt Index.

5.2. Density

The density is a more common property that can be measured with a densimeter or with some other method that determines the mass and volume of a certain sample. Density has strong correlation with the number of short chain branches. With a higher degree of short chain branches, the polymeric chains have more difficulty to pack and form the crystalline zones, leading to a decrease in polymer density. So, the polymer will become more amorphous.

Like for the previous case, many correlations were found in the literature for describing the relationship between density and the frequency of short chain branches. Sperati et al. [67] proposed the correlation in Equation (22). This equation is valid for a range of SCB/100 C between 0.4 and 50 but limits the density to a value of 0.9312 which is strange since there are LDPE grades with a greater density.

$$\rho \left(\frac{g}{cm^3} \right) = 0.9312 - 5.2 \times 10^{-3} \left(\frac{SCB}{100C} \right) \quad (22)$$

Like the relations for the melt index, Repsol also developed a relation between the density and the SCB [68].

$$\rho \left(\frac{g}{cm^3} \right) = \frac{0.793}{1.06 + 9.2 \times 10^{-4} \left(\frac{SCB}{100C} \right)} + 0.188 \quad (23)$$

As can be seen in Figure 21, none of the previous equations described well enough the plant data and so, a different linear relation was developed, leading to a R^2 of 0.96. Note that grade H is an outlier (neglected for generating the correlation and computing the R^2).

$$\rho \left(\frac{kg}{m^3} \right) = 944.7 - 0.574 \left(\frac{SCB}{1000 \text{ segments}} \right) \quad (24)$$

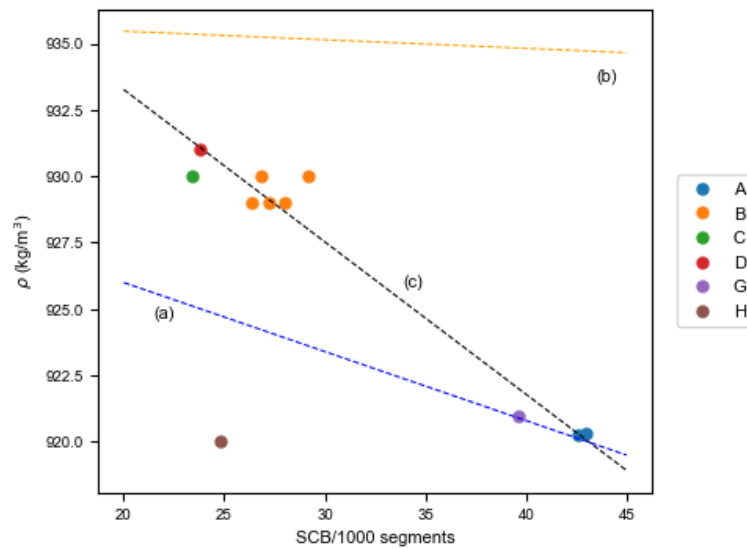


Figure 21. Relation between SCB and the final polymer density. Curve (a), (b) and (c) are generated with equations (22), (23) and (24), respectively.

6. Methodology

This chapter provides a clear description of the model developed in Aspen Plus® V11, new because the modelling of an autoclave reactor with five inlet streams has never been reported before.

6.1. Components definition

While the definition of the components is usually something that does not require much attention, the definition of polymers is a little bit different, as explained in chapter 1.3.1. Most of the components were available in the databases provided in Aspen Plus® V11. However, one of the initiators (initiator W) didn't exist in any database, so this compound was created from its molecular structure, with its properties being obtained from the Thermo Data Engine (TDE NIST) present in Aspen Plus® V11. The Ethylene Butyl Acrylate also didn't exist. Hence, it was defined as a generic polymer in which the segments that constitute it are later defined. Table 5 shows the compounds used in the simulation, their type, and the databank from where they were extracted.

Table 5. List of the compounds used in the simulation with their ID, type, and database.

ID	Component	Type	Database
ET	Ethylene	Conventional	APV110.PC-SAFT
ET-SEG	Ethylene Segment	Segment	APV110.SEGMENT
PEBD	LDPE	Polymer	APV110.POLYMER
ATA-BUT	Butane	Conventional	APV110.PC-SAFT
ATB-PROP	Propylene	Conventional	APV110.PC-SAFT
BA	Butyl Acrylate	Conventional	APV110.PURE37
BA-SEG	Butyl Acrylate segment	Segment	APV110.SEGMENT
EBA	Ethylene Butyl Acrylate	Polymer	APV110.POLYMER
O2	Oxygen	Conventional	APV110.PC-SAFT
N2	Nitrogen	Conventional	APV110.PC-SAFT
H2O	Water	Conventional	APV110.PC-SAFT
INI-X	Initiator X	Conventional	APV110.INITIATO
INI-Y	Initiator Y	Conventional	APV110.INITIATO
INI-W	Initiator W	Conventional	-----
INI-Z	Initiator Z	Conventional	APV110.INITIATO
INI-V	Initiator V	Conventional	APV110.INITIATO
ISOD	Iso-dodecane	Conventional	APV110.PURE37
ISOPAR	ISOPAR G	Conventional	APV110.PURE37

6.2. Thermodynamic model

The thermodynamic properties and the behavior of the different phases present in the different process units are an essential element of every simulation. There are numerous property methods available that can be clustered into two different categories.

The first is based on activity coefficients. This includes models like the Flory-Huggins, the NRTL modified for polymers (POLYNRTL), and others. These models are more appropriate for low-pressure, strongly non-ideal systems with multiple liquid phases.

The second category is based on Equations of State (EOS), including the Sanchez-Lacombe EOS, the Statistical Associating Fluid Theory EOS (SAFT), the Perturbed-Chain Statistical Associating Fluid Theory (PC-SAFT), etc. The equations of state present better predictions for high-pressure systems. Considering the pressures present in the polymerization of ethylene (above the critical pressure of ethylene) an EOS model was used [35–37].

Among the Equations of State, one of the most used due to its precision is the Perturbed-Chain Statistical Associating Fluid Theory (PC-SAFT). The major advantage of this model, when compared with other EOS such as the Sanchez-Lacombe EOS or the SAFT EOS, is the ability to also describe with accuracy the properties of conventional chemical compounds. It can do it with an accuracy comparable to the Peng-Robinson or other cubic equations of state used for smaller molecules. The PC-SAFT applies to a wide range of fluid systems. From systems with small and/or large molecules, such as hydrocarbons, water, alcohols, ketones, polymers, and copolymers and their mixtures [37].

6.2.1. PC-SAFT (Perturbed Chain Statistical Associating Fluid Theory)

In the models based on the EOS, one of the most used due to its precision is the Perturbed Chain Statistical Associating Fluid Theory (PC-SAFT). Developed by Gross and Sadowski, this state equation is an improvement over the SAFT EOS. The original SAFT EOS is based on the perturbation theory of classical statistical mechanics where the real fluid unknown properties are computed as a perturbation of the properties of a model system in which the molecular properties can be calculated. In the SAFT EOS, the reference fluid is a chain of hard spheres.

The main difference between SAFT and PC-SAFT lies in the perturbation term. The PC-SAFT EOS, unlike the SAFT EOS, doesn't base this term on argon's behavior, where the fluid is constituted by single spheres. In PC-SAFT, the perturbation term is based on the behavior of a fluid composed of a bonded sphere chain [54]. So, as it is represented in Figure 22, the idea is that the perturbation theory is employed for segments connected in a chain rather than between

isolated segments, as is the case in SAFT EOS [37]. This approach provides a more realistic view of how polymers, oligomers, hydrocarbons, and other chain molecules behave in solution.

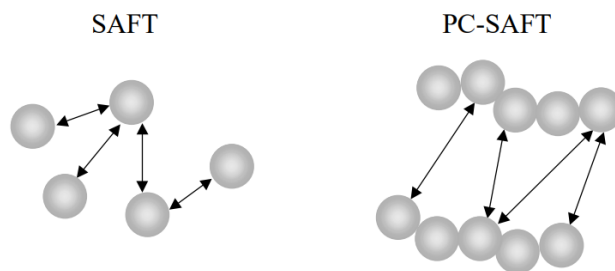


Figure 22. The main difference between SAFT and PC-SAFT.

For the PC-SAFT EOS application, three pure-component parameters for each compound present in the simulation are necessary. These parameters are the segment number, m (this is for the case of a conventional compound, if the compound is a segment, m is replaced by the ratio r), the segment diameter, σ , and the segment energy ϵ (it is usual that the segment energy is given as ϵ/k where k is the Boltzmann constant) [21,69]. Some parameters were unavailable for certain molecules, namely for the initiators and butyl-acrylate (both the conventional compound and segment). For missing parameters, the suggestion [37] is to use the following: $\sigma = 4.072$; $\epsilon/k = 269.67$ K, and if it is a conventional compound, $m = 0.02434M$, where M is the component's molar weight. In the case of a segment, m is replaced by r , which is set to 0.02434.

Normally for trace components, as the initiators, the segment number (m) should be set to a high value ($\Rightarrow 15$), to keep them in the liquid phase. We used $m=20$. The values of σ and ϵ parameters should be set to the key component's values, so they are miscible on the streams without polymer. The values considered were equal to the ethylene's parameters [36].

For the butyl-acrylate, the suggested values were considered only as an initial guess, since the parameters were fitted to the vapor pressure experimental data from Stull et al. [70]. The obtained parameters were $\sigma = 3.433$; $\epsilon/k = 381.34$ K and $m = 2.218$. For the butyl-acrylate segment, the parameters were found in the literature [71].

The parameters of ethylene and LDPE, although found in the databases, as these two are the main process components, will dominate process thermodynamics, so it is important to have a very precise description of their behavior. So, the PC-SAFT parameters were fitted using ethylene's experimental vapor pressure, supercritical density, and supercritical heat capacity data, to fit the PC-SAFT parameters. As the vapor pressure for the LDPE doesn't exist, only density data was used to estimate the parameters [54,69,72–75].

The PC-SAFT parameters utilized in the simulation are summarized in Table 6.

Table 6. PC-SAFT parameters used in the simulation.

ID	σ	ϵ/k (K)	m	r
ET	3.4372	179.540	1.557	----
ET-SEG	3.4751	267.179	---	0.0413
BA	3.4327	381.344	2.218	---
BA-SEG	3.9500	224	---	0.0259
INI-X	3.4372	179.540	20	---
INI-Y	3.4372	179.540	20	---
INI-W	3.4372	179.540	20	---
INI-Z	3.4372	179.540	20	---
INI-V	3.4372	179.540	20	---
ISOD	3.4372	179.540	20	---
ISOPAR	3.4372	179.540	20	---

Adding to the pure components parameters, PC-SAFT also accounts for the interaction between two different species, using a binary parameter (k_{ij}). This parameter was adjusted for the LDPE-ethylene mixture, considering the experimental vapor-liquid equilibrium data obtained by Rousseaux [76]. This was only to obtain a first approximation since, later, this parameter was changed in the fitting of the separation stages.

The Appendix in section B, contains the results for all the fits.

6.3. Process simulation

From the process description made previously on chapter 3.1. the flowsheet of the overall process was developed, starting from the reactor which was the main unit of the process. The reactor as it was seen is a 5-zone autoclave reactor. E. Topalis et al. [77] developed a model for autoclave reactors that approaches the autoclave as a series of CSTRs with external recycle and backflow. However, after a few tries, we found that such configuration led to prohibitive simulation times and so, a simpler approach was taken. The multi zone autoclave reactor was modeled as a series of five CSTRs, each representing one zone. The approach outlined is a conventional method of simulating reactors of this type. This is mainly because the reactor zones are separate compartments that are isolated from each other by plates connected to the agitator. The plates possess a diameter a bit smaller than the reactor's internal diameter. This arrangement permits the mixture to travel through a ring-shaped space with a narrow thickness that develops between the plate's edge and the reactor's internal wall. This configuration makes the back-mixing between

the reaction zones negligible. So, as an initial approximation, it is possible to consider each zone to be thoroughly mixed, thereby allowing the reactor to be modelled as a sequence of five CSTRs, as it is observed in Figure 23 [63,78].

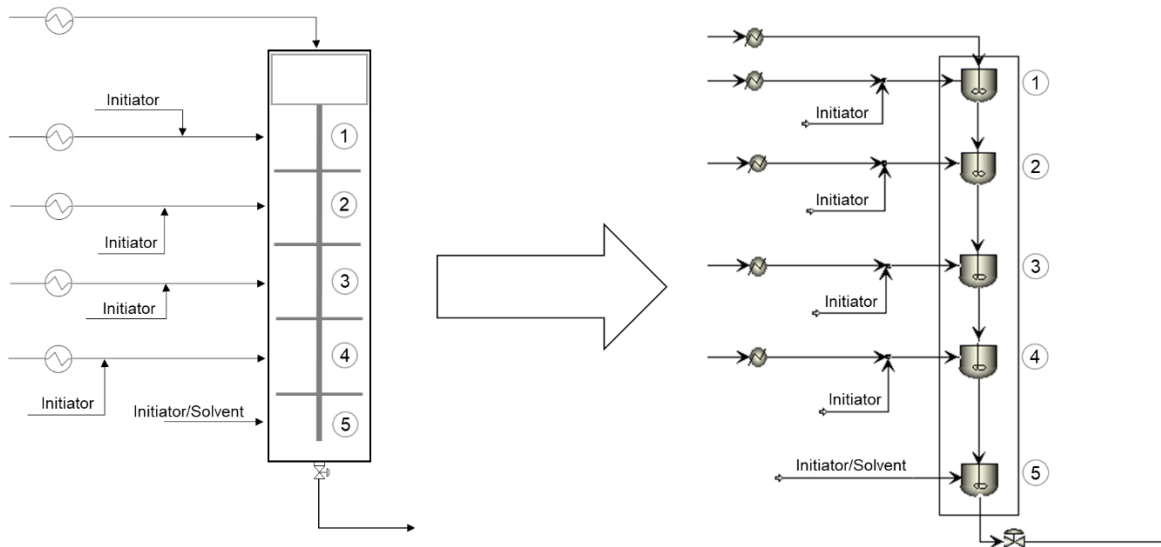


Figure 23. Conversion of the real reactor to the Aspen Plus[®] reactor model.

The reactor showed problems with the convergence of the mass balance for some conditions. The solution passed to manipulate some of the convergence parameters inside all the five CSTR blocks. The first change was the solver. As the default is to use the Broyden solver, which is a fast, but not the most stable solver. We opted to select the most stable solver available, which is Newton. With the Newton solver, the stabilization strategy was also changed from Dogleg to Line-Search, which is recommended for polymer kinetics [36]. The number of maximum iterations defines the number of mass balance iterations, and it is set at 50 as default. Sometimes this value was not enough for convergence and so it was incremented to 500. The error tolerance was fixed to 10^{-5} and so the mass balance will converge when the maximum scaled residual of conservation equation is lower than the specified tolerance. Note that there is a second criterion which is the root-mean-square scaled error. If the first criterion is reached but the root-mean-square scaled error is decreasing by a factor of 10 on each iteration, the model continues to iterate until this parameter reaches the specified function tolerance. This ensures a very tight convergence tolerance when the convergence is well behaved. The value chosen here needed to be small enough to ensure a good convergence, but not too small that would just increase unnecessarily the precision, leading to errors.

The initialization was another factor changed. The default is not to use integration, which makes the simulation faster, either by using saved results from the previous simulation or by providing estimates. The case where neither exists, the block will be initialized based on the mixed

feed stream. There were two other options: *Always use integration* and *initialize using integration*. The integration algorithm treats the CSTR as a dynamic stirred tank reactor. The conservation equations are numerically integrated from an initial condition to the steady-state conditions. The numerical integration is carried out until the residual terms are below the specified mass-balance tolerance. Afterwards, the model enters the solver and proceeds until convergence is reached. The difference between always using integration and initialize using integration is that the last is a hybrid initialization, taking advantage of the integration algorithm robustness to initialize the reactor during the first pass. On the following passes, when a previously converged solution is available, the solution algorithm goes directly to the trial-and-error solver. On other hand, the first option, as its name indicates, always uses the integration, which makes it the slowest of the three.

The damping factor controls the step size. Decreasing the damping factor will result in smaller steps where the outcome is a larger number of smaller but more stable steps. This factor was diminished down to 0.1. The last parameter changed was the scaling method. When the solver is Newton, the default scaling method is *Substream-based*, where the scaling factors are constant for each class of variables. The method employed was the Component based method where the variables are scaled against their estimated magnitude.

After the reactor, the rest of the flowsheet was implemented with the separation and compression stages. However, certain aspects of the process were simplified. The gas that comes out of the separator, usually carries the oligomers produced (a wax) which is removed in a series of cooling stages where each stage is then followed by cyclones to remove the wax. The wax formation was not initial considered since its production is not significant. Thus, the RMP (circuit of stream 11 through 13, in Figure 10) is only simulated with a heat exchanger to ensure the final temperature of the circuit. There are also some bypasses used for control purposes that are not considered. Finally, the simulation stopped in the low-pressure flash, where the polymer goes to the extruder, not considering the further stages.

In the process model, some calculator blocks were developed using FORTRAN language. The first cluster of calculators configured is to incorporate the end user correlation allowing to do the translation of the polymer properties given in the Aspen Plus® V11, to the properties measured in the plant (these include the density and the melt index). The second is related to the output variables that need to be calculated, more specifically, the conversion of the monomer and of the termination agents. The third group are calculators used to simplify the required inputs. These include a block to force all the CSTRs to work with the same pressure (so it makes only necessary to introduce the pressure in the first reactor and not in all five reactors), a block that stores the initiator information (the composition of the initiators in the different zones according to the grade that is being simulated), a block normalizing the kinetic constants. This last block was created to decrease the magnitude of the activation energy and pre-exponential factor, making it easier to perform the fitting. At the end to make the model the most user-friendly as possible it was created a calculator where all the required inputs can be introduced.

6.3.1. Data Fit tool

The parameters regression was performed using the Data Fit tool available in Aspen Plus® V11. The Data fit tool is implemented based on the N2SOL (an adaptive nonlinear-squares algorithm) developed by Dennis et al. [79]. Using a few adjustments, this is a trust region unconstrained optimization method. The idea is that at point x_k , the objective function is represented by a simpler local quadratic function (q_k) that inside a certain region is trusted to represent the objective function [79,80]. A step is made on the varying variable with the aim to minimize q_k , and then the new objective function value is computed. In the case where the new value computed is smaller than the previous value, the step is accepted. Otherwise, the trust region is shrunk, or the approximation model is changed.

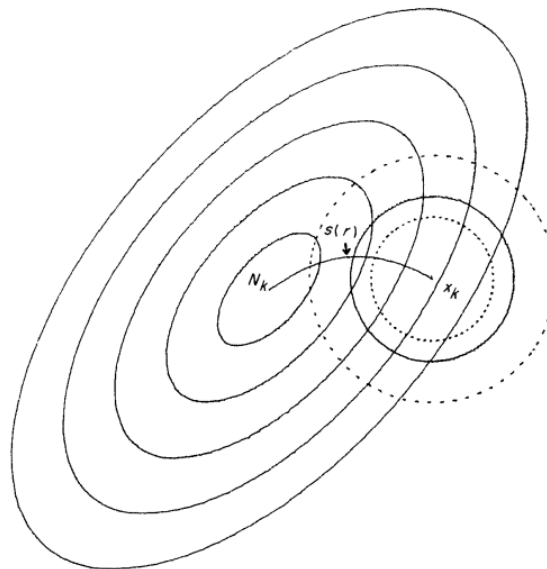


Figure 24. Trust Region Optimization [79].

Figure 24 illustrates the algorithm just described. The ellipses are contour lines representing different values of the objective q_k , the circles represent the trust region (the initial, in solid, an expanded, and a shrunk region). The point x_k is the current point from where the algorithm proceeds, and N_k is the global minimizer of the quadratic model. The curve $s(r)$ represents the locus of minimizers of q_k [35,79].

The objective function created in the Data Fit is the one in Equation (25) [36,37].

$$\min_{X_p, X_{ri}} \frac{1}{2} \sum_{i=1}^{N_{sets}} \left(W_i \times \left(\sum_{j=1}^{N_{exp\ i}} (term1 + term2) \right) \right) \quad (25)$$

$$term1 = \sum_{l=1}^{N_{ri}} \left(\frac{X_{mri} - X_{ri}}{\sigma_{X_{mri}}} \right)^2 \quad (26)$$

$$term2 = \sum_{m=1}^{N_{rr}} \left(\frac{X_{mrr} - X_{rr}}{\sigma_{X_{mrr}}} \right)^2 \quad (27)$$

Where:

N_{sets} is the number of data sets specified in the regression.

$N_{exp\ i}$ is the number of experiments in data set i .

N_{ri} is the number of reconciled input variables.

N_{rr} is the number of measured results variables.

W_i is the weight of the data set i in the regression case.

X_p is the vector of varied parameters.

X_{mri} are measured values of the reconciled input variables.

X_{ri} are the calculated values of the reconciled input variables.

X_{mrr} are the measured values of the result variables.

X_{rr} are the estimated values of the result variables.

σ is the specified standard deviation for the measured variables.

When performing the fitting, some parameters were modified maximize the likelihood convergence and to achieve better estimations. These parameters were the maximum passes through the flowsheet, the absolute and relative function tolerances, X convergence tolerance, the minimum step tolerance, the initial step size, and the relative perturbation size. The maximum passes through the flowsheet have as default value 1000, however in some cases this was not enough for the algorithm to achieve convergence (typically the value was increased up to around 2500-5000). The absolute function tolerance (default =0.01), the relative function tolerance (default =0.002) and the X convergence tolerance (default =0.002) control if the problem is converged or not. The default values are all of them very conservative, so they were increased

up to 0.1 for the first parameter and up to 0.01 for the other two. The minimum step tolerance (default = 1×10^{-10}) controls if the solution is suboptimal or not. If a step with a scaled length of at least Minimum Step Tolerance is attempted but denied, the Data Fit returns suboptimal solution. Like the previous parameters, this had a very conservative value set by default. The values were changed in a range of 10^{-15} to 10^{-30} . The initial step size parameter defines the initial step size of the trust region, this parameter affects the algorithm's performance, with different values leading to different local minima. The values were change between 0.1 and 100. The other parameter changed was the relative perturbation size, with values between 0.0001 and 0.1.

At the end of the data fit process, the following information is returned:

- 1) Summary:
 - Initial and final value of the objective function.
 - The number of iterations performed.
 - Number of converged flowsheet passes used to solve the Data Fit problem.
 - Chi-squared values for the fitted data.
- 2) Manipulated variables:
 - Initial and estimated values.
 - Standard deviation.
- 3) Fitted Data:
 - Measured and estimated values.
 - Standard deviation of the estimated values (the 95% confidence interval is computed multiplying these values by 1.96).
 - Normalized residues.
- 4) Iteration History:
 - Objective Function and its variations for each iteration.
 - Varied/reconciled variables for each iteration.

6.3.2. Parameters estimation

The problem is broken down in stages. In the first stage, the reaction parameters that can describe all the grades produced in the plant are regressed. At this stage, a simulation only with the reactor was done to facilitate the convergence and make the simulation faster. The first idea here was starting with LDPE and then move to EBA, since the homopolymer has less parameters to be regressed, due to the lack of the crossed reactions present in the copolymer.

After achieving a reactor model capable of describing all the grades, the separation phases were added to the flowsheet (the separator, the high-pressure flash, and the low-pressure flash). Here, the thermodynamic model binary parameters were manipulated to reproduce the amount of gas exiting both flashes.

Then the compressors were added. Here the main goal was having the energy consumption of each compressor. The manipulated variables were the mechanical and polytropic efficiencies of each compressor stage.

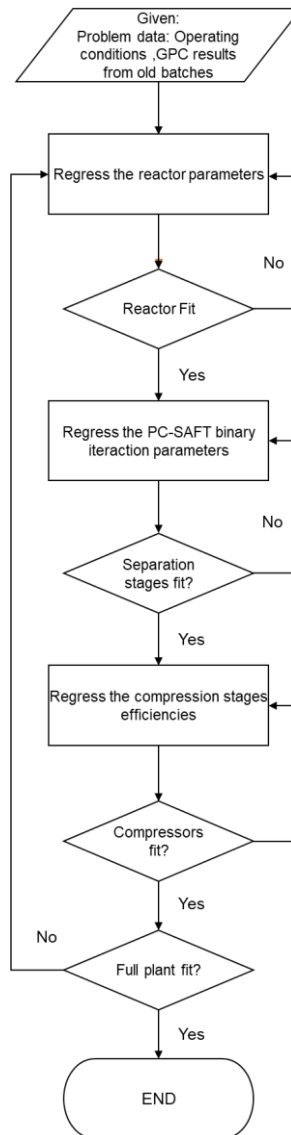


Figure 25. Flowchart of the methodology used to treat the full plant.

6.3.2.1. Reactor

To assess how the system behaved with the kinetic parameters presented in the literature compared to the plant real values, an analysis was conducted. This analysis involved gathering data on the production conditions and product properties, for several campaigns across eight

different grades. The results are presented over the next figures, where each point represents a campaign.

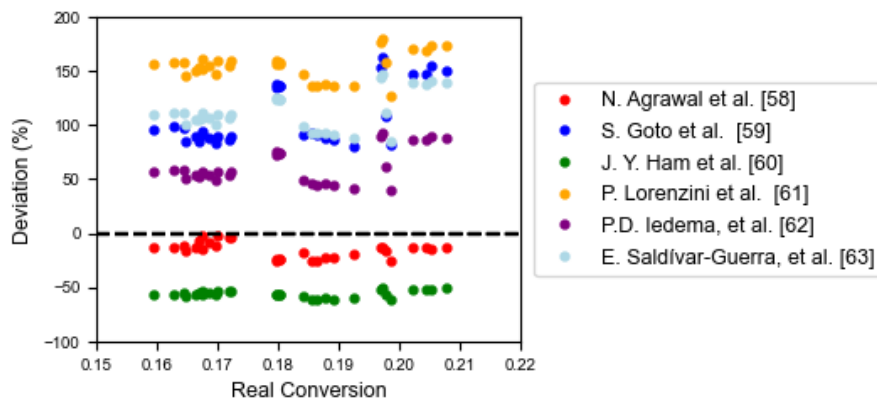


Figure 26. Deviations between the model predictions and experimental conversions when using the kinetic parameters taken from the literature.

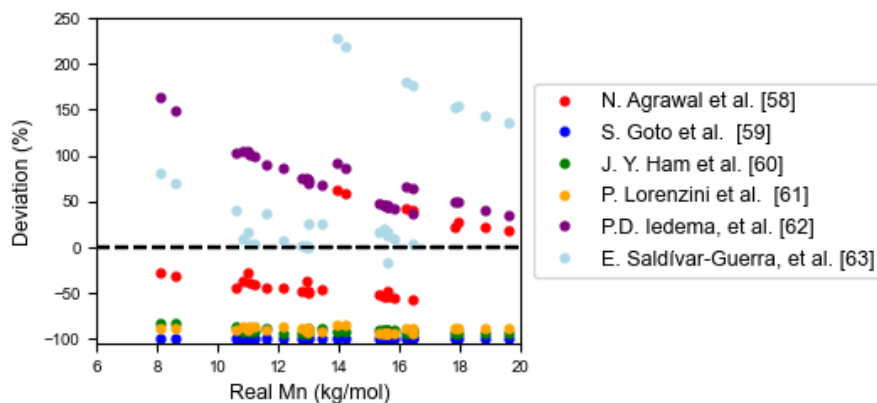


Figure 27. Deviations between the model predictions and experimental M_n when using the kinetic parameters taken from the literature.

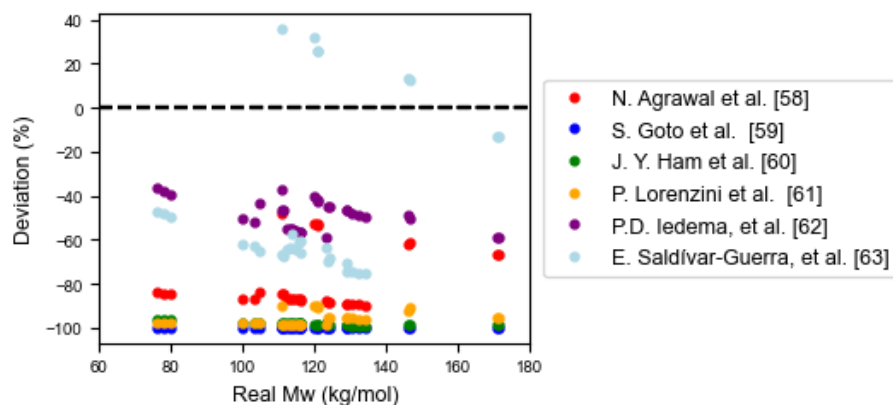


Figure 28. Deviations between the model predictions and experimental M_w when using the kinetic parameters taken from the literature.

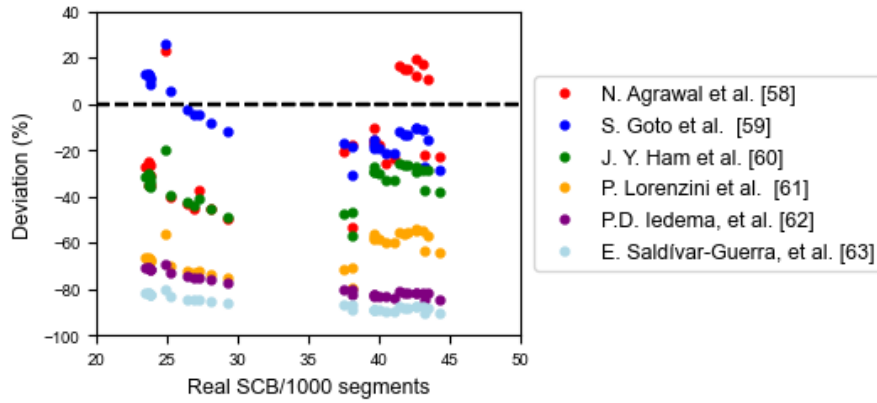


Figure 29. Deviations between the model predictions and experimental SCB when using the kinetic parameters taken from the literature.

Figure 26 shows that the parameters proposed by Agrawal et al. [58] generate results that are very close to those observed in the plant. Unfortunately, other sources lead to better results for the other output parameters, especially for the M_w in Figure 28. To have a more quantitative comparison between all the kinetic parameters studied, we resorted to the Root Mean Squared Error (RMSE). In equation (28), \hat{y}_i is the model predicted value for observation i , y_i is the real value, and n the number of observations.

$$RMSE = \sqrt{\frac{\sum_{i=1}^n (\hat{y}_i - y_i)^2}{n}} \quad (28)$$

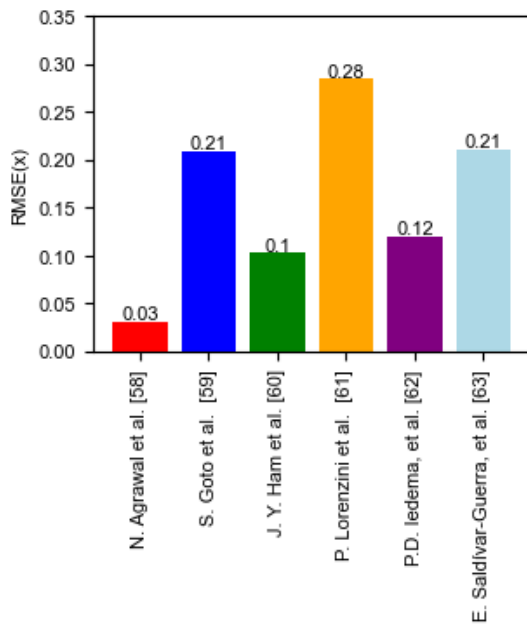


Figure 30. Conversion RMSE for the different kinetic sets.

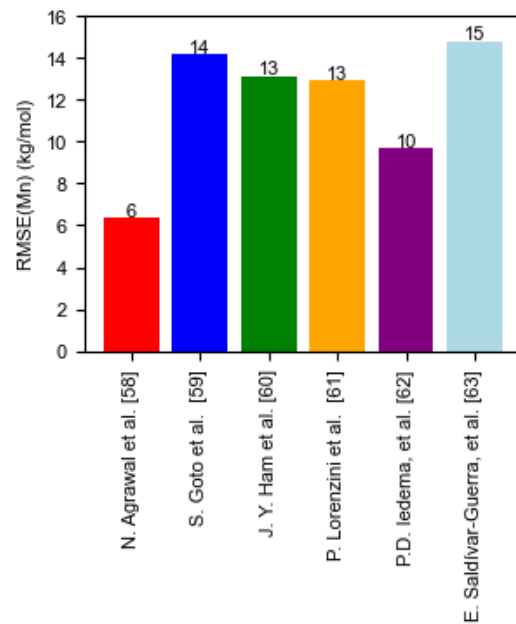


Figure 31. M_n RMSE for the different kinetic sets.

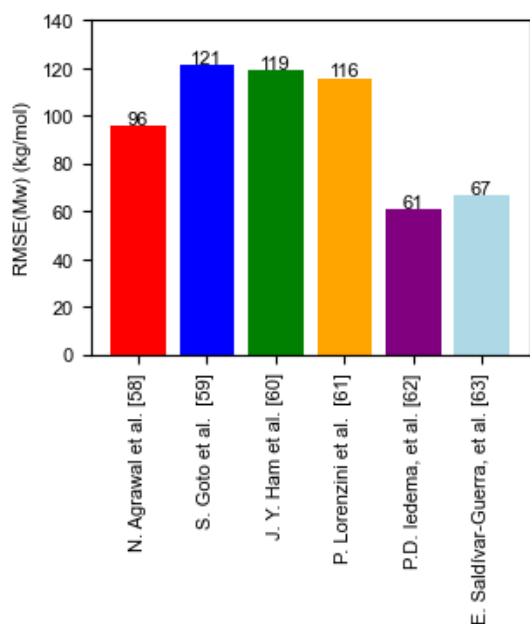


Figure 32. M_n RMSE for the different kinetic sets.

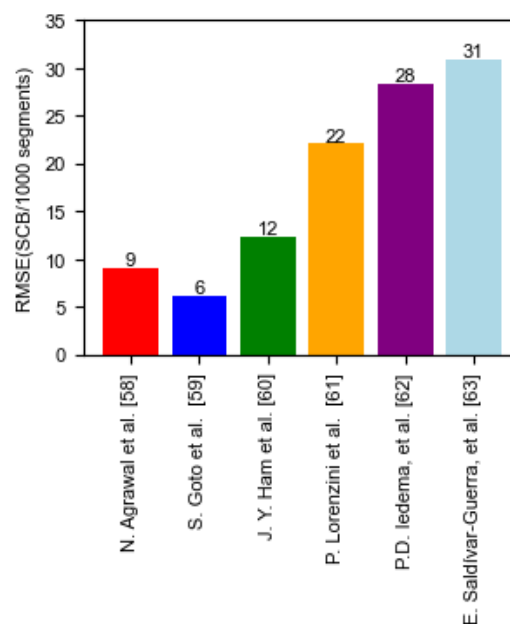


Figure 33. SCB RMSE for the different kinetic sets.

From the previous four figures, it is clear that the best kinetic parameters are the ones of Agrawal et al. [58]. However, they are not good enough to provide an accurate description of the system. Nevertheless, the data from Agrawal et al. [58] can be used to initialize the kinetic parameters of the following reactions: propagation, chain transfer to monomer, chain transfer to polymer, chain transfer to butane, chain transfer to propylene, termination by disproportionation, termination by combination, and backbiting. Data Fit was performed using as inputs the operating conditions in the reactor, and all product properties as reactor outputs (see Table 7).

Table 7. List of inputs and outputs for Data Fit.

Inputs	Outputs
Reactor Pressure	Monomer conversion
Temperatures of the 5 zones	Termination Agent conversion
Inlet streams temperatures	Number-Average Molecular Weight (M_n)
Ethylene and Termination Agents inlet flows	Weight-Average Molecular Weight (M_w)
Initiators inlet flows	Polydispersity Index (PDI)
Grade	Short Chain Branches (SCB)

As it will be seen on the next chapter, this first approach did not produce satisfactory results for the polymer quality and so, another approach was tried. In the literature [35], there exist two publications where the kinetic parameters of the LDPE polymerization reactions were regressed. In both works, an iterative process was employed where the output variables were sequentially fitted one at the time by manipulating the parameters of a limited number of reactions.

Although the previous studies differed from the current one, a similar approach was taken due to the analogous nature of the problem: regressing the kinetic parameters for the free-radical ethylene polymerization reactions. However, differences in the measured outputs between the current and previous works required the development of an adapted iterative scheme.

The first step of the iterative scheme is to evaluate how the reaction influences the output variables. Here we relied on the information coming from the analysis performed in chapter 4.8, which was crucial to select which adjusted parameters will be used to fit a specific output variable. The coupling was made based on the parameter with the most significant effect on a given output variable and is detailed in Table 8. However, as noted before, some reactions affect more than one output variable, so the fitting may require some iterations.

Table 8. Coupling between validation variables and adjusted parameters.

Validation variables	Adjusted parameters
Conversion	Propagation
Conversion of butane	Chain transfer to butane
Conversion of propylene	Chain transfer to propylene
Number-Average Molecular Weight	Chain transfer to monomer
Weighted-Average Molecular Weight or PDI	Chain transfer to polymer
Frequency of Short Chain Branches	Backbiting

The sequence followed to fit-regress the parameters was developed in a way that the next fit would not have much impact on the previous one. The propagation was the first reaction manipulated to fit the ethylene conversion because it significantly influences most properties. After this fit, we utilized chain transfer reactions that do not affect ethylene conversion (thus not disturbing the previously performed fit) to adjust other outputs. We started by tackling the chain transfer to butane and to propylene for fitting their respective conversion. This was done before fitting M_n and M_w since these reactions impact both molecular weights, but the conversion of butane and propylene are only affected by these reactions, therefore no subsequent fits will change these two fitted outputs. Then, as there does not exist a reaction that only affects M_n without affecting M_w , the M_n was fitted first by manipulating the chain transfer to monomer and then the M_w was fitted with the chain transfer to polymer which mainly impacts the M_w , leaving the M_n fit almost intact. Finally, the SCB was fitted with the backbiting reaction which does not influence any output beside the SCB. This sequence resulted in fewer iterations. The iterative scheme explained is synthesized in Figure 34.

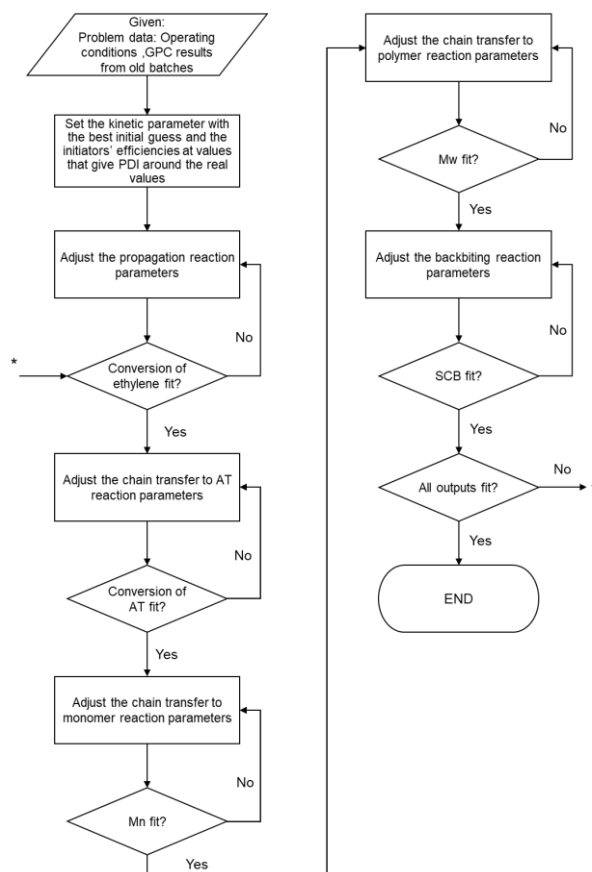


Figure 34. Flowchart of the iterative strategy to regress the kinetic parameters.

Although the results showed improvement, they were still unsatisfactory, for the reasons to be explained in the next chapter. So, for troubleshooting, the kinetic model was simplified by discarding many reactions. The firsts to be removed were the transfer to polymer and the β -scission reactions. The reason for neglecting these two reactions and not the others, was because it makes the method of instantaneous properties valid, i.e., the curve obtained in Aspen Plus® will have the same average properties as the ones that are being fitted. Therefore, the full MWD will be available in Aspen Plus®, which is a plus because these curves are obtained in another Repsol site and not in the plant. After a few tests, we also decided to deactivate the chain transfer to monomer and to propylene, which forced us to ignore the propylene grade.

Here in this stage, the PDI was taken as the key parameter since it relates both molecular weights. The number of parameters in this case were more limited, but it was found out that by manipulating the initiators' efficiencies, it was possible to obtain polymers with decent PDI. Although it may not make sense, Aspen Plus® V11, permits efficiencies to exceed 1, and so the upper limit for the efficiencies was extended past such value. The goal was obtaining polymers with a PDI near 10. From a kinetic standpoint, manipulating the efficiencies is not very different from manipulating the pre-exponential factor, since the reaction rate is directly proportional to both

parameters. Manipulating the efficiency of initiator X and Z, allowed to obtain polymers with PDIs between 5 and 12 which is around the real values. The efficiencies were set at 1200 and 300 for initiator X and Z, respectively.

After this first approximation to the optimal kinetic parameters, we concluded that it was not reasonable to include all result variables in the same Data Set. Specifically, it was not possible to fit the conversion and the quality parameters at the same time: the solutions obtained either exhibit good fits for the conversion but a poor fit for the quality parameters, or vice versa. Thus, we decided to proceed by focusing only on the PDI, M_n and SCB quality parameters. Unfortunately, the Data Fit still didn't perform as expected, which led us to develop the strategy represented in the flowchart of Figure 35.

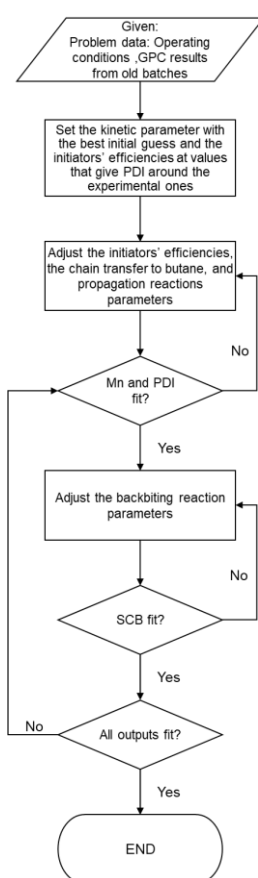


Figure 35. Flowchart of the strategy to regress the kinetic parameters related with the quality output variables.

After improving the results for polymer's quality, the focus switched to the conversion.

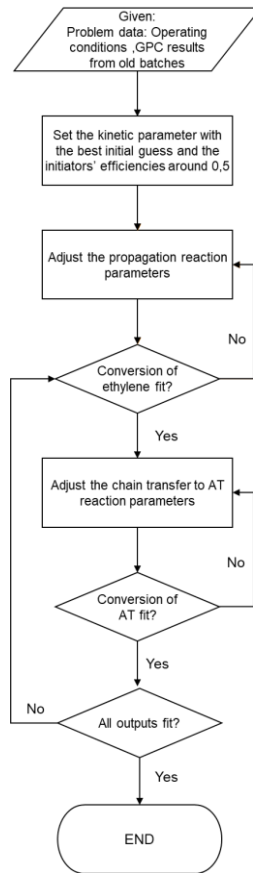


Figure 36. Flowchart of the strategy to regress the kinetic parameters related with the conversion output variables.

In summary, we decided to use two different sets of kinetic parameters to replicate the plant's data, forcing us to duplicate the reactor blocks representing the autoclave reactor. This can be seen in Figure 37, where the Duplicator block in Aspen Plus® V11 was used to clone the reactor's feed streams. The red streams are linked to the polymer's quality output, while the blue streams are used to compute the conversions. Then, a calculator block was implemented to guarantee that the reactors operate under the same conditions (zone temperatures and pressure).

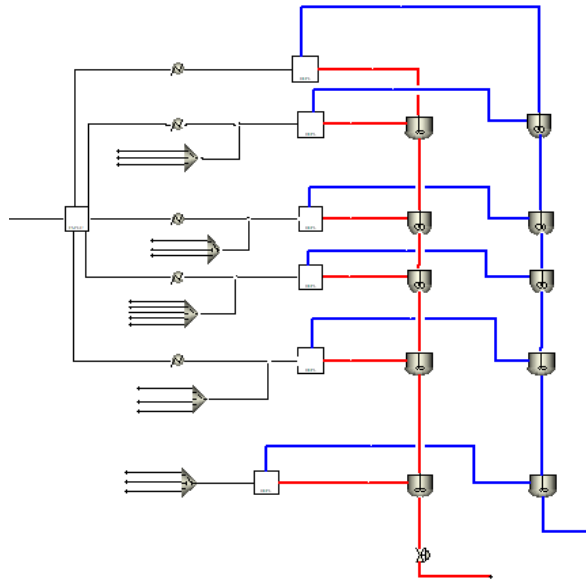


Figure 37. Flowsheet with the two reactor systems (one for each set of kinetic parameters).

6.3.2.2. Separation System

With the reactor giving reasonable results, the following step was implementing the separation stages, with the separator, the high-pressure flash, and the low-pressure flash. Here the goal was finding the best thermodynamic parameters that would describe the outlet streams of each block, based on the temperature and pressure conditions. All the separating stages consist of three simple liquid-vapor flashes, which follow a sequence of lower pressures and about the same temperature, to promote the removal of the gas from the liquid polymer.

In Aspen Plus® V11, the three stages are simulated using three 2-Flash blocks, where the temperature and pressure are defined. Then to replicate the separation, a Data Fit is performed, where the PC-SAFT binary parameters (between ethylene and LDPE, and butane and LDPE; the LDPE-propylene was not part since the grade which used propylene was neglected) are manipulated to achieve the same flows of the flashes' top outlet streams (streams 15 and 17 in Figure 10). These two parameters were chosen as the target due to availability of the measures at the plant. The inputs of the Data Set used were essentially the same as the ones used in the reactor, to have the separator inlet stream. The inlet stream is defined by a calculator block that extract the desired results from each reactor outlet stream. In addition to the inputs used in the reactor's Data Fit, we added the pressure and temperature of the three flashes. While the output variables were only the two outlet streams of the high and low-pressure flashes. At this point, the flowsheet is represented in Figure 38.

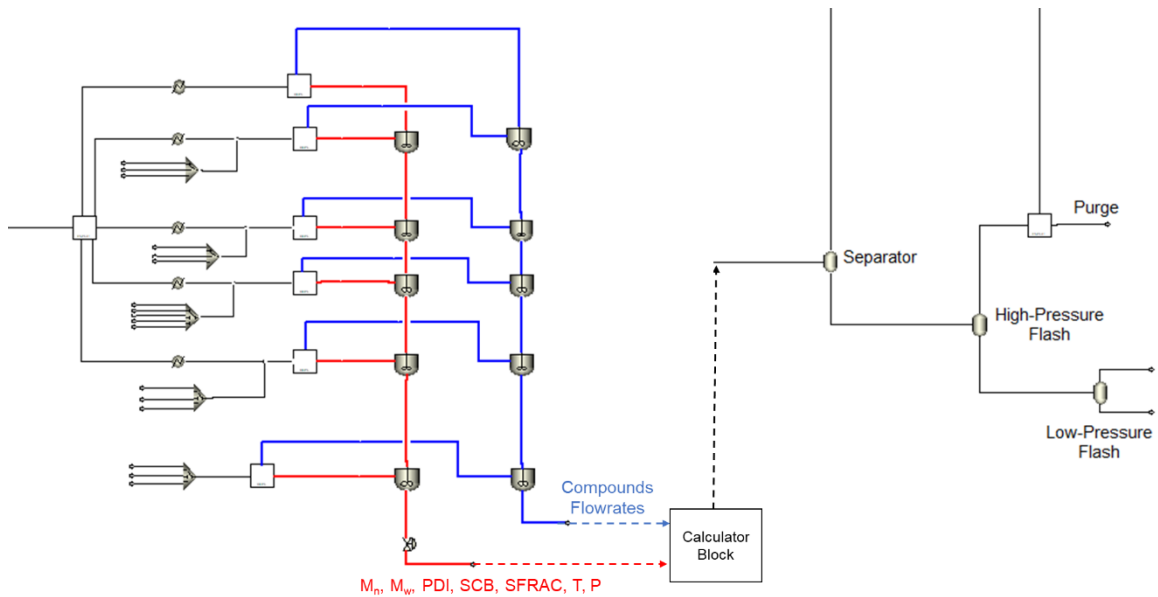


Figure 38. Flowsheet with the separation stages.

6.3.2.3. Compression

The next phase was to insert the compressors and close the flowsheet. The flow of the purge stream, measured in the plant, was not enough to ensure no accumulation of ethylene and butane in the system. As a first approach, we created a design spec to meet this target. So, the spec was that the sum of all the ethylene flow in the streams that leave the system plus the amount of ethylene consumed in the reactor minus the sum of all the ethylene flow in the streams entering the system is equal to zero. The varying variable, at a first attempt even being measured, was the purge stream itself. Unfortunately, this was not enough to achieve the target, leading to a complete purge of this stream.

The solution was to create a “false” purge at the stream coming from the separator (does not exist at the plant). This option showed improvement relative to previous one. However, the secondary compressor’s inlet stream had values that differed from the ones measured at the plant, and if the simulation was restarted, then the values would be very different (it would be about 3 to 4 times lower than it should be). Thus, the target of the design spec was changed. For the new target it was created a parameter (with a calculator) that would receive the flow value entering the secondary compressor. Then the spec was this new parameter minus the actual value of the stream in the simulation. The target was also set to zero. This solution worked well for most cases. The problem was that this design spec would only compensate when the outlet gas was in excess. When there was a deficit of gas, this design spec was not able to converge. The problem relied on not having a source of gas that would compensate negative deviations.

The data from the ethylene stream coming from the Steam-Cracker had a lot of noise. So, we placed the hypothesis of using this stream as the manipulating variable. This is a robust solution to the problem, since when there was an excess of gas, this stream flow will be reduced, and by opposition, when there was not enough gas, the flow would increase.

With the flowsheet closed, the compressing phase was fitted. The main goal was predicting the energy consumption in both compressors. As a second objective, the outlet temperature of each compressor stages was also evaluated.

The primary compressor is the smallest compressor, and it is constituted by 3 stages with inter-cooling. In Aspen Plus® V11, there is a block which simulates a multistage compressor (the *MCompr* block). This block receives as inputs, the outlet pressure of each stage, the outlet temperature after the cooling, and the efficiencies of each stage (default values are available in Aspen). The compressor model type was positive displacement since the compressor in the plant is a piston operated reciprocating compressor. This model uses a polytropic compression process.

The Data Fit performed here it had as target the outlet temperature of each stage, and the total brake-horsepower. The inputs used were the inlet flow, the inlet temperature and pressure, the outlet pressure of each stage, and the outlet cooling temperature. As manipulated variables, the mechanical and polytropic efficiencies of each stage were used. The polytropic efficiencies will essentially fit the outlet temperatures because this efficiency is used to correct the enthalpy change per mole of gas (Δh) for a compression process, which is given by Equation (29), where V is the molar volume, P_1 and P_2 are the inlet and outlet pressures, and η is the polytropic efficiency.

$$\eta\Delta h = \int_{P_1}^{P_2} VdP \quad (29)$$

To compute the integral, information regarding the path followed by the fluid from the inlet to the outlet is required. The following equation relates P and V for polytropic compression [81], where n is the polytropic exponent and C a constant. The polytropic efficiency is assumed to be the same along the integration path.

$$PV^n = C \quad (30)$$

With the enthalpy change per mole of gas, it is computed the indicated horsepower (IHP), which is the total enthalpy change in the stream, by multiplying the molar flow rate (F) by the enthalpy change per mole of gas. However, to obtain the brake horsepower (BHP), corresponding to the total work, the IHP must be corrected using the mechanical efficiency (η_m) [81]. So, after using the polytropic efficiency to fit the temperatures, the mechanical efficiency will adjust the BHP.

$$BHP = \frac{IHP}{\eta_m} \quad (31)$$

The secondary compressor is a larger compressor, composed by two stages, where the first stage has two cylinders and the second stage four. For the simulation, 6 compressor blocks were used, 2 to simulate the first stage and the other four for the second stage. In these blocks, we defined the outlet pressure and the type of compressor (which once again was positive displacement, since the compressor is a plunger operated hyper compressor). Inter-stage cooling was implemented with four *Heater* blocks. The Data Fit here was very similar to the one performed before, with the targets being the outlet temperatures from each compressor, and the total brake-horsepower. The manipulated variables were also the polytropic and mechanical efficiencies of each stage. A calculator block was developed to ensure that the outlet pressures of the first two cylinders and of the last four cylinders are the same (but different between the two groups).

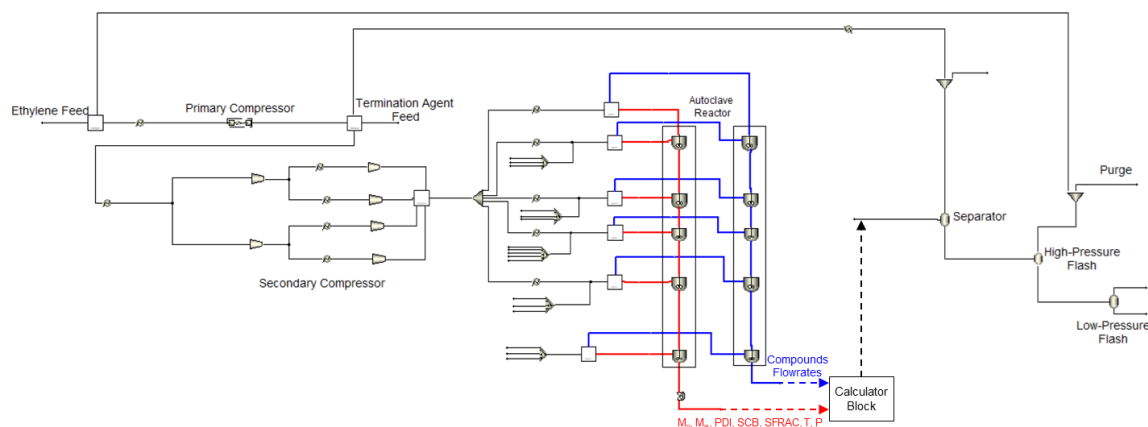


Figure 39. Final Flowsheet.

7. Results and Discussion

In this chapter, the results of the methodology proposed in the previous chapter will be presented and analyzed. But first let's recapitulate what was the problem and the steps followed. The construction of the process was divided into sections. In the first section, the reactor was fitted to reproduce the polymers production and quality. After choosing the initial kinetic parameters, three different approaches were tried on.

Initial case: This will be the base scenario, using the literature parameters, without any change.

Case 1: The scenario where all the data is considered in one Data Set, and most of the kinetic parameters are changed at the same time.

Case 2: The scenario where an iterative process was used.

Case 3: Corresponds to the case with the two-reactor system for decoupling the quality indicators from the production rate outputs.

Then, we will present the results obtained at the other stages of the flowsheet (separations and compressors).

7.1. Reactor

7.1.1. Initial Case

In the previous chapter we have shown that the literature parameters providing a better approximation of the real system were the ones by Agrawal et al. [58]. These results are shown here once again, now using one color for each grade, to facilitate the comparison to the results obtained in this work. Specifically, we want to understand if the upgraded kinetic parameters provide significant improvements.

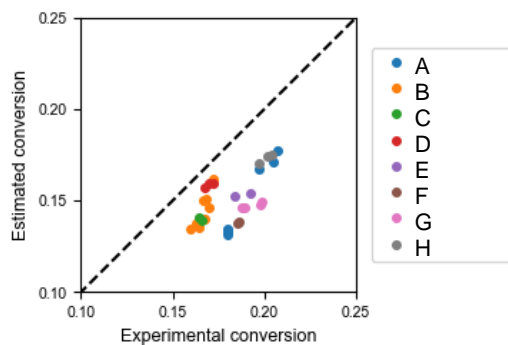


Figure 40. Experimental vs estimated ethylene conversion (initial case).

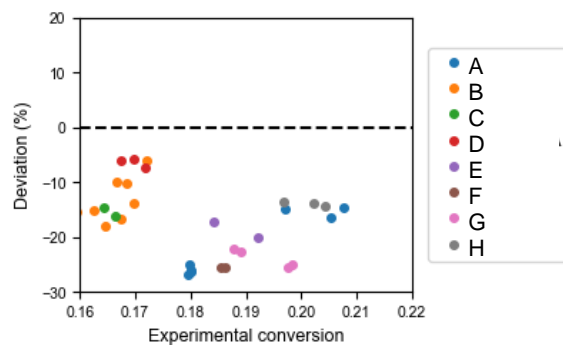


Figure 41. Deviation of the estimated ethylene conversion (initial case).

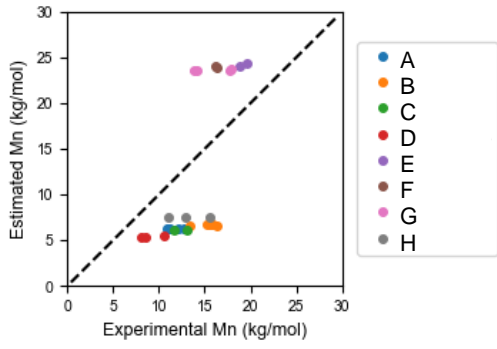


Figure 42. Experimental vs estimated M_n (initial case).

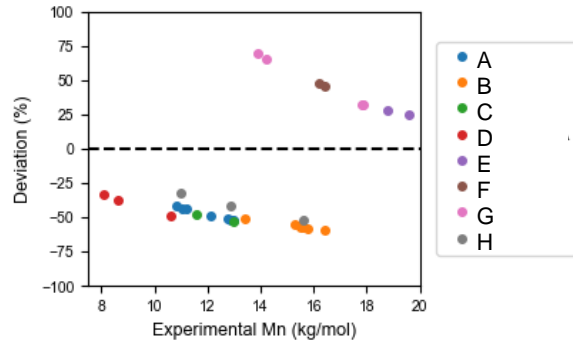


Figure 43. Deviation of the estimated M_n (initial case).

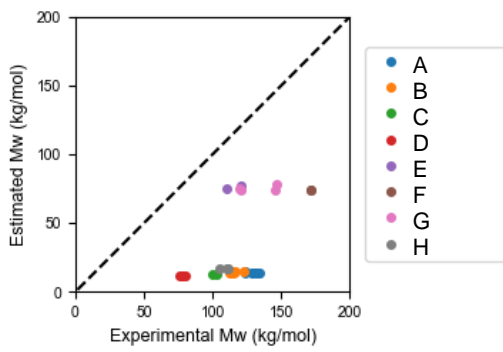


Figure 44. Experimental vs estimated M_w (initial case).

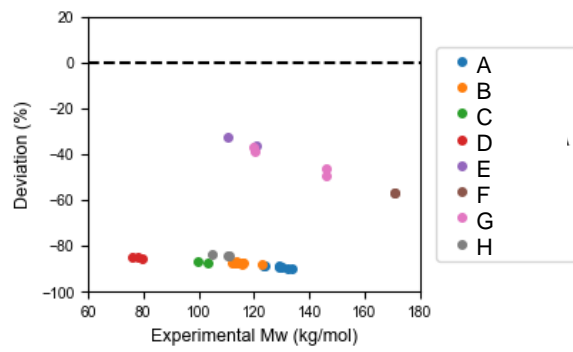


Figure 45. Deviation of the estimated M_w (initial case).

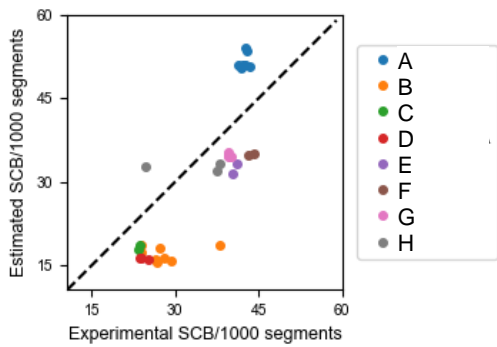


Figure 46. Experimental vs estimated SCB (initial case).

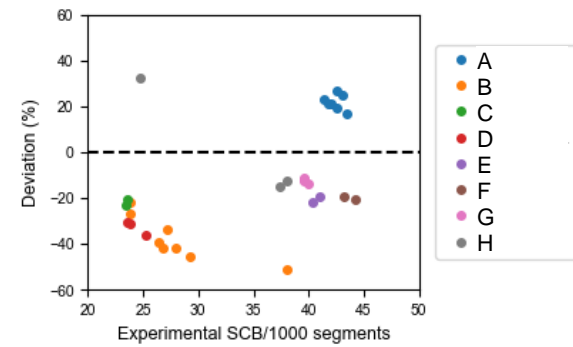


Figure 47. Deviation of the estimated SCB (initial case).

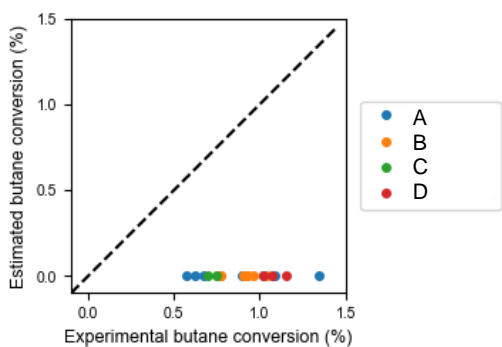


Figure 48. Experimental vs estimated butane conversion (initial case).

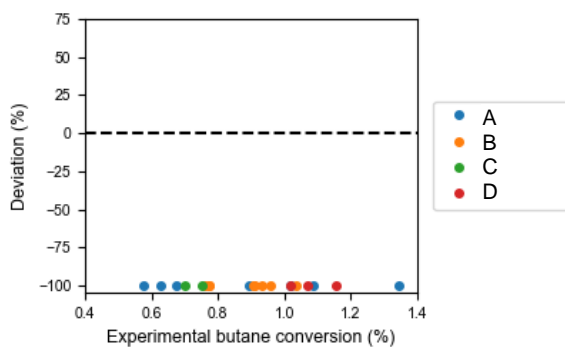


Figure 49. Deviation of the estimated butane conversion (initial case).

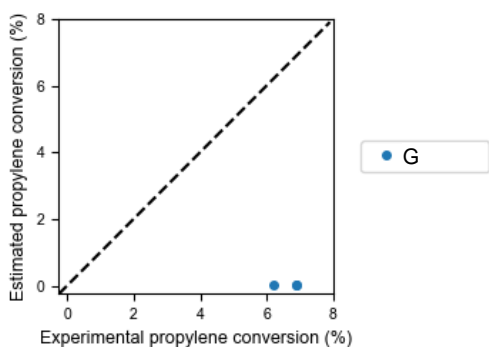


Figure 50. Experimental vs estimated propylene conversion (initial case).

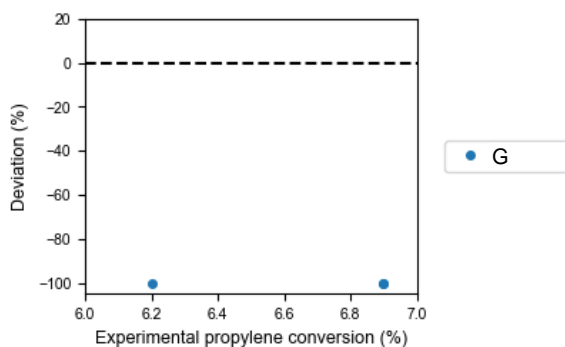


Figure 51. Deviation of the estimated propylene conversion (initial case).

From the previous figures, we can infer that the conversions are really low for both termination agents. In fact, they almost do not react. This suggests a big gap between the actual and the optimal kinetic parameters for the transfer to butane and propylene reactions. The rest of the variables show a big deviation for certain grades.

7.1.2. Case 1

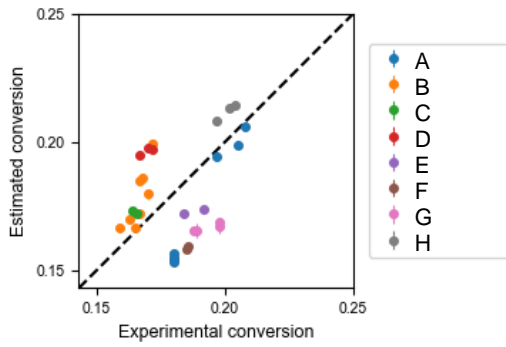


Figure 52. Experimental vs estimated ethylene conversion (case 1).

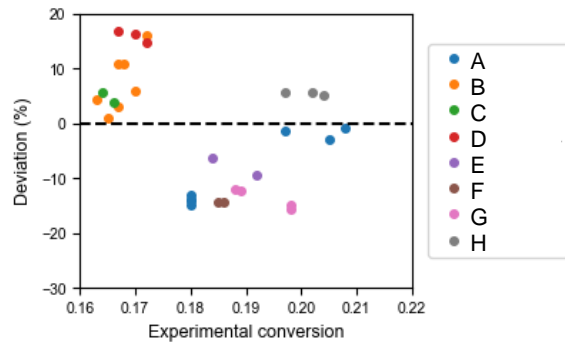


Figure 53. Deviation of the estimated ethylene conversion (case 1).

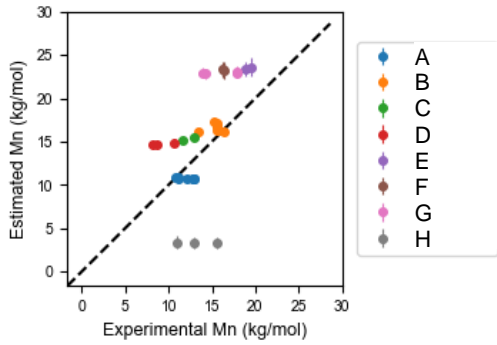


Figure 54. Experimental vs estimated M_n (case 1).

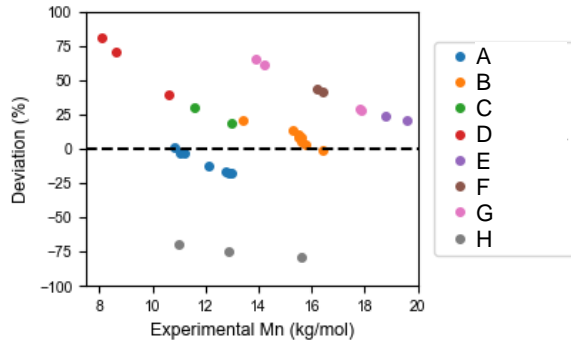


Figure 55. Deviation of the estimated M_n (case 1).

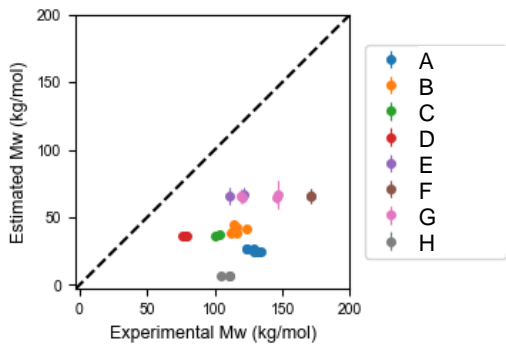


Figure 56. Experimental vs estimated M_w (case 1).

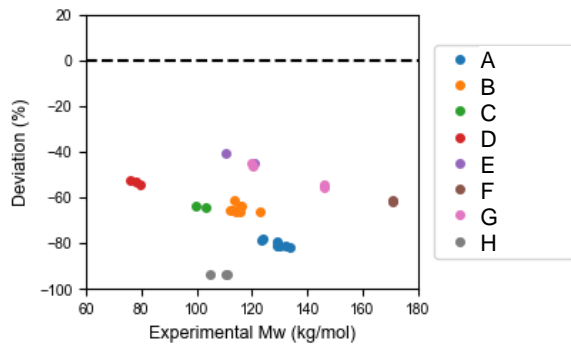


Figure 57. Deviation of the estimated M_w (case 1).

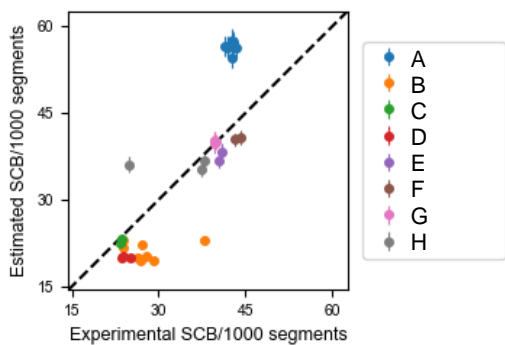


Figure 58. Experimental vs estimated SCB (case 1).

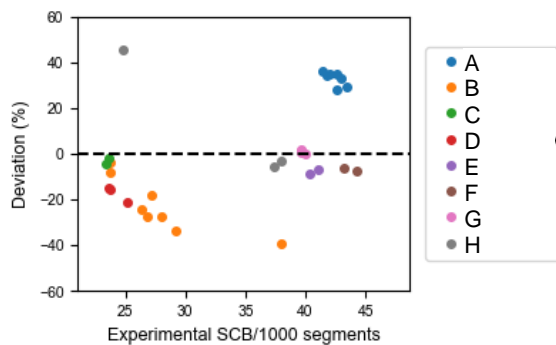


Figure 59. Deviation of the estimated SCB (case 1).

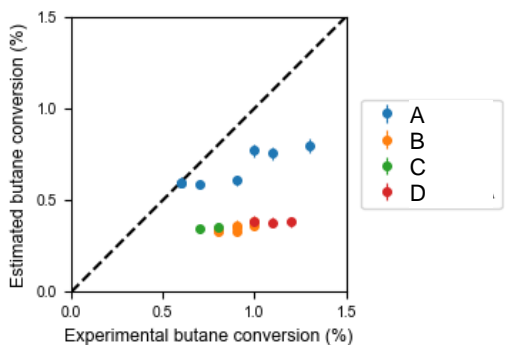


Figure 60. Experimental vs estimated butane conversion (case 1).

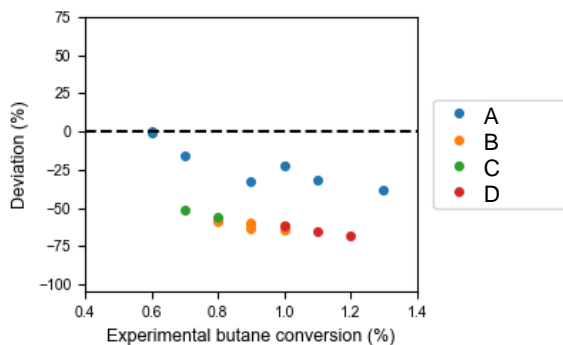


Figure 61. Deviation of the estimated butane conversion (case 1).

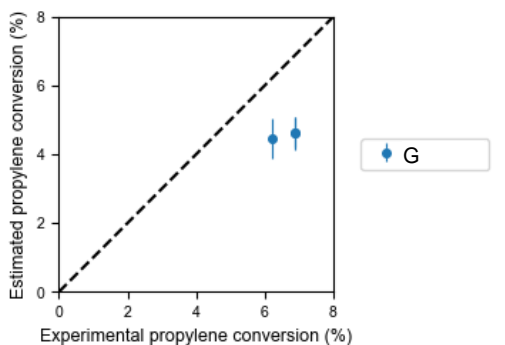


Figure 62. Experimental vs estimated propylene conversion (case 1).

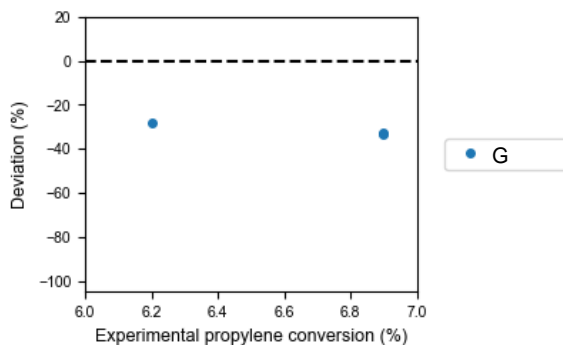


Figure 63. Deviation of the estimated propylene conversion (case 1).

Considering all outputs in one data set leads to a clear improvement compared to the base case. The conversion of the monomer exhibited the best results, with deviations within $\pm 20\%$. This means that the production of the polymer is well described by these new kinetic parameters. In contrast, M_w was consistently underestimated. Interestingly, this trend did not hold for the M_n , indicating that the PDI of the simulated polymers was notably low. In terms of the molecular weight distribution (MWD) curve, and in analogy to a normal distribution, our simulation

appears to align well with the mean but exhibits a significantly lower standard deviation compared to the actual data distribution.

7.1.3. Case 2

The previous results led us to try deconstructing what the Data Fit was doing and so the iterative approach that was described in chapter 6.3.2 was developed.

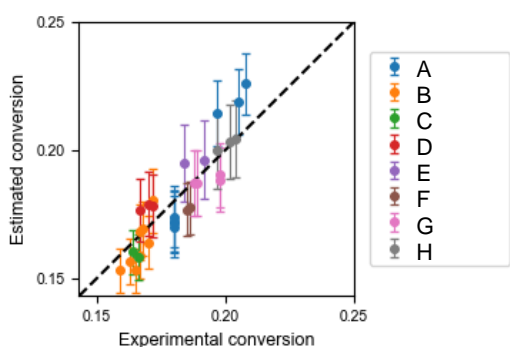


Figure 64. Experimental vs estimated ethylene conversion (case 2).

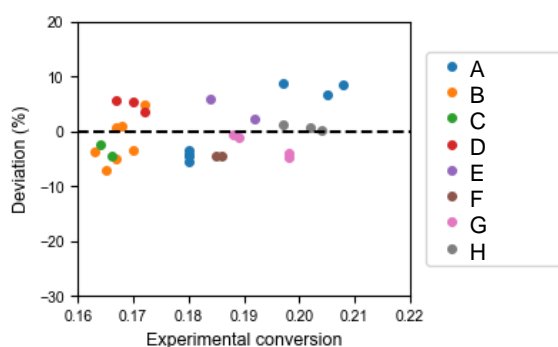


Figure 65. Deviation of the estimated ethylene conversion (case 2).

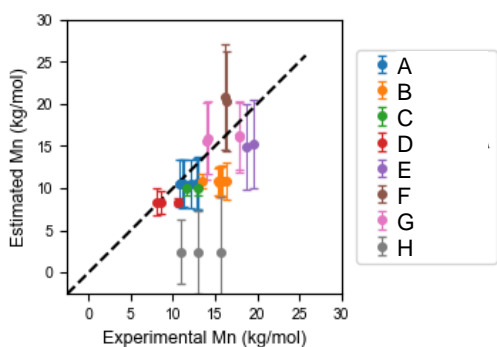


Figure 66. Experimental vs estimated M_n (case 2).

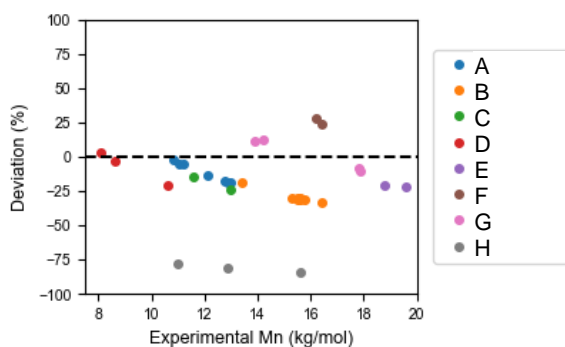


Figure 67. Deviation of the estimated M_n (case 2).

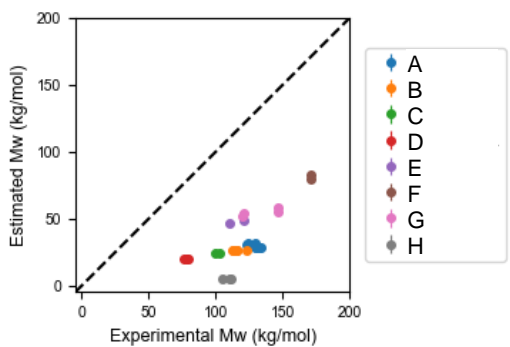


Figure 68. Experimental vs estimated M_w (case 2).

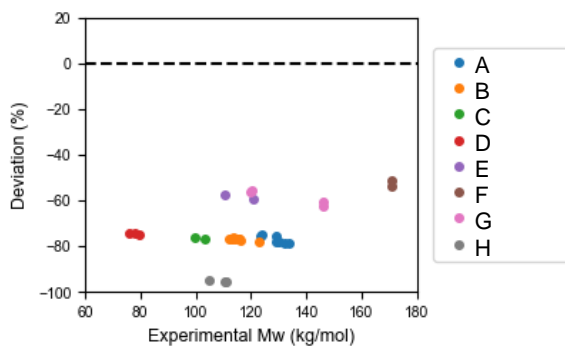


Figure 69. Deviation of the estimated M_w (case 2).

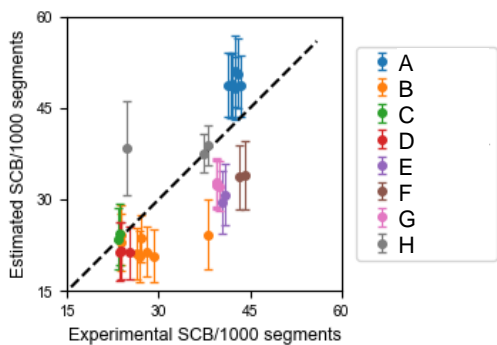


Figure 70. Experimental vs estimated SCB (case 2).

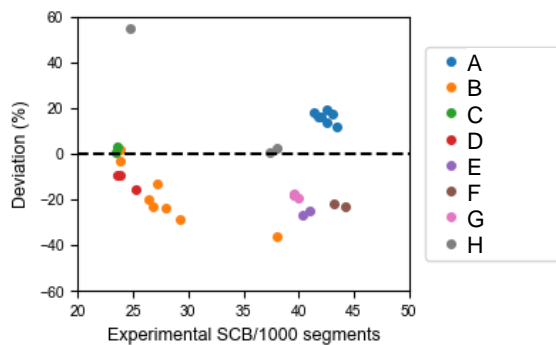


Figure 71. Deviation of the estimated SCB (case 2).

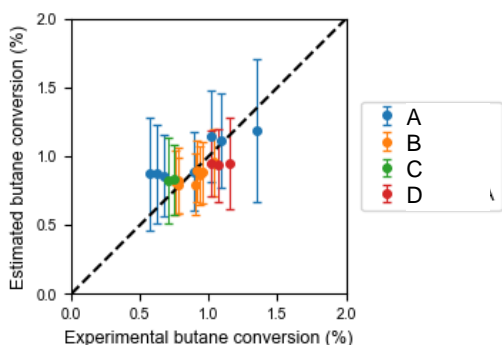


Figure 72. Experimental vs estimated butane conversion (case 2).

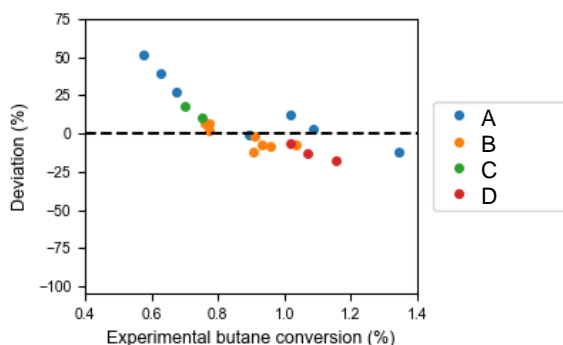


Figure 73. Deviation of the estimated butane conversion (case 2).

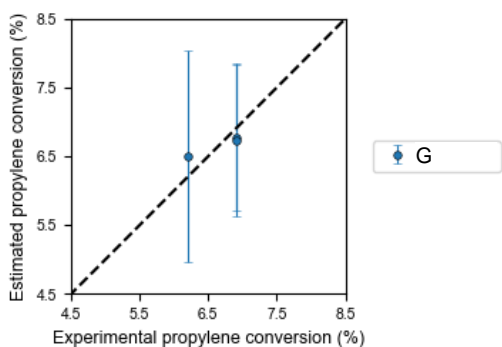


Figure 74. Experimental vs estimated propylene conversion (case 2).

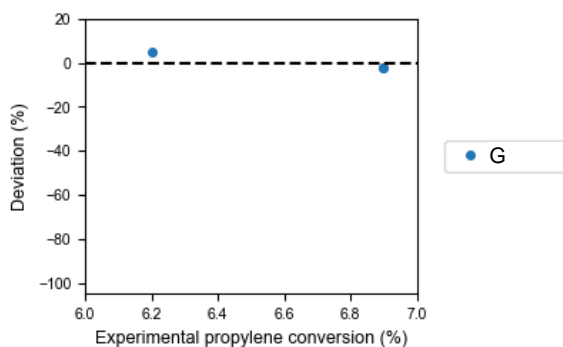


Figure 75. Deviation of the estimated propylene conversion (case 2).

Further improvements were observed. The ethylene conversion, which had already presented promising results, now has deviations of $\pm 10\%$, which considering that we are dealing with an industrial process, is more than acceptable. The conversion of termination agents also showed major enhancements. The butane has some points that are a little off for the A grade, but overall, the rest of the points fall in the range of $\pm 25\%$. For propylene, as it has just three points, the fitting was nearly perfect, but would take more data points to validate it. A typical rule of thumb

used in parameter estimation is to have a minimum of three data points for each estimated parameter to avoid overfitting the data [82].

Still regarding the transfer to propylene reaction, in Figure 66, Figure 67, Figure 68, and Figure 69 there is an interesting trend (already observed for the previous case, see Figure 54, Figure 55, Figure 56, and Figure 57). The only grade using propylene as the termination agent (H) exhibits very low M_n and M_w estimates, which suggests that the chains are being excessively “cut”. This could mean that propylene, due to its nature, could be copolymerizing, and so its conversion is not exclusively due to the transfer agent reaction, as it is being supposed.

However, it is important to note that this hypothesis remains unvalidated due to the limited dataset available for the grades that use propylene as termination agent, consisting of only the three points of the H grade. This limited dataset poses challenges because the introduction of propylene as comonomer significantly increases the complexity of the system. The complexity arises from the need to include not only the propylene-propylene reactions but also the crossed reactions (propylene-ethylene and ethylene-propylene). Since the number of parameters to be estimated far exceeds the limited number of data points available, it was decided to discard the H grade from further analysis.

The SCB did not show any major changes. The M_w continues with the same problem as before, but now we noticed something new. As mentioned in chapter 6.3.1, there are a couple of parameters inside the Data Fit that affect the results. In this case, it was found that the results for M_w would go for absurd values (over 10^9 g/mol) or were too low, as presented in the results. Instead of trying to fit the M_w , we attempted to fit the PDI. The results were basically the same, with the values falling to around 2 or going to ridiculous values (10^6).

A better understanding of what was going on with the system while attempting to perform this fit was obtained with a sensitivity analysis. The manipulated variables used to perform the fit were the parameters of the transfer to polymer reaction. The variable varied was the pre-exponential factor (scaled). The sensitivity analysis showed that there is a point where the system is unstable, beyond which there is no trend, with the data points appearing almost randomly. It was also noticed that once the system entered this unstable region, the only way to get out of it was by reinitializing the simulation. This was demonstrated by executing the analysis with the base case scenario (pre-exponential factor scaled=1) before or after the cases in analysis. When the base case was executed first, the M_w value was normal as it is in Figure 76. When it was performed after, the value of M_w went to somewhere around 10^9 .

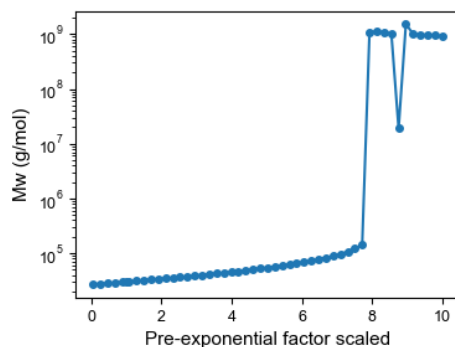


Figure 76. System instability sensitivity analysis.

The cause for the Data Fit problem must lie on something like what is happening in the sensitivity analysis. The iterations go as far as they can in the stable region. However, once it enters the unstable one, it cannot get out, leading to meaningless results. It is important to note that the instability is not only due to the transfer to polymer reaction, because sometimes during the iterative process, even before performing this fit, the system was already with these large M_w values.

7.1.4. Case 3

In the third and final case, the model was simplified by neglecting the transfer to polymer and the β -scission reaction (as explained in section 6.3.2.1). Neglecting the transfer to polymer affects the microstructure, since this is the reaction responsible for the formation of LCB present in LDPE, although allowing to obtain the MWD curve. Without this reaction, the microstructure of the polymer will be similar to the HDPE and the LLDPE, a linear polymer with only SCB. (See Figure 2)

Initially, the estimated values for M_n were too low, compared to the real ones. As it was seen in chapter 4.8, the reactions with the most impact on the molecular weights are the propagation, and the chain transfer reactions. The Data Fit was leading to low values for the pre-exponential factor of the transfer chain to monomer and so, we deactivated this reaction to allow the chains to grow more and get a better solution, as mentioned in section 6.3.2.1.

With good enough values for the PDI and M_n , we proceeded to fit the SCB, by adjusting just the kinetic parameters of the backbiting reaction. These two stages produced the following results.

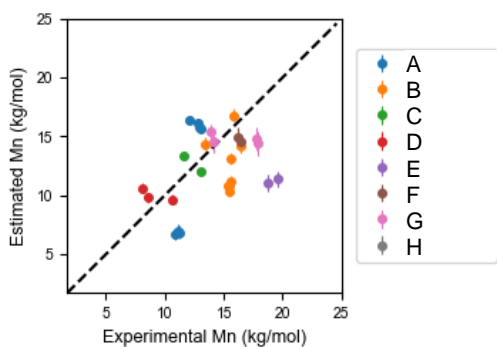


Figure 77. Experimental vs estimated M_n (case 3).

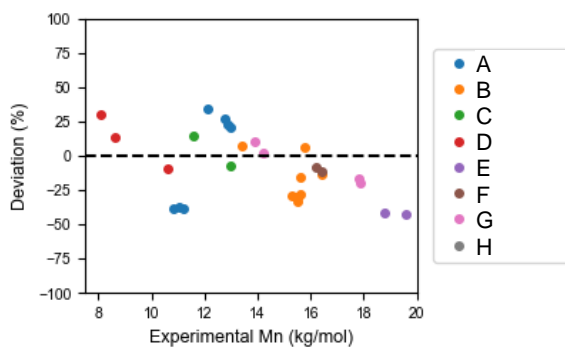


Figure 78. Deviation of the estimated M_n (case 3).

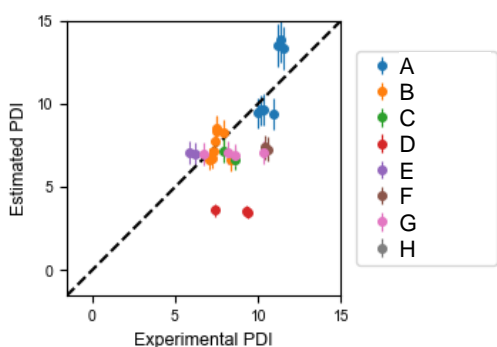


Figure 79. Experimental vs estimated PDI (case 3).

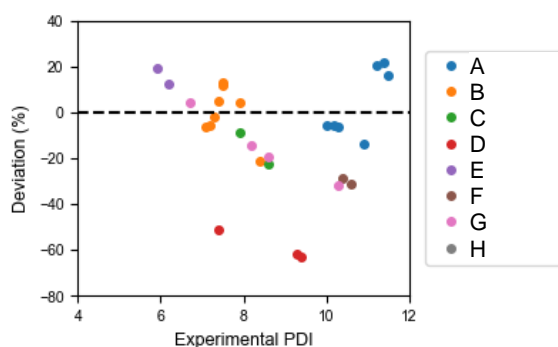


Figure 80. Deviation of the estimated PDI (case 3).

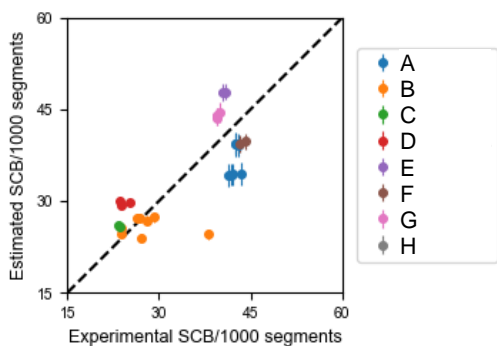


Figure 81. Experimental vs estimated SCB (case 3).

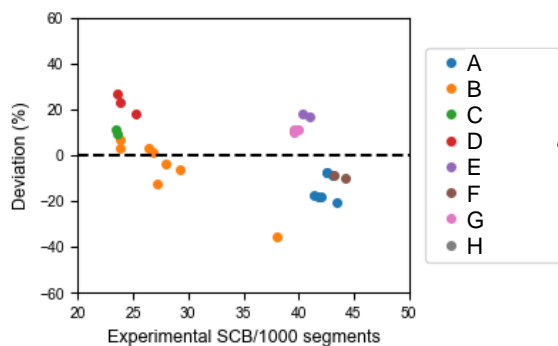


Figure 82. Deviation of the estimated SCB (case 3).

In the previous figures, an improvement over the previous Data Fit can be noticed, especially for the PDI (previously adjusted via M_w), which before was giving values either around 2 or meaningless ($>10^6$). The M_n did not show major improvements over the second case. In fact, there are some points that got a slightly higher deviation. The SCB is better with only one point falling off the $\pm 30\%$ range. The fitted kinetic parameters are available in Table 9.

Table 9. Kinetic parameters used to predict quality attributes- set number 1.

	k_0 (SI)	E_A (kJ/mol)	V_A (cm ³ /mol)	T_{ref} (°C)	# Radicals	Efficiency
INI-X	3.79×10^{-8}	153.5	0	60	2	960.4
INI-Y	4.14×10^{-6}	124.9	0	60	2	3.0×10^{-3}
INI-W	9.30×10^{16}	154.1	0	1×10^{35}	4	1.0
INI-Z	2.82×10^{-5}	123.6	0	60	2	0.24
INI-V	1.17×10^{-4}	115.5	0	60	2	117.6
Chain initiation	3.70×10^5	17.6	-17.1	1×10^{35}	----	----
Propagation	3.70×10^5	17.6	-17.1	1×10^{35}	----	----
Chain Transfer to butane	1.00	1.6×10^4	25.3	1×10^{35}	----	----
Termination by disproportion	1.08×10^9	13.2	12.1	1×10^{35}	----	----
Termination by combination	1.08×10^9	13.2	12.1	1×10^{35}	----	----
Backbiting	2.57×10^4	5.9×10^{-4}	49.3	1×10^{35}	----	----

Recall from section 6.3.2.1 that we will be estimating two sets of kinetic parameters, one for the polymer quality and another for the conversion of ethylene and butane. The second reactor system is only used to reproduce the conversions, and so it does not need to have complex kinetics. Hence, the kinetic scheme was simplified, with almost the same reactions as previously for fit the quality output being deleted (the transfer to polymer, monomer, and the β -scission). This will help the model to perform faster when introducing the recycling streams. The manipulated parameters were thus related to the propagation, and transfer to butane reactions. The results can be found in the following charts.

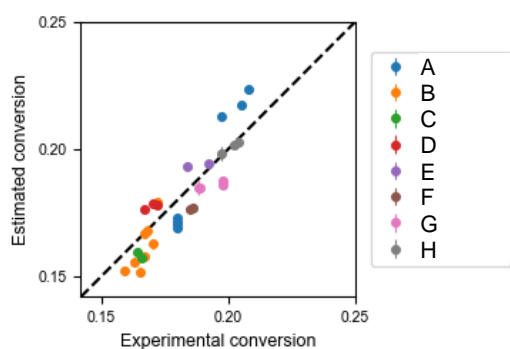


Figure 83. Experimental vs estimated ethylene conversion (case 3).

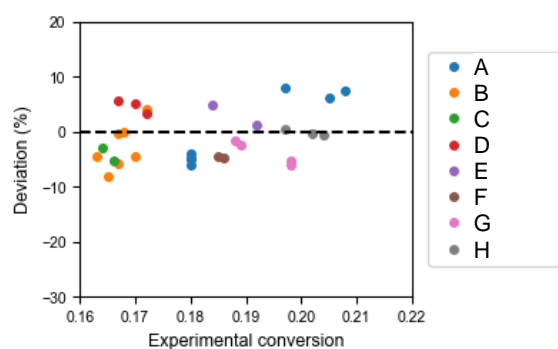


Figure 84. Deviation of the estimated ethylene conversion (case 3).

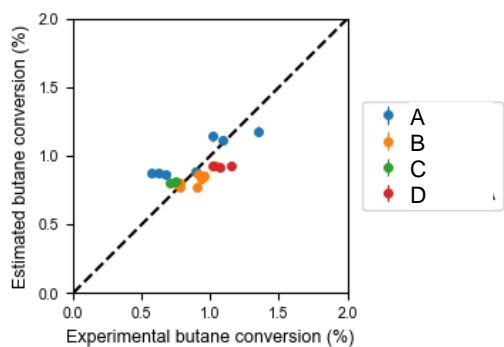


Figure 85. Experimental vs estimated butane conversion (case 3).

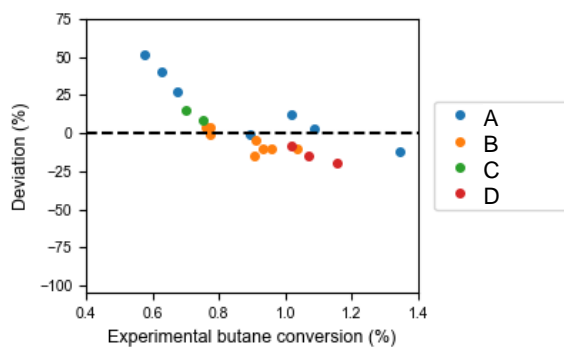


Figure 86. Deviation of the estimated butane conversion (case 3).

These results are very similar to the ones of the second case, with the ethylene conversion, presenting a deviation of $\pm 10\%$. For the butane conversion, two points present large deviations (both from grade A), while the others stay within $\pm 25\%$.

Table 10. Kinetic parameters used to predict conversion- set number 2.

	k_0 (SI)	E_A (kJ/mol)	V_A (cm ³ /mol)	T_{ref} (°C)	# Radicals	Efficiency
INI-X	3.79×10^{-8}	153.5	0	60	2	0.5
INI-Y	4.14×10^{-6}	124.9	0	60	2	0.5
INI-W	9.30×10^{16}	154.1	0	1×10^{35}	4	0.5
INI-Z	2.82×10^{-5}	123.6	0	60	2	0.5
INI-V	1.17×10^{-4}	115.5	0	60	2	0.5
Chain initiation	7.84×10^5	18.2	-8.9	1×10^{35}	----	----
Propagation	7.84×10^5	18.2	-8.9	1×10^{35}	----	----
Chain Transfer to butane	3.94×10^4	19.2	-11.9	1×10^{35}	----	----
Termination by disproportion	8.70×10^8	15.3	9.2	1×10^{35}	----	----
Termination by combination	8.70×10^8	15.3	9.2	1×10^{35}	----	----
Backbiting	1.20×10^{10}	60.5	0.0	1×10^{35}	----	----

The comparison with respect to RMSE for the output variables and the four different cases is clearer. The following figures confirm that all cases provide improvements with respect to the base case.

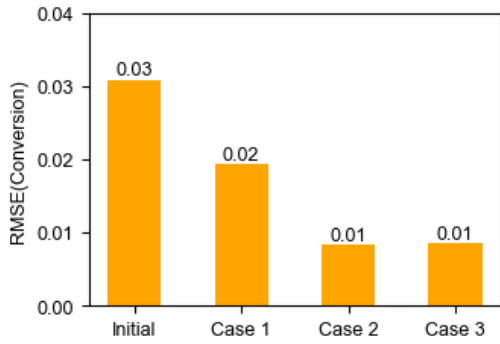


Figure 87. RMSE of the ethylene conversion for the different scenarios.

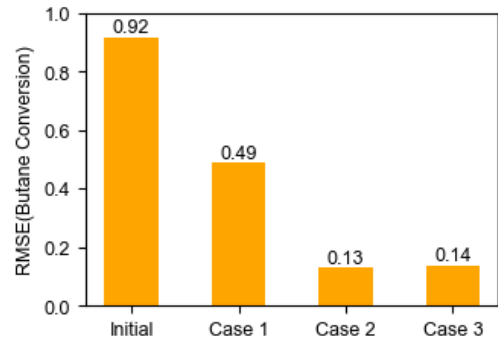


Figure 88. RMSE of the butane conversion for the different scenarios.

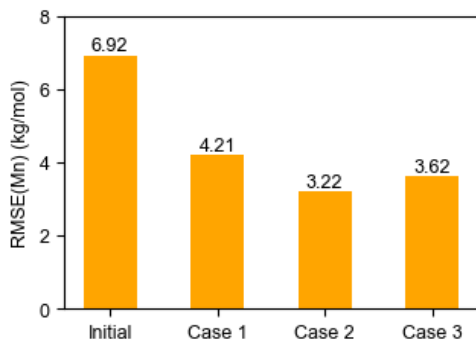


Figure 89. RMSE of the M_n for the different scenarios.

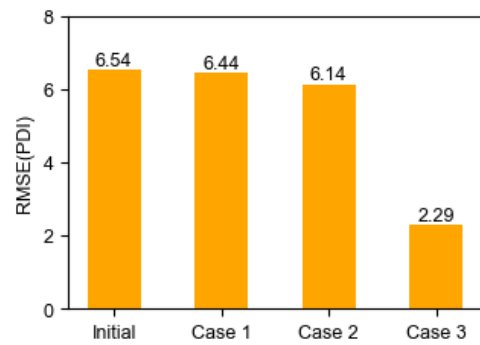


Figure 90. RMSE of the PDI for the different scenarios.

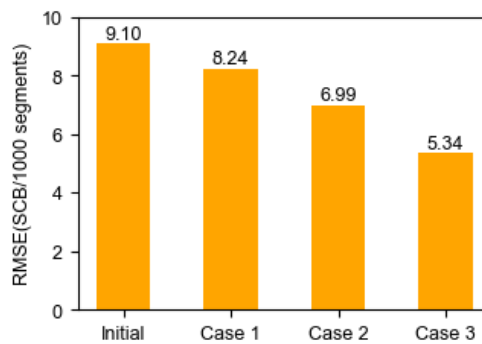


Figure 91. RMSE of the SCB for the different scenarios.

For the first case, there are output variables where the RMSE variation did not change significantly. These include the PDI and the SCB, with reductions of 2% and 9%, respectively. In

contrast, the RSME for ethylene conversion, butane conversion and the M_n , presented decreases of 38%, 47% and 39% respectively. For the second case, the PDI and the SCB were further reduced by 5% and 15%. The ethylene conversion decreased 57%, but the variable where the RMSE varied the most was the butane conversion, with a difference of 73%. The M_n decreased 24% from the first to the second scenario.

Finally, in the third and final scenario, and compared to the second case, some variables improved while others worsened. The monomer conversion did not show any changes compared to the second case. The RMSE was already small, thus there is no noticeable difference between the two scenarios. The butane conversion and the M_n got worse. For butane conversion, the difference is minor, 5%, while for M_n , the variation is 12%. The RMSE for SCB decreased by 24%. The biggest takeaway in this final scenario is the improvement on the prediction of the PDI, that showed a 63% reduction in RMSE.

Summarizing, this last scenario allows having a polymer with a better estimate of the SCB, which implies that the density of the polymer is well estimated. Regarding the PDI and M_n , by having a better PDI estimation, the MWD curve width will meet the ones observed at the plant. However, with the M_n slightly worse, this means that the curve would be shifted to the right (for positive deviations) or to the left (for negative deviations) compared to the experimental MWD. Concluding, this last case was seen as the more advantageous and thus it was the one used to move on with the construction of the flowsheet.

7.2. Separation Stages

After achieving a reactor model capable of predicting the quality and conversion of the LDPE production, the separation stages were simulated. The base scenario was based on the binary parameters from Aspen Plus[®] database and the ones previously regressed with the data from Rousseaux et al. [76].

The process operation at high pressures inhibits flow measurements and the compositions are even less measured. Only the stream returning to the Steam-Cracker unit (the mix between stream 18 and 19, in Figure 10) is periodically analyzed. The separator operates at around 300 barg so no outlet stream flows are measured. The high-pressure and the low-pressure flashes operate at about 15 barg and 0.3 barg, respectively. Therefore, only measures of the top outlet stream exist. So, these were the variables used to fit and validate the separation model.

The initial case results are the following.

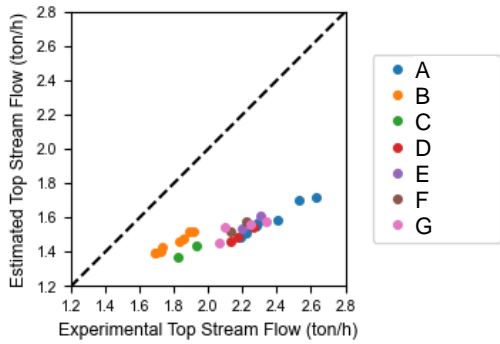


Figure 92. Experimental vs estimated high-pressure flash top output stream (before the fit).

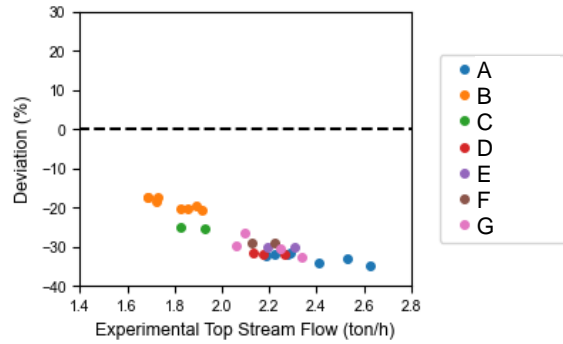


Figure 93. Deviation of the estimated high-pressure flash top output stream (before the fit).

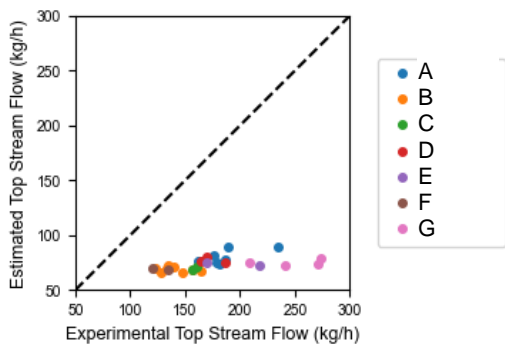


Figure 94. Experimental vs estimated low-pressure flash top output stream (before the fit).

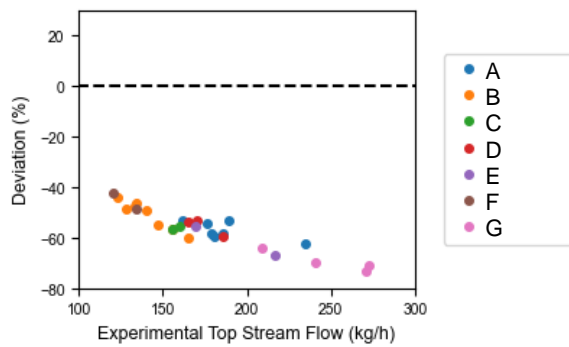


Figure 95. Deviation of the estimated low-pressure flash top output stream (before the fit).

The results in Figure 92, Figure 93, Figure 94 and Figure 95, show that both flashes are underestimating the amount of gas exiting at the top (streams 15 and 17, in Figure 10). Although the polymer was leaving the low-pressure flash with an acceptable amount of gas (a very residual amount that is later removed in the silos), the separator was removing an excessive amount of gas. There are a couple of possible explanations for these results. The first, is that the liquid-vapor separators are not operating under equilibrium conditions, as it was explored by Buchelli et al. [69]. However, this scenario was not assessed since we did not have the time nor resources to perform a vapor-liquid equilibrium study. Therefore, it was just assumed that the equipment was operating under equilibrium conditions. The second hypothesis was that the binary parameters (k_{ij}) used are not describing the equilibrium well. Thus, these parameters were adjusted to match the separation process results, as it was explained on section 6.3.2.2.

The Data Fit was performed using the polymer coming from the reactor, and defining the operating temperatures and pressures of each block as input variables and the top outlet streams of both flashes (streams 15 and 17 in Figure 10) as output variables. The results in Figure 96 to

Figure 99 show an improvement in both separation stages, with no longer an excess of gas removed on the separator (at least not for all the grades). The initial and regressed parameters can be found in Table 11.

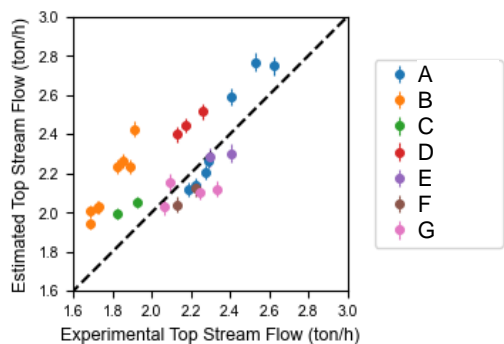


Figure 96. Experimental vs estimated high-pressure flash top output stream (after the fit).

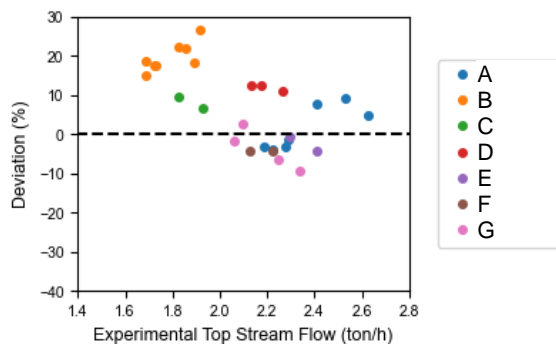


Figure 97. Deviation of the estimated high-pressure flash top output stream (after the fit).

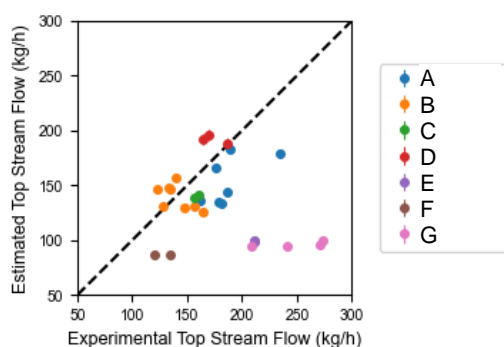


Figure 98. Experimental vs estimated low-pressure flash top output stream (after the fit).

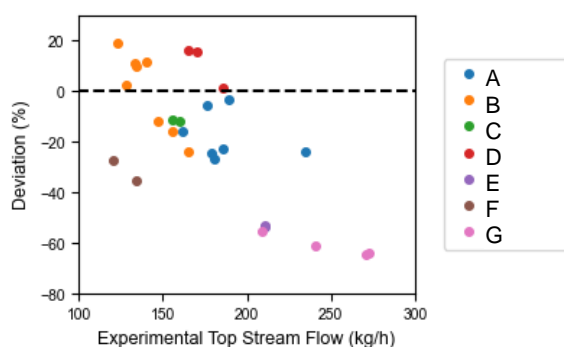


Figure 99. Deviation of the estimated low-pressure flash top output stream (after the fit).

Table 11. PC-SAFT binary parameters before and after the fit.

k_{ij}	Initial value	Estimated value
Ethylene – Ethylene Segment	-0.0562	-0.0996
Butane – Ethylene Segment	0	-0.119

7.3. Compressors

Although the compressors do not affect the mass balance, they are important to estimate the energy consumption. Due to the high pressures required in this process, the compressors

represent a significant parcel of the total energy consumption at the LDPE plant. This part was done on a separate flowsheet taking the mass flows as input variables in the Data Set.

Here there were not many things that could be adjusted since the outlet pressures and the outlet temperature of the cooler between stages are defined. The only thing that could be manipulated were the efficiencies of each stage. For validation, we used the stages outlet temperatures and the total power of the compressor. By default, the software assumes a polytropic efficiency of 0.72 while the mechanical is 1.

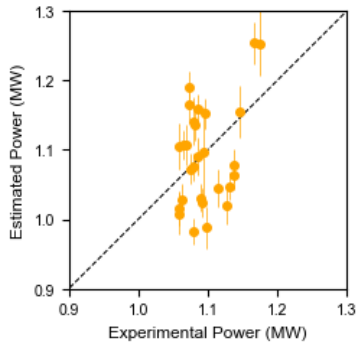


Figure 100. Experimental vs estimated CP power (after the fit).

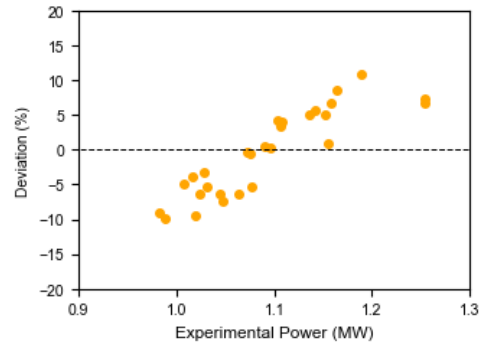


Figure 101. Deviation of the estimated CP power (after the fit).

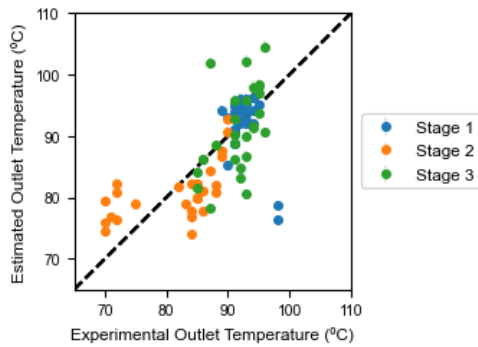


Figure 102. Experimental vs estimated output temperatures in each CP stage (after the fit).

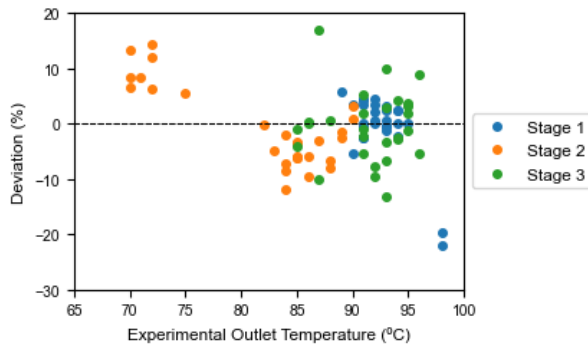


Figure 103. Deviation of the estimated output temperatures in each CP stage (after the fit).

The primary compressor exhibited compelling results, with power estimates within $\pm 15\%$ the real values. For the temperatures, we got slightly higher deviations, between -25% and $+20\%$. These results are interesting, because the mass flow entering the compressor is not very accurate on the simulation, since a design spec is being used for manipulating the fresh ethylene feed and

also because a bypass in the plant was neglected, where the part of the gas after the compressor is sent back to the feed drum to cool the ethylene, in order to allow sending more mass forward.

Table 12. Primary compressor efficiencies after the fit.

Stage	Polytropic Efficiency	Mechanical Efficiency
1	0.89	0.64
2	0.96	1.00
3	0.98	0.45

The polytropic efficiency results for the primary compressors appear to be unrealistic. The modern design compressors have polytropic efficiencies under 85%, and considering the age of the plant's compressors, these values are not realistic. We suspect that the reason behind these values lies in the low accuracy of the data used for the second stage output pressure and temperature. It was used measurements made once a shift with no track of the time. Therefore, the value is a momentaneous value, or at best is an average value of 2/3 reads. While the rest of the data are time averages for the entire batch production.

The mechanical efficiencies are also not very credible. The power losses on couplings are usually lower than 3-4%, hence, mechanical efficiencies of 0.45 are unlikely. Here the reason may be due to the incorrect flow passing through the compressor. Since as was explained this compressor as receives a by-pass which the flowrate is unknown and was not considered. Therefore, the IHP will be lower and consequently, to achieve the same BHP, the mechanical efficiency will come lower than expected.

For the secondary compressor, the idea was the same with the difference that there are only two stages, although the first stage has two cylinders, and the second stage has four.

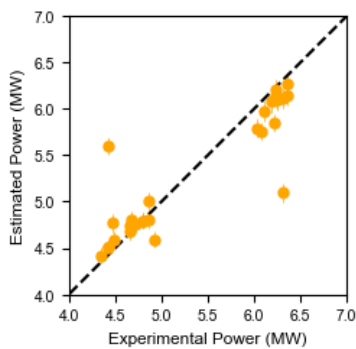


Figure 104. Experimental vs estimated CS power (after the fit).

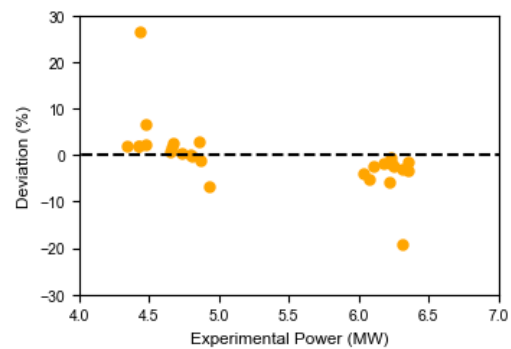


Figure 105. Deviation of the estimated CS power (after the fit).

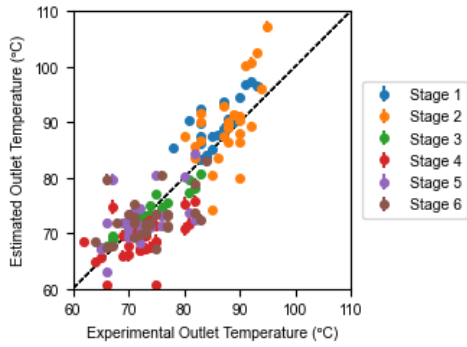


Figure 106. Experimental vs estimated output temperatures in each CS stage (after the fit).

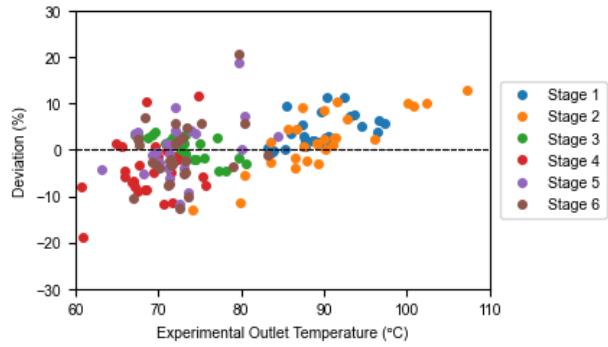


Figure 107. Deviation of the estimated output temperatures in each CS stage (after the fit).

The results were a little more disperse than the ones from the primary compressor. For estimated power, the first thing that is noticed in Figure 104 and Figure 105 is the existence of two points with a much larger deviation than the others. These must be outliers, since all the other point falls in the range of $\pm 10\%$. For the outlet temperatures, most of the points have deviation in module equal or lower than 20%.

Table 13. Secondary compressor efficiencies after the fit.

Stage	Polytropic Efficiency	Mechanical Efficiency
1	0.79	0.67
2	0.76	1.00

7.4. Full plant

With the compression stage done, the flowsheet was complete. To make sure that the results did not suffer major changes, (i.e., the separation did not have a significant impact on the reactor configuration) a sensitivity analysis was performed where all the inputs of the system were placed, and the most important output variables were checked. The results did not show any significant changes for the main variables.

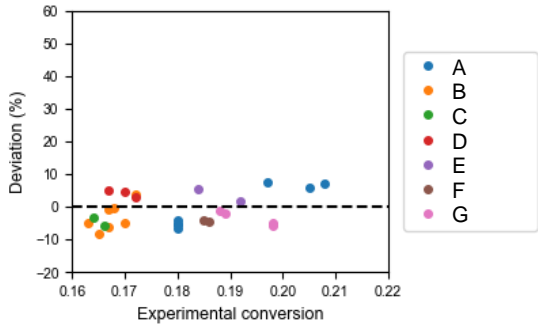


Figure 108. Deviation of the estimated conversion (full plant scenario).

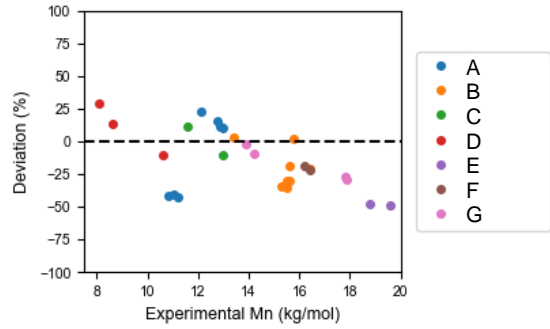


Figure 109. Deviation of the estimated M_n (full plant scenario).

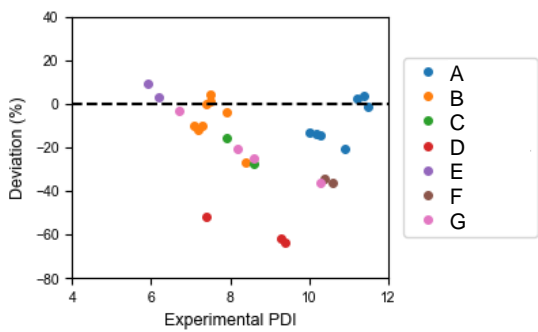


Figure 110. Deviation of the estimated PDI (full plant scenario).

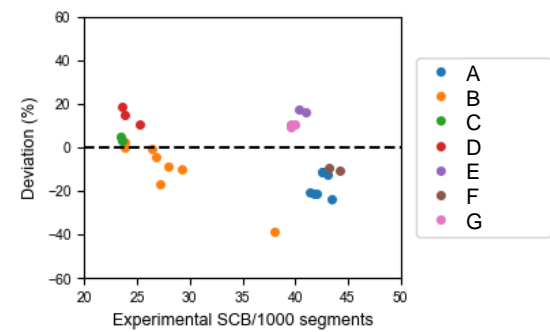


Figure 111. Deviation of the estimated SCB (full plant scenario).

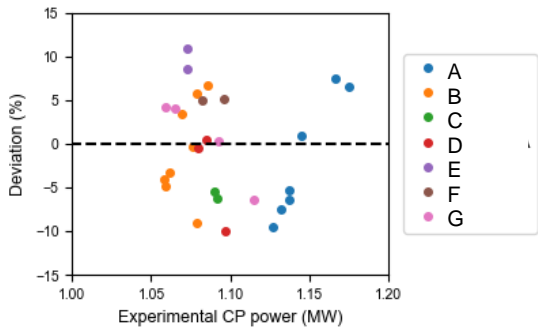


Figure 112. Deviation of the estimated CP power (full plant scenario).

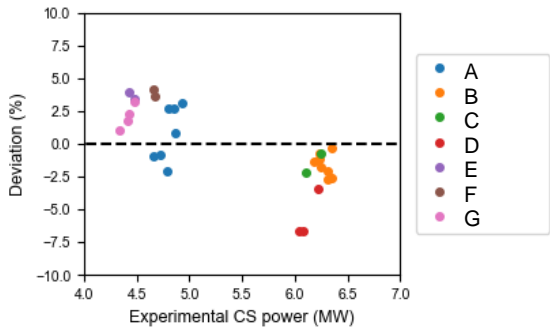


Figure 113. Deviation of the estimated CS power (full plant scenario).

Some runs were also independently done, to compare the MWD curve obtained by the model and the ones experimentally obtained. Not all the grades had the experimental MWD available, with some of them just coming with the output variables. In Figure 114 are presented the MWD for at least one representative batch of each grade with the MWD available. Although not a bad approximation, with the MWD curves placed almost at the right place and with widths not far from the reality, they are far from being perfect.

If we observe Figure 114, the MWD for the grade B, that run exhibits deviations for the M_n and PDI of approximately 2% and -12%, respectively. While these deviations are within an acceptable range, the curve significantly differs from what would be expected given these deviations. The same can be said of the (a) curve that have deviations of 12% and -13% for M_n and PDI, respectively. This leads to the hypothesis that the average properties fitted are not enough to estimate the entire MWD curve, and so more information regarding the curve is needed to perform the fit.

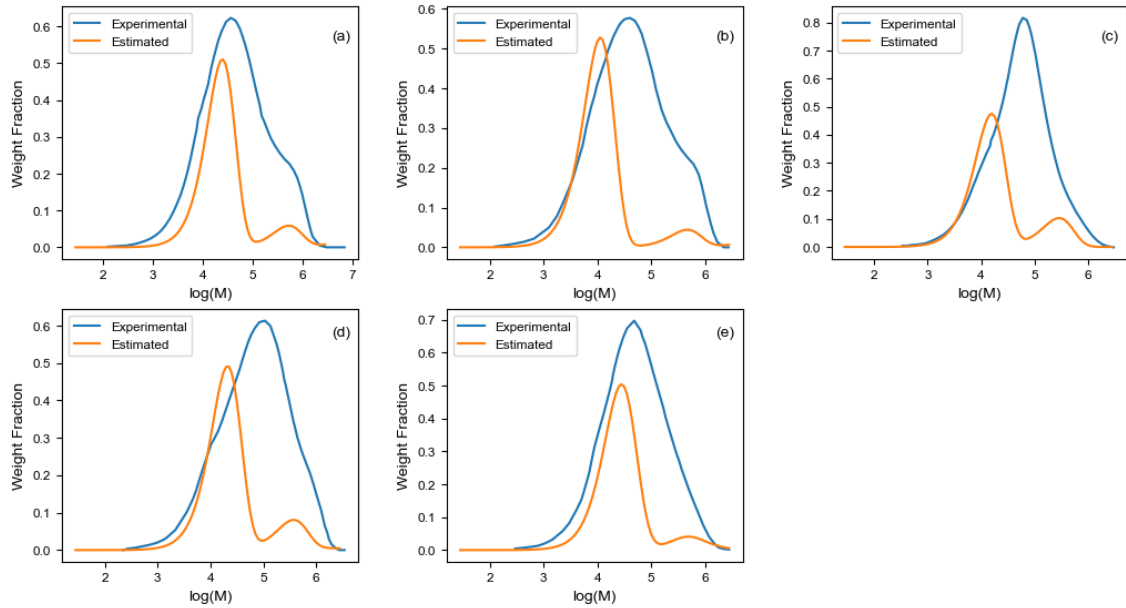


Figure 114. Estimated and experimental MWD for different grades. (a) and (b) are the A but with different batches with different protocols, (c) is E, (d) F, and (e) B.

8. Conclusions and Future Work

Multiple approaches were developed to estimate the kinetic parameters of the ethylene free-radical polymerization for the autoclave process, using industrial data. Beyond the reactor, the model was extended to the rest of the plant, integrating the compression and separation stages. From what it was found in the literature, there are no references to an Aspen Plus® simulation model applied to a full LDPE autoclave process. The closest works are from Alleyne [35] with a model for an EVA plant (where the MWD was neglected since the focus was to optimize transitions tracking the melt index), and Bokis [21], which is a model for a different type of reactor and again, only the average properties were considered. The model was shown to give a good description of the process, allowing to predict the polymer production rate, the quality parameters (M_n , PDI, and SCB) with the obtention of the Molecular Weight Distribution (MWD), and the energy consumption related with the compressors.

Since the number of points used to develop the model was limited to the number of available GPC tests, it would be important in a near future to test the model for other grades and more batches even for some of the grades already present, because for most of them, only two or three points were used. On other hand, the fit to be performed should take into account more than just two points of the MWD if the objective is to reproduce the curve, because as we saw, there are some differences between the real MWD and the estimated by the model. It is recommended that future work uses for example the z-average molecular weight (M_z) as a third point of the MWD curve.

Other aspect to assess would be the fact that the model implemented does not account for the heat transfer limitation of the autoclave reactor, since the reactors were implemented at fixed temperatures. Over the years, the plant has been optimized, lowering the feed streams' temperatures, for maximizing the production, since the mass flow of the gas entering is bigger. However, these temperatures could not be too low, because it would cause the reaction to stop. Here is where this model fails to describe the reality, because in the model the inlet temperatures do not have an impact on the production. The only thing that they are doing is changing the required heat duty for each CSTR. At an initial stage, we considered fitting the duty or specify the duty and fit the temperatures. However, this idea was not carried out due to the lack of measurements for the heat duty. A thermal fluid flows around the body of the reactor but the flows are not exactly measured. But the major problem is that the fluid splits into 5 different ramifications that will go to different zones, and the outlet temperatures before the streams are mixed, are not measured. What is experimentally available is thus the overall heat exchanged and not the heat for each zone. Furthermore, the plant data has shown that there are zones where the temperature of the thermofluid is greater than the zone temperature (heating zone), and others where it is the other way around (cooling zone).

This plant produces 40 different grades with the client's orders being used to set the amount to produce for each grade. Therefore, grade transitions occur frequently, which are performed without the shutdown of the reactor or feed cut-off. During this grade transition, an amount of out-of-specification product is produced, which it is sold at a lower price. In the future, it would be interesting to move to a dynamic model, to predict the properties of the grades produced during the transition. This would allow to minimize the time spent during the grade transitions and maximize the profit.

Nowadays, data driven models are gaining more and more strength. As this is a mechanistic approach, considering the kinetics, thermodynamics, mass and energy balances of the process, it would be interesting to compare the results to the ones from data-driven techniques such as PLS or PCA.

9. References

- [1] J. Soares, T. McKenna, An in House Industrial Short Course on Olefin Polymerization Processes for Repsol, 2022. www.polyolefins.org.
- [2] Association of Plastics Manufacturers in Europe, Annual report, 2022.
- [3] J.B.P. Soares, T.F. McKenna, Polyolefin reaction engineering, Wiley-VCH, 2012.
- [4] J. Berzelius, Isomerie, Unterscheidung von damit analogen Verhältnissen, Jahres-Bericht Über Die Fortschritte Der Physischen Wissenschaften. (1833) 63–66.
- [5] W.B. Jensen, The origin of the polymer concept, J Chem Educ. 85 (2008) 624–625. <https://doi.org/10.1021/ED085P624>.
- [6] H. Staudinger, Über Polymerisation, Berichte Der Deutschen Chemischen Gesellschaft (A and B Series). 53 (1920) 1073–1085. <https://doi.org/10.1002/CBER.19200530627>.
- [7] H. Staudinger, J. Fritsch, Über Isopren und Kautschuk. 5. Mitteilung. Über die Hydrierung des Kautschuks und über seine Konstitution, Helv Chim Acta. 5 (1922) 785–806. <https://doi.org/10.1002/HLCA.19220050517>.
- [8] Polymer | Description, Examples, Types, Material, Uses, & Facts | Britannica, (n.d.). <https://www.britannica.com/science/polymer> (accessed September 11, 2023).
- [9] D.B. Malpass, Introduction to Industrial Polyethylene: Properties, Catalysts, and Processes, John Wiley and Sons, 2010. <https://doi.org/10.1002/9780470900468>.
- [10] M.A. Spalding, A.M. Chatterjee, Handbook of Industrial Polyethylene Technology, Wiley Blackwell, 2016. <https://doi.org/10.1002/9781119159797>.
- [11] History and Future of Plastics | Science History Institute, (n.d.). <https://sciencehistory.org/education/classroom-activities/role-playing-games/case-of-plastics/history-and-future-of-plastics/> (accessed September 13, 2023).
- [12] R.B. Seymour, Tai. Cheng, Advances in Polyolefins : the World's Most Widely Used Polymers, in: Springer US, 1987: p. 568.
- [13] R.J. Young, P.A. Lovell, INTRODUCTION TO POLYMERS, 3rd ed., CRC Press, 2011. <https://doi.org/10.1201/9781439894156>.
- [14] S.M. Benito, Functionalized Polymer Nanocontainers for Targeted Drug Delivery, (2006).

- [15] Polyolefin | Chemical Compound, Plastics & Polymer | Britannica, (n.d.). <https://www.britannica.com/science/polyolefin> (accessed July 28, 2023).
- [16] C.S.F. Simões, Solubility of Polyethylenes in Different Solvents, Instituto Superior Técnico, 2019.
- [17] D.W. Green, M.Z. Southard, Perry's Chemical Engineers' Handbook, n.d.
- [18] J.B.P. Soares, Introduction to Polyolefin Types, Microstructures, and Catalysts, (2022). www.polyolefins.org.
- [19] K.S. Whiteley, T.G. Heggs, H. Koch, R.L. Mawer, W. Immel, Polyolefins, John Wiley & Sons, Ltd, Weinheim, Germany, 2000. https://doi.org/10.1002/14356007.A21_487.
- [20] N.H. Kolhapure, Computational fluid dynamics for design and optimization of tubular low-density polyethylene reactors, Iowa State University, 2001.
- [21] C.P. Bokis, S. Ramanathan, J. Franjione, A. Buchelli, M.L. Call, A.L. Brown, Physical properties, reactor modeling, and polymerization kinetics in the low-density polyethylene tubular reactor process, Ind Eng Chem Res. 41 (2002) 1017–1030. <https://doi.org/10.1021/IE010308E>.
- [22] D. Jeremic, Polyethylene, John Wiley & Sons, Ltd, 2014. https://doi.org/10.1002/14356007.A21_487.PUB3.
- [23] M. Neilen, J. Bosch, Tubular LDPE has the EC future, in: n.d.
- [24] T. Meyer, J.T.F. Keurentjes, Handbook of Polymer Reaction Engineering, Wiley-VCH, 2008. <https://doi.org/10.1002/9783527619870>.
- [25] S. Freinkel, Plastic: a toxic love story, Text Publishing, 2011.
- [26] Global plastics production forecast 2025-2050 | Statista, (n.d.). <https://www.statista.com/statistics/664906/plastics-production-volume-forecast-worldwide/> (accessed September 13, 2023).
- [27] Plastic production worldwide 2021 | Statista, (n.d.). <https://www.statista.com/statistics/282732/global-production-of-plastics-since-1950/> (accessed September 11, 2023).
- [28] Low Density Polyethylene Market | Global Sales Analysis Report - 2029, (n.d.). <https://www.futuremarketinsights.com/reports/low-density-polyethylene-market> (accessed September 14, 2023).

- [29] The Circular Economy for Plastics – A European Overview • Plastics Europe, 2022. <https://plasticseurope.org/knowledge-hub/the-circular-economy-for-plastics-a-european-overview-2/> (accessed September 14, 2023).
- [30] Why Polyolefins Are The Polymers To Watch | Wood Mackenzie, (n.d.). <https://www.woodmac.com/news/opinion/why-polyolefins-are-the-polymers-to-watch/> (accessed September 11, 2023).
- [31] A. Peacock, Handbook of Polyethylene : Structures: Properties, and Applications, CRC Press, 2000. <https://doi.org/10.1201/9781482295467>.
- [32] Growth in HDPE, LDPE and LLDPE Global Trade Volume | International Trader Publications Blog, (n.d.). <https://blog.itpweb.com/growth-in-hdpe-ldpe-and-lldpe-global-trade-volume/#more-2957> (accessed September 11, 2023).
- [33] Low Density Polyethylene Market - LDPE - Industry Analysis & Size, (n.d.). <https://www.mordorintelligence.com/industry-reports/low-density-polyethylene-market> (accessed September 11, 2023).
- [34] C. Kiparissides, G. Verros, J.F. MacGregor, Mathematical Modeling, Optimization, and Quality Control of High-Pressure Ethylene Polymerization Reactors, Journal of Macromolecular Science, Part C. 33 (1993) 437–527. <https://doi.org/10.1080/15321799308021566>.
- [35] I.R. Alleyne, Optimal grade transition policies for a high pressure EVA polymerization plant, 2006. <https://doi.org/10.7939/R3-YNRN-XB21>.
- [36] Aspen Plus®: Process Simulation with Aspen Polymers (AspenTech Customer Education Training Manual), (2022).
- [37] Aspen Physical Property System, Aspen Technology, Inc., 2019.
- [38] Aspen Polymers: Unit Operations and Reaction Models, 2013. <http://www.aspentech.com>.
- [39] A.E. Hamielec, H. Tobita, Polymerization Processes, John Wiley & Sons, Ltd, Weinheim, Germany, 2000. https://doi.org/10.1002/14356007.A21_305.
- [40] P.P. Shirodkar, G.O. Tsien, A mathematical model for the production of low density polyethylene in a tubular reactor, Chem Eng Sci. 41 (1986) 1031–1038. [https://doi.org/10.1016/0009-2509\(86\)87189-5](https://doi.org/10.1016/0009-2509(86)87189-5).

- [41] C.H. Chen, J.G. Vermeychuk, J.A. Howell, P. Ehrlich, Computer model for tubular high-pressure polyethylene reactors, *AIChE Journal*. 22 (1976) 463–471. <https://doi.org/10.1002/AIC.690220308>.
- [42] S. Agrawal, C.D. Han, Analysis of the high pressure polyethylene tubular reactor with axial mixing, *Aiche Journal*. 21 (1975) 449–465. <https://doi.org/10.1002/AIC.690210305>.
- [43] K.H. Lee, J.P. Marano, Free-Radical Polymerization: Sensitivity of Conversion and Molecular Weights to Reactor Conditions, *ACS Symposium Series*. (1979) 221–251. <https://doi.org/10.1021/BK-1979-0104.CH010>.
- [44] A. Brandolin, M.H. Lacunza, P.E. Ugrin, N.J. Capiati, High Pressure Polymerization of Ethylene. an Improved Mathematical Model for Industrial Tubular Reactors, *Polymer Reaction Engineering*. 4 (1996) 193–241. <https://doi.org/10.1080/10543414.1996.10744475>.
- [45] M. Asteasuain, A. Brandolin, Modeling and optimization of a high-pressure ethylene polymerization reactor using gPROMS, *Comput Chem Eng*. 32 (2008) 396–408. <https://doi.org/10.1016/J.COMPCHEMENG.2007.02.011>.
- [46] M.L. Dietrich, C. Sarmoria, A. Brandolin, M. Asteasuain, LDPE Production in Tubular Reactors: Comprehensive Model for the Prediction of the Joint Molecular Weight-Short (Long) Chain Branching Distributions, *Ind Eng Chem Res*. 58 (2019) 4412–4424. <https://doi.org/10.1021/ACS.IECR.8B05713>.
- [47] Repsol Polímeros, (n.d.). <https://sines.repsol.pt/pt/index.cshtml> (accessed September 23, 2023).
- [48] APQuímica- Repsol Polímeros, (n.d.). <http://www.portal-apquimica.pt/pt/diretorio/empresas-industriais/repsol-polimeros-unipessoal-lda> (accessed September 23, 2023).
- [49] Plan de Sostenibilidad 2023, (n.d.). <https://sines.repsol.pt/content/dam/repsol-complejos-industriales/sines/plan-sostenibilidad-sines-2023.pdf> (accessed September 23, 2023).
- [50] N.A. Dotson, *Polymerization Process Modeling*, Wiley-VCH, 1996.
- [51] Libro de Tecnología PEBD, 2006.
- [52] W.G. Oakes, R.B. Richards, 619. The thermal degradation of ethylene polymers, *Journal of the Chemical Society (Resumed)*. (1949) 2929–2935. <https://doi.org/10.1039/JR9490002929>.

- [53] M.J. Roedel, The Molecular Structure of Polyethylene. I. Chain Branching in Polyethylene during Polymerization, *J Am Chem Soc.* 75 (1953) 6110–6112. <https://doi.org/10.1021/JA01120A005>.
- [54] E.L. Cheluget, C.P. Bokis, L. Wardhaugh, C.C. Chen, J. Fisher, Modeling polyethylene fractionation using the perturbed-chain statistical associating fluid theory equation of state, *Ind Eng Chem Res.* 41 (2002) 968–988. <https://doi.org/10.1021/IE010287O>.
- [55] Licensor Documentation: “Cinetique de Polymerisation,” 1978.
- [56] E.H.I. and E.A.G. J. Brandrup, *Polymer Handbook 2 Volumes Set*, 4th ed., John Wiley & Sons, Inc., 1999.
- [57] Nouryon - Your partner in essential solutions for a sustainable future, (n.d.). <https://www.nouryon.com/> (accessed April 19, 2023).
- [58] N. Agrawal, G.P. Rangaiah, A.K. Ray, S.K. Gupta, Multi-objective optimization of the operation of an industrial low-density polyethylene tubular reactor using genetic algorithm and its jumping gene adaptations, *Ind Eng Chem Res.* 45 (2006) 3182–3199. <https://doi.org/10.1021/IE050977I>.
- [59] S. GOTO, Y. K, F. S, S. M, COMPUTER MODEL FOR COMMERCIAL HIGH-PRESSURE POLYETHYLENE REACTOR BASED ON ELEMENTARY REACTION RATES OBTAINED EXPERIMENTALLY, (1981).
- [60] J.Y. Ham, H.K. Rhee, Modeling and control of an LDPE autoclave reactor, *J Process Control.* 6 (1996) 241–246. [https://doi.org/10.1016/0959-1524\(95\)00052-6](https://doi.org/10.1016/0959-1524(95)00052-6).
- [61] P. Lorenzini, M. Pons, J. Villermaux, Free-radical polymerization engineering-IV. Modelling homogeneous polymerization of ethylene: determination of model parameters and final adjustment of kinetic coefficients, *Chem Eng Sci.* 47 (1992) 3981–3988. [https://doi.org/10.1016/0009-2509\(92\)85147-4](https://doi.org/10.1016/0009-2509(92)85147-4).
- [62] P.D. Iedema, M. Wulkow, H.C.J. Hoefsloot, Modeling molecular weight and degree of branching distribution of low-density polyethylene, *Macromolecules.* 33 (2000) 7173–7184. <https://doi.org/10.1021/MA991711O>.
- [63] B. López-Carpy, E. Saldívar-Guerra, I. Zapata-González, C. García-Franco, B. López-Carpy, E. Saldívar-Guerra, I. Zapata-González, C. García-Franco, Mathematical Modeling of the Molecular Weight Distribution in Low Density Polyethylene. I. Steady-State Operation of Multizone Autoclave Reactors, *Macromol React Eng.* 12 (2018) 1800013. <https://doi.org/10.1002/MREN.201800013>.

- [64] D1238 Standard Test Method for Melt Flow Rates of Thermoplastics by Extrusion Plastometer, (n.d.). <https://www.astm.org/d1238-10.html> (accessed June 5, 2023).
- [65] C.A. Sperati, W.A. Franta, H.W. Starkweather, The Molecular Structure of Polyethylene. V. The Effect of Chain Branching and Molecular Weight on Physical Properties¹, *J Am Chem Soc.* 75 (1953) 6127–6133. <https://doi.org/10.1021/JA01120A009>.
- [66] A. López, K.S. Whiteley, Nuevas correlaciones para MFI en PEBD/EVA, n.d.
- [67] C.A. Sperati, W.A. Franta, H.W. Starkweather, The Molecular Structure of Polyethylene. V. The Effect of Chain Branching and Molecular Weight on Physical Properties¹, *J Am Chem Soc.* 75 (1953) 6127–6133. <https://doi.org/10.1021/JA01120A009>.
- [68] A. López, J.J. Pedraza, Ampliación del modelo S2 para la simulación de un CSTR depolimerización de PEBD a alta presión. Modelo S3. III, n.d.
- [69] A. Buchelli, M.L. Call, A.L. Brown, C.P. Bokis, S. Ramanathan, J. Franjione, Nonequilibrium Behavior in Ethylene/Polyethylene Flash Separators, *Ind Eng Chem Res.* 43 (2004) 1768–1778. <https://doi.org/10.1021/ie0302037>.
- [70] D.R. Stull, Vapor Pressure of Pure Substances. Organic and Inorganic Compounds, *Ind Eng Chem.* 39 (1947) 517–540. <https://doi.org/10.1021/IE50448A022>.
- [71] F. Becker, M. Buback, H. Latz, G. Sadowski, F. Tumakaka, Cloud-point curves of ethylene-(meth)acrylate copolymers in fluid ethene up to high pressures and temperatures—experimental study and PC–SAFT modeling, *Fluid Phase Equilib.* 215 (2004) 263–282. <https://doi.org/10.1016/J.FLUID.2003.10.011>.
- [72] National Institute of Standards and Technology | NIST, (n.d.). <https://www.nist.gov/> (accessed March 25, 2023).
- [73] A. Michels, T. Wassenaar, The vapour pressure of ethylene, *Physica.* 16 (1950) 221–224. [https://doi.org/10.1016/0031-8914\(50\)90018-8](https://doi.org/10.1016/0031-8914(50)90018-8).
- [74] O. Olabisi, R. Simba, Pressure-Volume-Temperature Studies of Amorphous and Crystallizable Polymers. I. Experimental, *Macromolecules.* 8 (1975) 206–210. <https://doi.org/10.1021/MA60044A022>.
- [75] A. Michels, T. Wassenaar, The vapour pressure of ethylene, *Physica.* 16 (1950) 221–224. [https://doi.org/10.1016/0031-8914\(50\)90018-8](https://doi.org/10.1016/0031-8914(50)90018-8).
- [76] P. Rousseaux, D. Richon, H. Renon, Ethylene—polyethylene mixture: Saturated liquid densities and bubble pressures up to 26.1 MPa and 493.1 K, *Journal of Polymer Science:*

Polymer Chemistry Edition. 23 (1985) 1771–1785.
<https://doi.org/10.1002/POL.1985.170230617>.

- [77] E. Topalis, P. Pladis, C. Kiparissides, I. Goossens, Dynamic modelling and steady-state multiplicity in high pressure multizone LDPE autoclaves, *Chem Eng Sci.* 51 (1996) 2461–2470. [https://doi.org/10.1016/0009-2509\(96\)00102-9](https://doi.org/10.1016/0009-2509(96)00102-9).
- [78] E. Saldivar-Guerra, A. Ordaz-Quintero, R. Infante-Martínez, J. Herrera-Ordóñez, L. Villarreal-Cárdenas, D. Ramírez-Wong, E. Rivera-Rodríguez, R. Flores-Flores, L. Miramontes-Vidal, Some Factors Affecting the Molecular Weight Distribution (MWD) in Low Density Polyethylene Multizone Autoclave Polymerization Reactors, *Macromol React Eng.* 10 (2016) 123–139. <https://doi.org/10.1002/MREN.201500030>.
- [79] J.E. Dennis, J.R. University, D.M. Gay, R.E. Welsch, *An Adaptive Nonlinear Algorithm Least-Squares*, (1981).
- [80] J.E. Dennis, D.M. Gay, R.E. Welsch, Algorithm 573: NL2SOLAn Adaptive Nonlinear Least-Squares Algorithm [E4], *ACM Transactions on Mathematical Software (TOMS)*. 7 (1981) 369–383. <https://doi.org/10.1145/355958.355966>.
- [81] Compressor Background - Aspen Plus Support File, (n.d.).
- [82] B. Satola, Thermodynamic & Chemical Process Simulation Expert at Eastman, Personal Communication, (2023).

Appendix

A. MWD

Here is shown the difference between the calculated average properties between the two methods, when the instantaneous is not valid, due to the presence of some reactions.

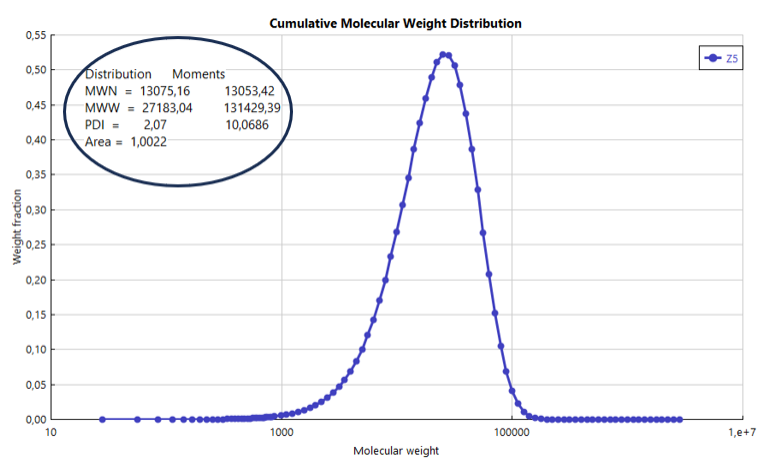


Figure 115. Invalid distribution due to the presence of some side reactions.

B. PC-SAFT

Here are presented the regressions initially performed for the PC-SAFT parameters, using the experimental data point available in the literature.

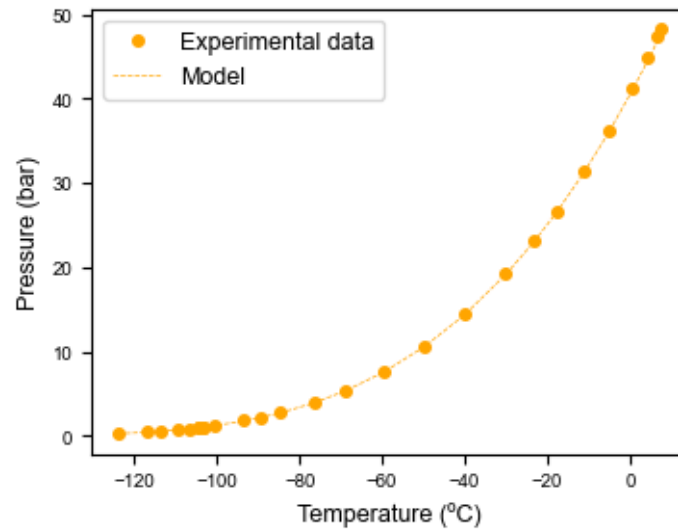


Figure 116. Ethylene vapor pressure with the PC-SAFT [75]

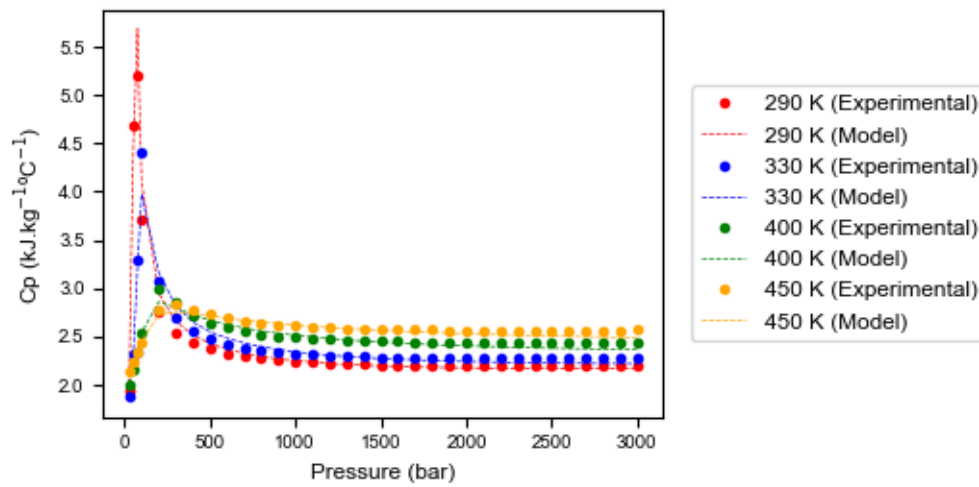


Figure 117. Supercritical ethylene calorific capacity with the PC-SAFT [72]

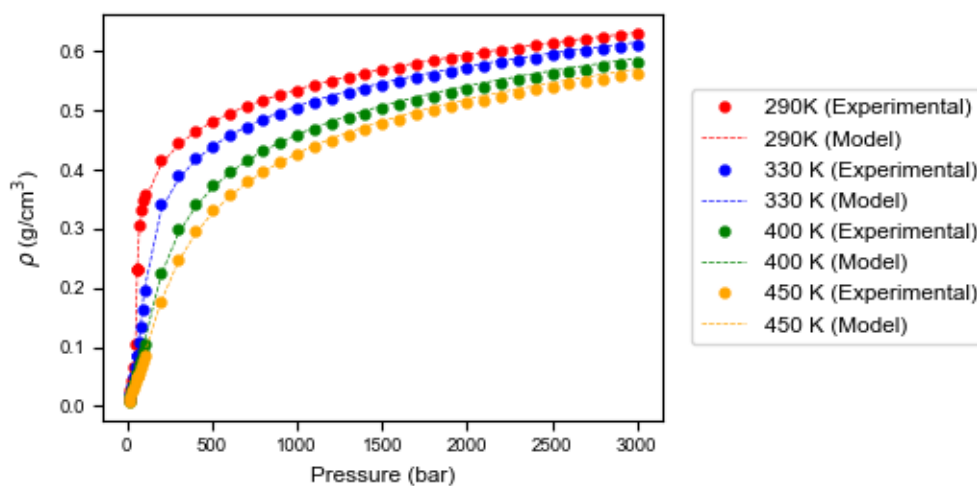


Figure 118. Supercritical ethylene density with PC-SAFT [72]

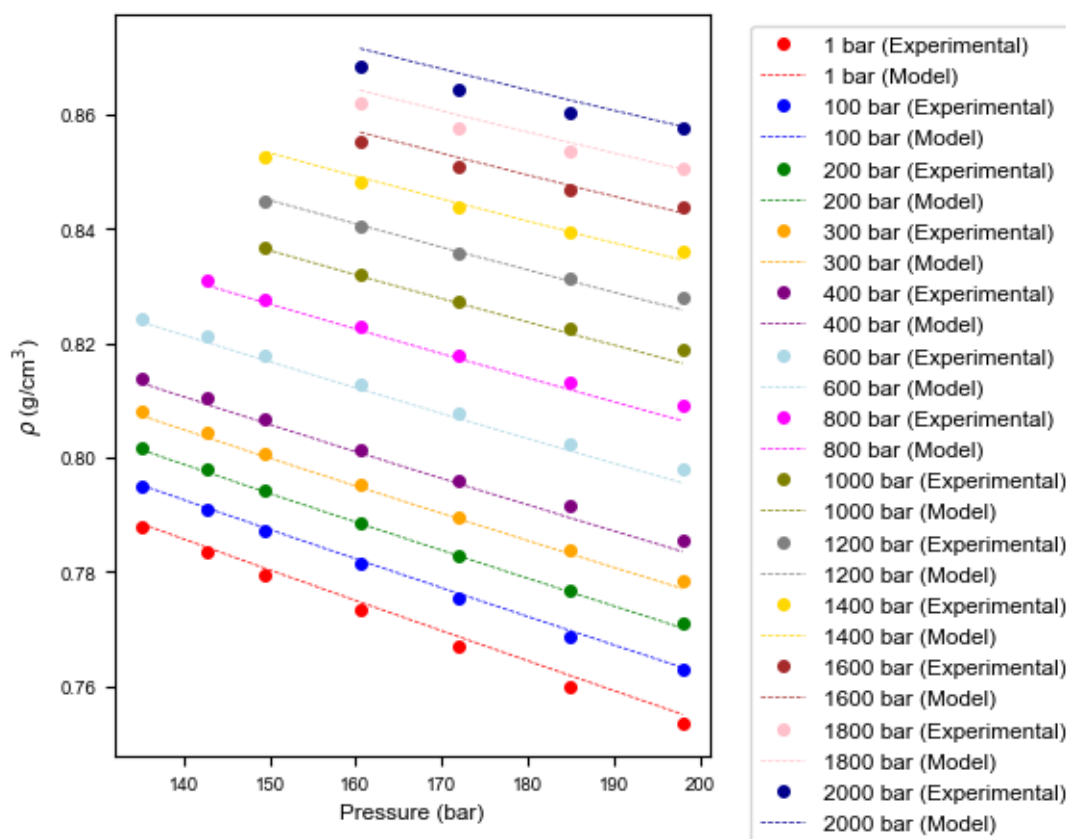


Figure 119. LDPE density with PC-SAFT [74]

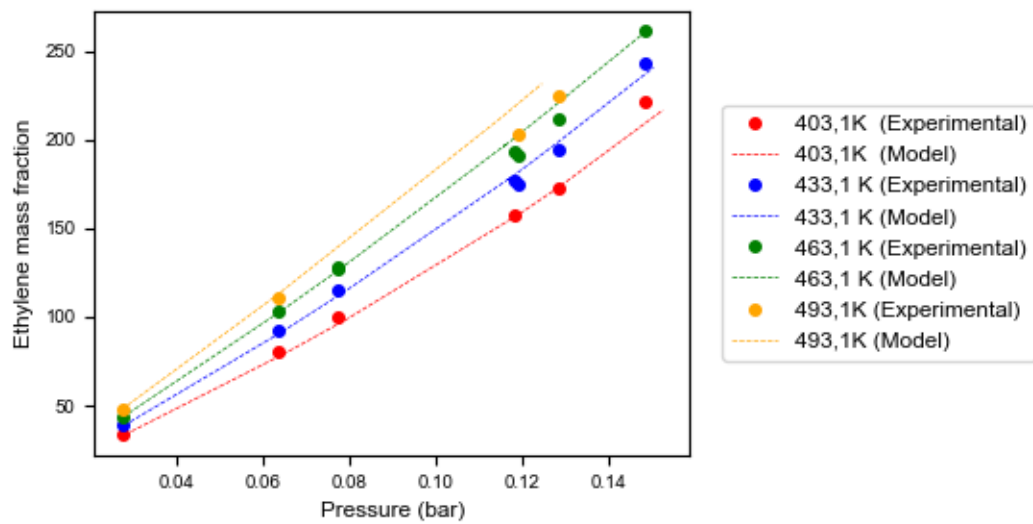


Figure 120. Liquid-Vapor equilibrium between LDPE and ethylene with PC-SAFT [76]

C. Reactor conditions

Table 14. Data for the reactor inputs for the grades with butane as termination agent

Grade	T1	T2	T3	T4	T5	P (barg)	Butane (kg/h)	Stream 5 (ton/h)	Stream 6 (ton/h)	Stream 7 (ton/h)	Stream 8 (ton/h)	Stream 9 (ton/h)	Stream 5 (°C)	Stream 6 (°C)	Stream 7 (°C)	Stream 8 (°C)	Stream 9 (°C)
A	1,3	1,3	1,4	1,4	1,5	1435	58	7.4	7.4	13.9	14.1	5.4	52	52	52	52	52
A	1,3	1,3	1,4	1,4	1,5	1436	49	7.2	7.2	13.6	13.8	5.4	52	52	52	52	52
A	1,3	1,3	1,4	1,4	1,5	1437	51	7.0	7.0	13.1	13.3	5.3	52	52	52	52	52
A	1,3	1,3	1,4	1,4	1,5	1440	49	7.2	7.1	13.8	13.7	5.1	52	52	52	52	52
A	1,2	1,2	1,4	1,4	1,7	1440	65	8.4	6.4	13.5	10.7	6.4	52	52	52	52	52
A	1,2	1,2	1,4	1,4	1,7	1440	68	8.7	6.6	13.9	11.1	6.6	52	40	40	40	40
A	1,2	1,2	1,4	1,4	1,7	1439	70	8.7	12.4	13.1	9.3	2.7	52	46	40	40	20
B	1,2	1,1	1,2	1,2	1,4	1950	77	7.7	7.5	14.4	13.4	5.2	55	55	39	36	34
B	1,2	1,1	1,2	1,2	1,4	1951	76	7.6	7.5	14.4	13.4	5.2	40	40	39	36	34
B	1,1	1,1	1,1	1,2	1,4	1951	91	7.7	7.4	14.3	13.3	5.2	41	41	39	36	34
B	1,1	1,1	1,1	1,2	1,4	1951	80	7.6	6.8	16.3	11.9	7.0	42	40	40	40	36
B	1,1	1,1	1,1	1,2	1,4	1949	81	7.9	6.6	15.6	11.7	6.8	50	40	40	40	35
B	1,1	1,0	1,1	1,2	1,4	1949	81	7.9	6.7	15.7	11.8	6.5	50	50	40	40	35
B	1,0	1,0	1,0	1,2	1,4	1951	80	7.9	6.6	15.6	11.8	6.4	50	50	40	40	35
B	1,1	1,1	1,1	1,2	1,4	1949	76	6.6	6.6	16.7	11.2	7.2	60	60	40	40	38
C	1,1	1,1	1,1	1,2	1,4	1934	87	7.6	7.4	16.4	10.2	5.7	55	55	35	35	30
C	1,1	1,1	1,1	1,2	1,4	1950	85	7.7	7.5	17.2	10.4	5.9	43	43	36	35	31
D	1,1	1,0	1,0	1,1	1,4	1946	121	6.5	6.5	16.5	10.6	5.3	52	51	43	40	35
D	1,1	1,0	1,0	1,1	1,4	1951	120	6.7	6.7	17.0	10.9	5.4	40	40	40	40	35
D	1,1	1,0	1,0	1,1	1,4	1948	116	6.5	6.5	16.5	10.6	5.3	45	45	41	40	36

...	Initiator 1 (kg/h)	Initiator 2 (kg/h)	Initiator 3 (kg/h)	Initiator 4 (kg/h)	Initiator 5 (kg/h)	Conversion	M _n (kg/mol)	M _w (kg/mol)	PDI	SCB/1000 segments
...	9.9	8.5	6.8	3.9	3.4	0.180	12.9	128.9	10.0	43.4
...	8.3	8.6	6.1	3.8	3.2	0.180	12.1	132.3	10.9	41.4
...	7.9	8.0	5.6	3.5	3.2	0.180	12.8	130.1	10.2	42
...	7.9	7.5	6.3	3.7	3.4	0.180	13.0	133.9	10.3	41.8
...	11.4	12.3	6.4	5.5	11.2	0.197	11.1	123.4	11.2	42.6
...	11.9	15.0	7.3	6.4	11.8	0.205	11.2	129.0	11.5	43
...	27.1	11.9	6.8	1.7	11.9	0.208	10.8	123.9	11.4	42.6
...	6.4	5.7	4.3	3.9	2.4	0.163	13.4	112.3	8.4	38
...	7.3	5.8	4.3	3.9	2.3	0.167	16.4	115.9	7.1	23.8
...	7.3	5.8	3.7	4.1	1.6	0.165	15.6	113.3	7.3	23.8
...	10.7	4.8	6.5	6.1	1.4	0.170	15.6	123.2	7.9	28
...	11.8	5.1	6.5	6.3	1.4	0.168	15.5	115.7	7.5	26.4
...	10.9	4.5	6.6	7.2	1.3	0.167	15.5	116.0	7.5	26.8
...	11.9	5.3	7.8	8.4	2.0	0.172	15.3	113.8	7.4	29.2
...	5.8	3.6	5.0	5.3	2.0	0.159	15.8	114.4	7.2	27.2
...	8.0	5.0	4.4	3.2	3.0	0.164	11.6	99.9	8.6	23.6
...	9.5	5.3	4.6	3.3	2.4	0.166	13.0	103.1	7.9	23.4
...	9.8	6.5	5.6	3.6	4.6	0.167	8.1	76.0	9.4	23.8
...	11.9	7.2	5.8	3.7	4.6	0.172	10.6	78.1	7.4	25.2
...	11.2	7.0	5.7	3.4	4.6	0.170	8.6	79.7	9.3	23.6

Table 15. Data for the reactor inputs for the grades with propylene as termination agent

Grade	T1	T2	T3	T4	T5	P (barg)	Propylene (kg/h)	Stream 5 (ton/h)	Stream 6 (ton/h)	Stream 7 (ton/h)	Stream 8 (ton/h)	Stream 9 (ton/h)	Stream 5 (°C)	Stream 6 (°C)	Stream 7 (°C)	Stream 8 (°C)	Stream 9 (°C)
H	1,2	1,2	1,3	1,4	1,6	1928	163	7.3	7.1	13.4	13.4	4.4	60	60	45	36	36
H	1,2	1,2	1,2	1,4	1,6	1951	177	7.4	7.4	13.6	13.6	4.4	40	40	40	36	36
H	1,2	1,2	1,2	1,4	1,6	1951	177	7.5	7.5	13.7	13.7	4.1	42	42	41	36	36

...	Initiator 1 (kg/h)	Initiator 2 (kg/h)	Initiator 3 (kg/h)	Initiator 4 (kg/h)	Initiator 5 (kg/h)	Conversion	M _n (kg/mol)	M _w (kg/mol)	PDI	SCB/1000 segments
...	4.7	4.8	4.7	6.3	2.4	0.197	11.0	104.7	9.5	38
...	5.8	5.3	4.8	6.2	2.4	0.204	15.6	111.3	7.1	24.8
...	5.8	5.2	5.0	5.5	2.4	0.202	12.9	110.6	8.6	37.4

Table 16. Data for the reactor inputs for the grades without termination agent

Grade	T1	T2	T3	T4	T5	P (barg)	Stream 5 (ton/h)	Stream 6 (ton/h)	Stream 7 (ton/h)	Stream 8 (ton/h)	Stream 9 (ton/h)	Stream 5 (°C)	Stream 6 (°C)	Stream 7 (°C)	Stream 8 (°C)	Stream 9 (°C)
E	1,1	1,1	1,1	1,3	1,6	1236	7.8	7.6	13.0	8.9	10.2	68	68	45	41	40
E	1,1	1,1	1,1	1,3	1,6	1238	7.4	7.3	13.6	9.5	9.8	41	41	40	42	40
F	1,2	1,1	1,2	1,4	1,6	1318	7.4	7.1	15.2	8.5	9.6	69	68	50	41	41
F	1,2	1,1	1,2	1,4	1,6	1322	7.5	7.2	15.4	8.5	9.7	67	67	50	40	40
G	1,1	1,1	1,2	1,4	1,6	1258	7.5	7.5	15.0	9.6	7.7	65	65	42	38	38
G	1,2	1,1	1,2	1,4	1,6	1262	7.0	6.4	16.0	9.6	7.5	41	41	40	38	36
G	1,1	1,1	1,2	1,4	1,6	1259	6.7	6.4	15.0	9.5	8.7	40	40	40	36	36
G	1,1	1,1	1,2	1,4	1,6	1251	6.6	6.6	14.7	9.3	8.5	59	58	45	36	36

...	Initiator 1 (kg/h)	Initiator 2 (kg/h)	Initiator 3 (kg/h)	Initiator 4 (kg/h)	Initiator 5 (kg/h)	Conversion	M _n (kg/mol)	M _w (kg/mol)	PDI	SCB/1000 segments
...	8.4	13.7	8.0	12.3	6.1	0.184	18.8	110.6	5.9	41
...	9.8	15.0	8.7	9.5	5.9	0.192	19.6	121.0	6.2	40.4
...	7.1	9.2	8.2	6.3	3.1	0.185	16.4	171.2	10.4	44.2
...	7.3	9.7	8.4	6.5	3.0	0.186	16.2	171.0	10.6	43.2
...	10.5	10.2	11.9	5.4	4.0	0.189	17.9	120.6	6.7	39.6
...	8.1	12.3	11.7	4.8	3.8	0.198	17.8	146.0	8.2	39.6
...	10.6	11.2	11.9	4.3	3.9	0.198	14.2	146.3	10.3	39.6
...	8.6	10.4	11.9	5.3	3.5	0.163	13.4	112.3	8.4	38

The prediction measures for the flowrates of the several initiators were obtained using a correlation between the pump strokes/min and the flowrates. The points were available in the documentation of the licensor.

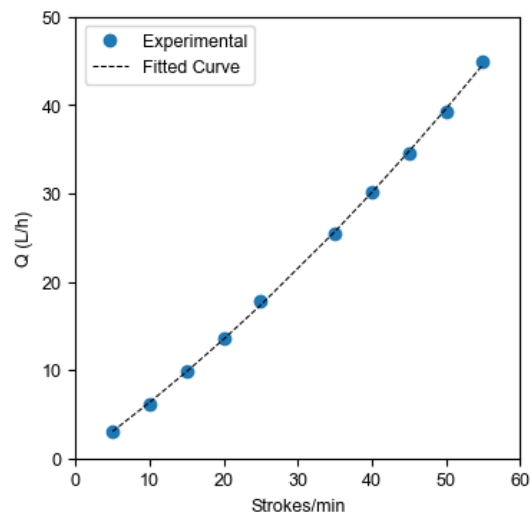


Figure 121. Relation between the flowrate and the strokes/min of the initiator pumps.
 $Q(L/h) = 0.0038(\text{Strokes/min})^2 + 0.6004(\text{Strokes/min}) - 0.0521$, $R^2=0.9996$.